

INTERIM REPORT

Accession No. _____

Report No. EGG-TFBP-5222

Contract Program or Project Title:

Subject of this Document: MEASURED EFFECTS OF FUEL ROD INTERNAL GAS PRESSURE
AND XENON CONCENTRATION IN OPERATING FUEL RODS AND
A COMPARISON WITH BASIC THEORY AND FRAP CALCULATIONS

Type of Document: Preliminary

Author(s): R. W. Miller
A. D. Appelhans

Date of Document: August 1980

Responsible NRC Individual and NRC Office or Division: G. P. Marino

This document was prepared primarily for preliminary or internal use. It has not received full review and approval. Since there may be substantive changes, this document should not be considered final.

EG&G Idaho, Inc.
Idaho Falls, Idaho 83415

Prepared for the
U.S. Nuclear Regulatory Commission
Washington, D.C.
Under DOE Contract No. DE-AC07-76ID01570
NRC FIN No. A6041

INTERIM REPORT

NRC Research and Technical
Assistance Report

8009260558

MEASURED EFFECTS OF FUEL ROD INTERNAL GAS PRESSURE
AND XENON CONCENTRATION IN OPERATING FUEL
RODS AND A COMPARISON WITH BASIC
THEORY AND FRAP CALCULATIONS

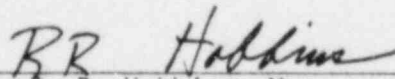
By

R. W. Miller

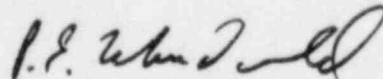
A. D. Appelhans

August 1980

Approved:



R. R. Hobbins, Manager
Program Development and Evaluation Branch



P. E. MacDonald, Manager
Light Water Reactor Fuel Research Division

ABSTRACT

Long term irradiations of instrumented fuel assemblies at the Heavy Boiling Water Reactor in Halden, Norway are being managed by EG&G Idaho, Inc. for the Nuclear Regulatory Commission. One of these instrumented fuel assemblies, IFA-430, was used to study the effects of fuel rod internal gas composition and pressure on fuel thermal behavior.

The fuel rod internal pressure and gas composition were varied, during nuclear operation, in the range 0.1 to 5.1 MPa and 0 to 10% Xe in He and the fuel thermal response measured. The results indicate that current gap conductance theory in general predicts the response of the fuel to changes in the gas composition and pressure and that the FRAP-T fuel behavior computer code calculates fuel temperatures within ~5% of the measured data.

ACKNOWLEDGEMENTS

The experiments reported herein were funded by the U.S. Nuclear Regulatory Commission; the support of that organization is appreciated. The assistance of K. Svanholm, Y. Minagawa, J. Aasgaard, T. Johnson and the rest of the Halden Project Staff is gratefully acknowledged. The reviews of E. Kolstad, D. Lanning, R. Hobbins, P. MacDonald, and L. Siefken are appreciated as is the aid of M. K. Charyulu in running the FRAP code and G. Reilly for data processing.

SUMMARY

The pressure and composition of the fill gas of light water reactor type fuel rods affects the thermal performance of the rods during both steady state and transient operation. As part of the U.S. Nuclear Regulatory Commission's Water Reactor Safety Research Fuel Behavior Program, the Thermal Fuels Behavior Program of EG&G Idaho, Inc., is conducting fuel rod behavior studies in the Heavy Boiling Water Reactor in Halden, Norway. The Instrumented Fuel Assembly-430 (IFA-430) operated in that facility is a multipurpose assembly designed to provide information on the effect of fill gas pressure and composition on fuel thermal performance, the axial gas flow characteristics of fuel rods, cracking and relocation of the fuel pellets, and the release of fission gases.

This report presents an analysis of the effects of fill gas pressure and composition on fuel thermal performance and compares the data with gap conductance models and the Fuel Rod Analysis Program (FRAP) fuel behavior code. The tests and comparison of the data with the FRAP code are intended to confirm the current gap conductance models used in analysis of fuel behavior under normal and accident conditions. The stored energy of the fuel is a controlling factor in the behavior of the fuel rod during accident situations and the gap conductance is the major factor in determining the stored energy in the fuel. The data are unique in that the fuel rod fill gas composition and pressure were varied during actual nuclear operation which removes the uncertainty in rod to rod variation present in typical tests of this type and permits a wide range of pressures and fill gases to be evaluated.

The IFA-430 test assembly contains four, 1.28-m-long fuel rods loaded with 10% enriched UO_2 pellet fuel. The two rods used in the fill gas pressure and composition tests, termed gas flow rods, are each instrumented with a centerline thermocouple and three axially spaced pressure sensors. These two rods have a fabricated diametral gap size of 0.10 mm and 0.23 mm, and are connected to a gas supply system. The other two rods,

prepressurized with 0.48 MPa of He, are not connected to the gas supply system and were not used in the fill gas pressure and composition tests.

The gas flow rods are connected, top and bottom, to a gas supply system which permits the fill gas composition and pressure to be changed while the fuel rods are operating. During the experiments reported herein the fill gas was systematically changed in both pressure and xenon concentration while the rods were operating. The fuel centerline temperatures were measured for fill gas pressures ranging from 0.1 to 5.1 MPa and xenon concentrations from 0 to 10%, at rod linear powers from 5 to 25 kW/m. The fuel had a burnup of ~ 2500 MWd/tUO₂ at the time of the experiments and was in a cracked but stable condition.

As an aid in interpreting the data, gap conductance theory and relationships based upon a concentric solid-pellet model are reviewed and the expected effects of fill gas pressure and composition discussed. The results of the experiments show that, with one exception, the qualitative and quantitative effects of fill gas pressure are adequately predicted by current gap conductance models which include a temperature jump distance term. The exception is for the 0.23 mm gap rod when the xenon concentration is >5% and the pressure above 2.0 MPa; for these conditions the gap conductance appears to continue to increase as the pressure increases above 2.0 MPa, contrary to the model's prediction of essentially constant gap conductance in this pressure range. This behavior, which is present at all power levels and consistently reproducible, is not understood. The qualitative effect of xenon concentration in the fill gas is also adequately predicted by current models. As expected, the quantitative agreement between the simple concentric pellet model (with no cracking or relocation of the fuel pellet) and the data was poor, the model predicting hot gap sizes $\sim 100\%$ greater than determined from the data.

The FRAP-T5 and -T6 (experimental) fuel behavior computer code models for gap conductance are reviewed and the FRAP-calculated fuel temperatures are compared with the test data. With the exception of the case of the

0.23 mm gap rod with 10% Xe at pressures above 2.0 MPa, the FRAP calculated centerline temperature response to varied fill gas pressures and Xe concentrations agree with the data. However, an apparent divergence between the data and FRAP-calculated centerline temperatures as the Xe concentration increases indicates that FRAP should be used with caution at Xe concentrations above 10%.

In general, the results of the experiments support the use of on-line fuel rod fill gas control and fuel-centerline temperature measurement as a viable, in-pile, non-destructive technique for measuring fuel-cladding heat transfer characteristics. Temperature changes resulting from variances in fill gas pressure and composition can be measured with sufficient precision to determine the temperature jump distance effect and measure small changes in fuel cladding gap conductance.

CONTENTS

ABSTRACT	iii
ACKNOWLEDGEMENT	iv
SUMMARY	v
1. INTRODUCTION	1
2. GAP HEAT TRANSFER DISCUSSION	3
2.1 The Influence of Gas Pressure	5
2.2 The Influence of Xenon Concentration	8
3. EXPERIMENT DESCRIPTION	11
3.1 Description of IFA-430	11
3.2 Status of the Fuel	11
3.3 Instruments	15
3.4 Experimental Procedure	15
4. RESULTS	19
4.1 Fuel Temperature as a Function of Power	19
4.2 The Influence of Pressure on Fuel Temperature	19
4.2.1 Form of Pressure Dependence	23
4.2.2 Dependence of Pressure Effects on Power	23
4.2.3 Dependence of Pressure Effects on Gap Width	27
4.2.4 Calculation of Temperature Jump Distance	27
4.3 The Influence of Xenon on Fuel Temperature	32
4.4 Calculation of Gap Width	36
4.5 Comparison with FRAP-T Calculations	39
4.5.1 Xenon Effects	43
4.5.2 Pressure Effects	45
5. CONCLUSIONS	53
6. REFERENCES	56
APPENDIX A - Compilation of Raw Data	58
APPENDIX B - Calculation and Table of T_{std}	66

CONTENTS (cont'd)

APPENDIX C - Discussion of Measurement Errors 67

APPENDIX D - Gas Exchange Procedure 77

APPENDIX E - Design Characteristics of IFA-430. 79

APPENDIX F - Calculation of R 82

1. INTRODUCTION

The U.S. Nuclear Regulatory Commission (NRC) through its contractor, EG&G Idaho Inc., is conducting fuel rod behavior studies in the Heavy Boiling Water Reactor (HBWR) at Halden, Norway as part of the NRC's Water Reactor Safety Research Fuel Behavior Program.¹ This report presents the results of selected experiments conducted using instrumented fuel assembly 430 (IFA-430). IFA-430 was designed to obtain data on (a) fuel rod axial gas flow characteristics, (b) the thermal response of the fuel rods as a function of various internal rod pressures and gas compositions and (c) on the release of fission gases for the purpose of developing and assessing fuel behavior models.

This report presents the results of experiments performed to determine the effects of fuel rod internal pressure and fill gas composition on fuel temperatures; specifically, how the pressure and fill gas composition affect the fuel-cladding gap conductance, and how current models for fuel behavior compare with the data. The tests and the comparison of the data with gap conductance models are intended to confirm the gap conductance models used in analyses of fuel behavior under normal and accident situations. The stored energy of the fuel is a controlling factor in the behavior of fuel rods during loss of coolant type accident situations and the gap conductance strongly influences the stored energy in the fuel.

The IFA-430 test assembly holds four, LWR-type fuel rods. Two rods (Rods 1 and 3), with diametral gap sizes of 0.10 and 0.23 mm, respectively, are pressurized to 0.48 MPa with helium and instrumented with centerline and off-center fuel thermocouples. The other two rods (Rods 2 and 4), termed gas flow rods, each has three axially distributed pressure transducers mounted directly to the cladding, a centerline thermocouple, and each is connected to an external gas supply system that allows the fill gas to be changed during operation. Rods 2 and 4 have the same diametral gap sizes as Rods 1 and 3, respectively.

A four-day sequence of tests was conducted during August of 1979 in which the gas in the gas flow rods was systematically changed from pure helium to 5% and 10% xenon in helium mixtures and the pressure varied from 0.1 to 5.1 MPa. Further tests were conducted in December of 1979 to critically test the experimental method and to obtain data at higher power levels. Preliminary results of these tests have been published.² This report provides extensive presentation and analysis of the data, and, in the appendices, information for modeling IFA-430.

Section 2 of the report provides a discussion of fuel-cladding gap heat transfer theory, using a simple model consisting of a solid pellet concentrically located in the cladding, to review basic gap heat transfer processes. Several relationships useful in interpreting the data are developed and it is shown that the effect of gas pressure on fuel center temperature is a separable effect from gap closure, although dependent upon pellet cracking. Expressions relating fuel centerline temperature changes to fill gas xenon concentration and fill gas pressure are presented.

The experimental procedures and a brief description of IFA-430 instrumentation is provided in Section 3. Results of the experiments together with interpretation of the data are presented in Section 4 along with a comparison of the experimental results with the Fuel Rod Analysis Program³ (FRAP) fuel behavior code calculations.

Conclusions are presented in Section 5 and details of the data, calculations, and the IFA-430 assembly are presented in the appendices.

2. GAP HEAT TRANSFER DISCUSSION

Both the fill gas pressure and the fill gas composition affect the fuel-cladding gap conductance. To assess the expected effect of each on the gap conductance a simple model is applied to the fuel rod. In a simple concentric fuel rod model the temperature drop across the fuel-cladding gap, TG, is related to heat flux by the equation

$$TG = \frac{q}{H_g + H_c} \quad (1)$$

where q is the heat flux (W/m^2), H_g is the gap conductance (W/m^2K) and H_c is the contact conductance. Since the IFA-430 fuel rods do not experience hard pellet-cladding contact, H_c is assumed to be zero. H_g is related to the gas conductivity, k_{gas} (W/mK), by

$$H_g = \frac{k_{gas}}{d + g_1 + g_2} \quad (2)$$

where d is the mechanical radial gap width (m) and g_1 and g_2 are, respectively, the temperature jump distances at the fuel and inside cladding surfaces. The temperature jump distance reflects the imperfect energy transfer between gas and solid molecules at surfaces. First described by Kennard⁴ and later by Lloyd⁵ and Loyalka⁶ as well as others, a generalized expression for g is given by Lanning and Hahn⁷ as

$$g = \frac{C k_{gas} \sqrt{T_{gas}}}{P} F(a_i, m_i, M_i) \text{ meters} \quad (3)$$

where T_{gas} (K) is the mean temperature of the interface gas, and P is the absolute gas pressure. The constant C and the function F , containing the accommodation coefficients a_i , mole fraction m_i and gram molecular weights, M_i , of each gas present in the gap, differ among authors and

have been summarized recently by Garnier and Begej.⁸ In the Lloyd model, the constant C takes on the value

$$C = 6.86 \times 10^{-3} \quad (4)$$

when F is defined, for a mixed gas, as

$$\bar{r} = \frac{1}{\sum_i \frac{a_i m_i}{M_i}} \quad (5)$$

For helium and xenon the accommodation coefficients can be expressed^{7,9} as

$$a_{\text{He}} = 0.425 - (2.3 \times 10^{-4})T_{\text{gas}} \quad (6)$$

$$a_{\text{Xe}} = 0.749 - (2.5 \times 10^{-4})T_{\text{gas}} \quad (7)$$

It has been proposed⁷ that the average gap gas temperature

$$T' = \frac{(T_{\text{fuel surface}} + T_{\text{clad surface}})}{2} \quad (8)$$

be used in Equations (3), (6), and (7) to obtain an average temperature jump distance, \bar{g} . With $H_C = 0$, Equation (1) then becomes

$$TG = \frac{q(d + g_1 + g_2)}{k_{\text{gas}}} = \frac{qd}{k_{\text{gas}}} + \frac{q \ 2\bar{g}}{k_{\text{gas}}} \quad (9)$$

Inserting Equation (3) into Equation (9) results in:

$$TG = \frac{qd}{k_{\text{gas}}} + 2qCF \left(\frac{\sqrt{T'}}{p} \right) \quad (10)$$

where the terms on the right hand side of Equations (9) and (10) represent the conventional temperature gradient across the gap, and combined temperature jump of the two surfaces, respectively. Note that it is only in the temperature jump term that the pressure occurs explicitly.

In a helium-xenon mixture at a typical fill gas operating temperature ($T_g = 600$ K), the combined jump distance for UO_2 and zircaloy, $2\bar{g}$, at 0.1 MPa varies from a pure helium value of about 0.006 mm down to about 0.004 mm for a mixture of 10% xenon. It might be concluded from such small values that for the two fuel rods in this study (with 0.05 and 0.12 mm fabricated radial gaps) the contribution of the second term in Equations (9) and (10) would be quite small. However, since both rods are known to have experienced considerable cracking and relocation in which the pellet fragments are much closer to the cladding and in contact with it in many places the temperature jump distances may have a significant effect on the total gap conductance.

2.1 The Influence of Gas Pressure

The fact that the pressure occurs only in the second term of Equation (10), suggests that the temperature jump expression can be evaluated by performing an experiment in which a fuel rod is maintained at constant power as the internal gas pressure is changed. The change in gap temperature drop from a standard pressure, P_0 , to any other pressure, P , will be

$$\Delta TG = TG_P - TG_{P_0} \quad (11)$$

$$= -2qCF \left[\frac{\sqrt{T'_0}}{P_0} - \frac{\sqrt{T'}}{P} \right] \quad (12)$$

where T'_0 and T' are the mean gap gas temperature at the two pressures. However, the root mean gap gas temperature changes by less than two percent due to pressurization for $P \leq 50 P_0$, thus

$$\sqrt{T'_0} = \sqrt{T'} \quad (13)$$

(for constant power) and Equation (12) becomes

$$\Delta TG = -2qCF \frac{\sqrt{T'_0}}{P_0} \left(1 - \frac{P_0}{P}\right) . \quad (14)$$

In IFA-430, thermocouples measure centerline fuel temperatures, TC, rather than gap temperature drop, TG, so that the relationship of these separate quantities must be introduced into Equation (14). From the concentric solid-pellet conduction equation:¹⁰

$$qF = \frac{2}{r_0} TS \int^{TC} k dT \quad (15)$$

(where r_0 is pellet radius, TS and TC are surface and centerline temperatures and F is the neutron flux depression factor). At constant power, a change in T_S must be offset by a change in TC to keep the conductivity integral, $I = \int k dT$, constant, that is,

$$\Delta TS \frac{dI}{dT_S} = \Delta TC \frac{dI}{dT_C} \quad (16)$$

Thus, the desired ratio between the fuel centerline and surface temperature changes, the transfer ratio, R, is

$$R = \frac{\Delta TC}{\Delta TS} = \frac{dI/dT_S}{dI/dT_C} = \frac{(k)_{TS}}{(k)_{TC}} \quad (17)$$

or, just the ratio of fuel conductivities at the two points. Finally, since the cladding inside temperature is independent of gap conductance, it follows that

$$\frac{\Delta TC}{\Delta TG} = \frac{\Delta TC}{\Delta TS} = R \quad (18)$$

and Equation (14) takes the form:

$$(\Delta TC)_q = -2RqCF \frac{\sqrt{T'_0}}{P_0} \left(1 - \frac{P_0}{P}\right) \quad (19)$$

or

$$(\Delta TC)_q = \frac{-Rq}{k_g} (2\bar{g})_0 \left(1 - \frac{P_0}{P}\right) \quad (20)$$

describing the dependence of fuel centerline temperature on pressure in an experiment in which power and fill gas composition are held invariant. From Equation (19) and its development the following is expected for temperature decrement data from variable pressure experiments:

1. The temperature decrement, $(\Delta TC)_q$, should follow the inverse-P relationship, $1 - (P_0/P)$ approaching a maximum as P becomes much greater than P_0 ;
2. The temperature decrement should be proportional to power (when adjusted by R) although a small deviation from proportionality can exist due to the $\sqrt{T'_0}$ term, which is weakly dependent upon power;
3. In experiments in which power is constant but gas composition is changed, the temperature decrement should change only in relation to the function F;

4. Temperature decrements should be independent of gap width since the gap width term, d , drops out when temperature differences are computed, although a small dependence on gap size remains in the $\sqrt{T'_0}$ term.
5. If values of R are available, Equation (20) indicates that an experimental measure of the combined temperature jump distance at any pressure, P , can be obtained by measuring the decrement at a higher pressure, P' , where $P' > P$.

2.2 The Influence of Xenon Concentration

Unlike the pressure term in Equation (10) which could be easily separated from the (unmeasurable) gap width and studied directly, xenon concentration is linked with the physical gap through its influence on the gas conductivity. Temperature drop in the gap, and fuel centerline temperature, T_C , are directly affected by the fuel-cladding gap size and, therefore, by any physical process affecting the gap, i.e. the gap gas composition.

The concentric, solid pellet model used to develop Equation (19) predicts nearly direct proportionality between fuel centerline temperatures and gas conductivity, deviating from this dependence only for gap widths that are of the same magnitude as the combined jump distance. The model, however, ignores many effects such as fuel cracking and relocation which can, at the same time, increase the jump distance effect and reduce the gap size effect. If one assumes, for instance, that a circumferential crack occurs immediately inside the pellet surface, then two pairs of solid-gas interfaces exist and the second term of Equation (10) is doubled. If the crack forms closer to the pellet center, the importance of the crack declines in direct proportion to the fractional power produced internal to the crack location. For a multitude of such cracks, the second term of Equation (10) would have to be multiplied by

$$(1 + \sum_i^n h_i)$$

where n is the total number of cracks and h_i is the fractional power remaining inside the crack. Further minor corrections would be required to account for the mean gas temperature and, possibly, surface properties of each crack.

The relative importance of gap size to the gap conductance is also affected by cracks. Cracks generally result in the original gap being redistributed inside the pellet where less heat flow is involved. It is apparent, then, that the present experimental measurements with different xenon concentrations cannot, with any confidence, be expected to compare well, in absolute terms, with solid pellet model predictions. In addition, eccentricity of the fuel pellets within the cladding can significantly affect the xenon-temperature relationship and this is also unaccounted for in the concentric pellet model. However, the solid, concentric pellet model can provide an estimate of the significant effects of Xe on the fuel temperature and identify trends. Combining Equations (9) and (18), the change in centerline temperature, ΔTC , from a pure helium fill gas to a fill gas with a xenon fraction, x , is

$$\Delta TC = R \left[TG_x - TG_{He} \right] \quad (21)$$

$$= Rq \left[\frac{d + 2\bar{g}_x}{k_x} - \frac{d + 2\bar{g}_{He}}{k_{He}} \right] \quad (22)$$

For the limited range of x in this study ($0 < x < 0.1$), gas conductivity can be approximated (to within 99% of the true value) by

$$k_x = k_{He} (1 - 3x), \quad (0 < x < 0.1). \quad (23)$$

Recalling the definition of \bar{g} and its components, Equations (3) to (7), Equation (22) becomes:

$$\Delta TC = Rq \left[\left(\frac{3x}{1-3x} \right) \frac{d}{k_{He}} - \frac{2C}{P} \left(\sqrt{T'_x} F_x - \sqrt{T'_{He}} F_{He} \right) \right] \quad (24)$$

where subscripts indicate values for xenon or helium. Applying estimates of T' and calculated F 's which are applicable to the present experiments, Equation (24) becomes:

$$\Delta TC \approx Rq \left[\left(\frac{3x}{1-3x} \right) \frac{d}{k_{He}} - \frac{2.25x}{P} \right], \quad (0 < x < 0.1) \quad (25)$$

Thus, using the simple model, Equation (25) predicts nearly linear increases in ΔTC proportional to physical gap size, less a small xenon effect from the temperature jump terms.

3. EXPERIMENT DESCRIPTION

The IFA-430 design, instrumentation and the experimental procedure used during the tests are presented in the following sections.

3.1 Description of IFA-430

IFA-430, shown schematically in Figure 1, contains four full length (1.28-m) fuel rods with 10% enriched conventional pellet fuel. Two of the rods, termed thermocouple rods and shown in Figure 2, are equipped with two centerline thermocouples and three off-center thermocouples each and are pressurized to 0.48 MPa with helium. The other two rods, termed gas flow rods and shown in Figure 3, in addition to having a fuel centerline thermocouple each have three pressure transducers mounted directly to the cladding to measure internal gas pressure. The gas flow rods are connected, top and bottom, to a gas supply system, shown in Figures 4 and 5, which can impose steady or pulsed gas pressures in the top plenum to drive gas axially through each rod. The gas system is capable of providing pressures from 0.1 to 15 MPa as well as introducing new gases and gas mixtures. Valves located within the assembly permit selection of either gas flow rod for gas flow experimentation. The two gas flow rods differ in design only in the fabricated gap size. Rod 2 has a diametral gap size of 0.23 mm, Rod 1 a gap size of 0.10 mm. The two different gap sizes allow gap-size effects to be studied by comparing the thermal behavior of the two rods. Downstream gas lines are monitored, either by batch process or by continuous gamma spectrometry, for identification of radioactive fission products. Additional characteristics of the IFA-430 experiment are listed in Appendix E, and a complete description has been published.¹¹

3.2 Status of the Fuel

At the time the first gas exchange experiments were conducted, all four fuel rods had reached burnups of about 3500 MWd/t UO₂. Average power levels during this burnup were below about 26 kW/m and axial peak powers were less than about 31 kW/m. Peak fuel centerline temperatures have been below 1700 K; thus no fuel restructuring is expected. Some cracking and relocation of the fuel was observed¹¹ during the first few

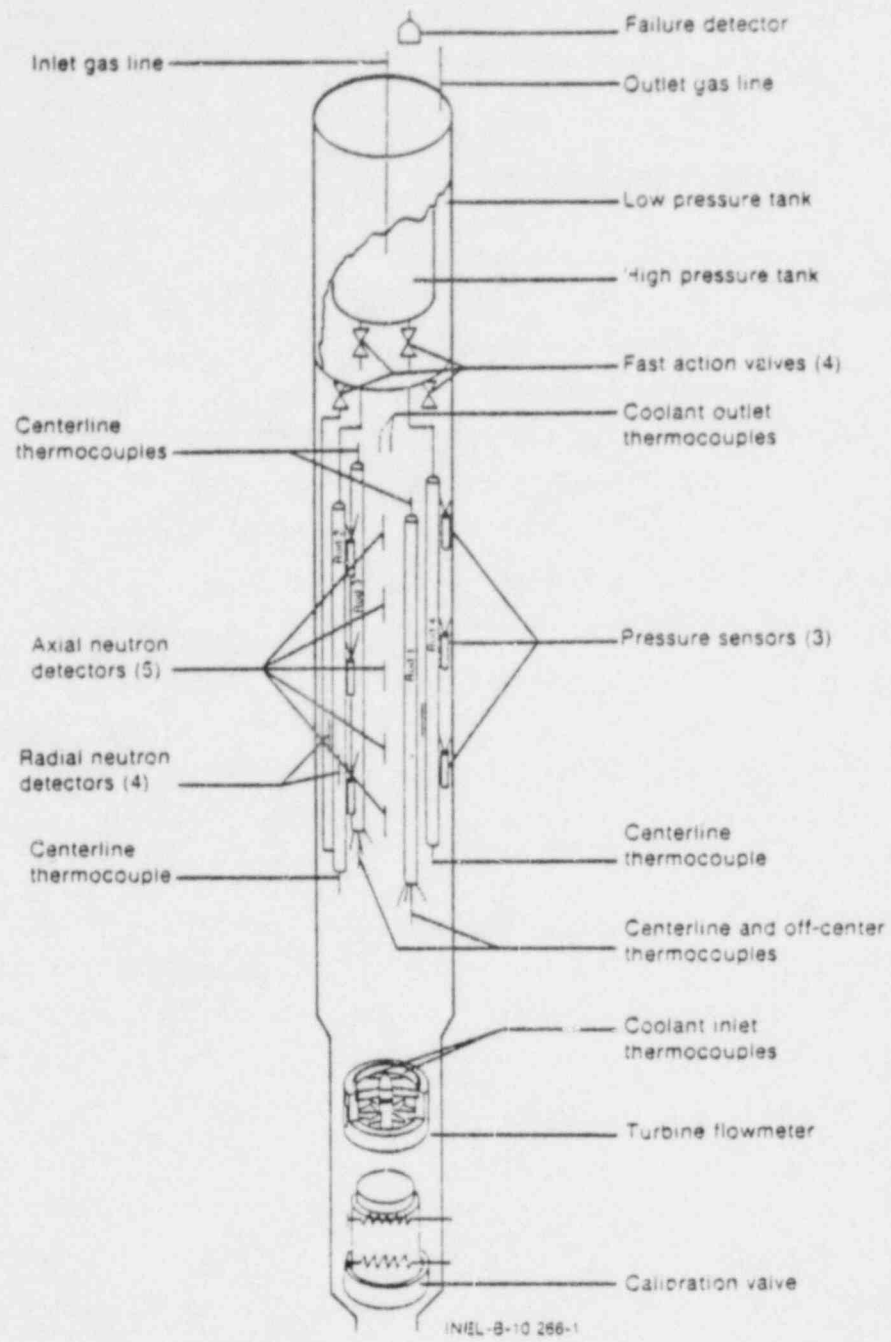


Fig. 1 Schematic of IFA 430 assembly.

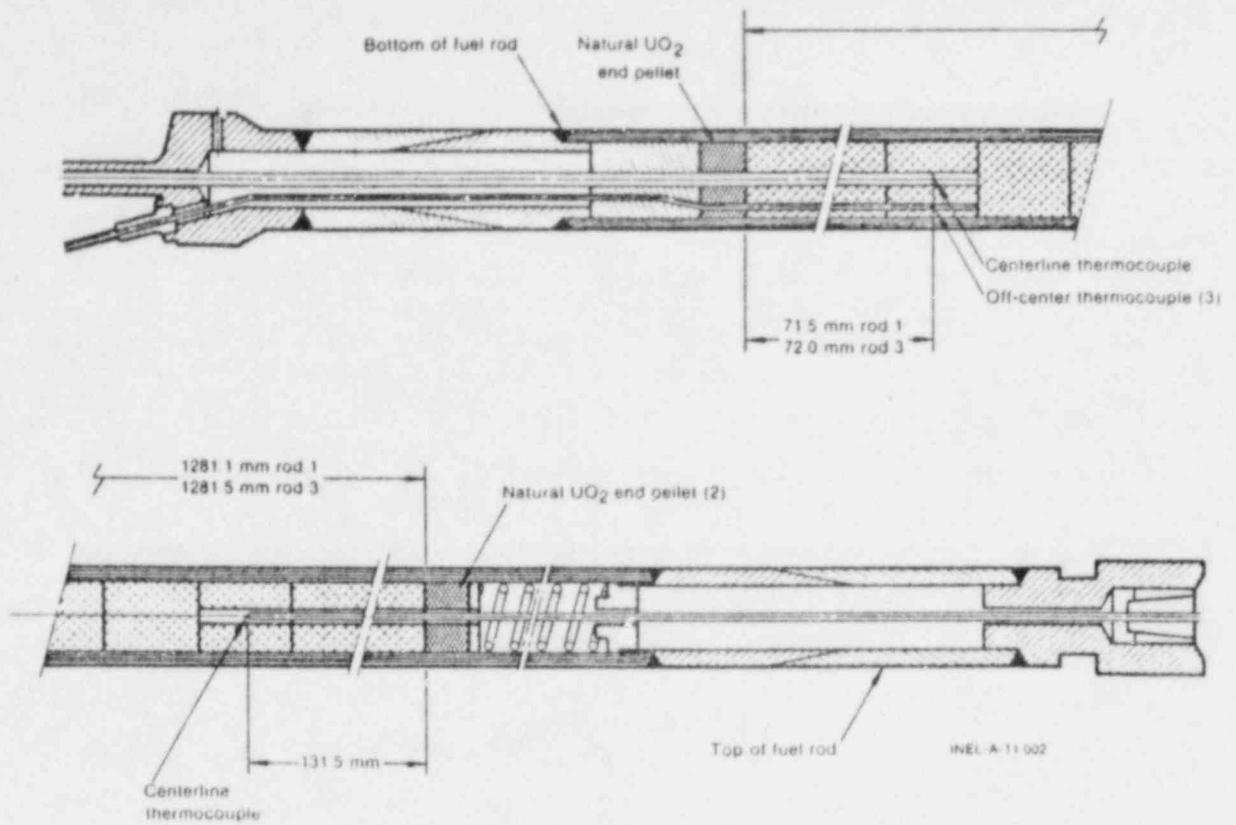


Fig. 2 Features of the two sealed, thermal performance fuel rods, rods 1 and 3.

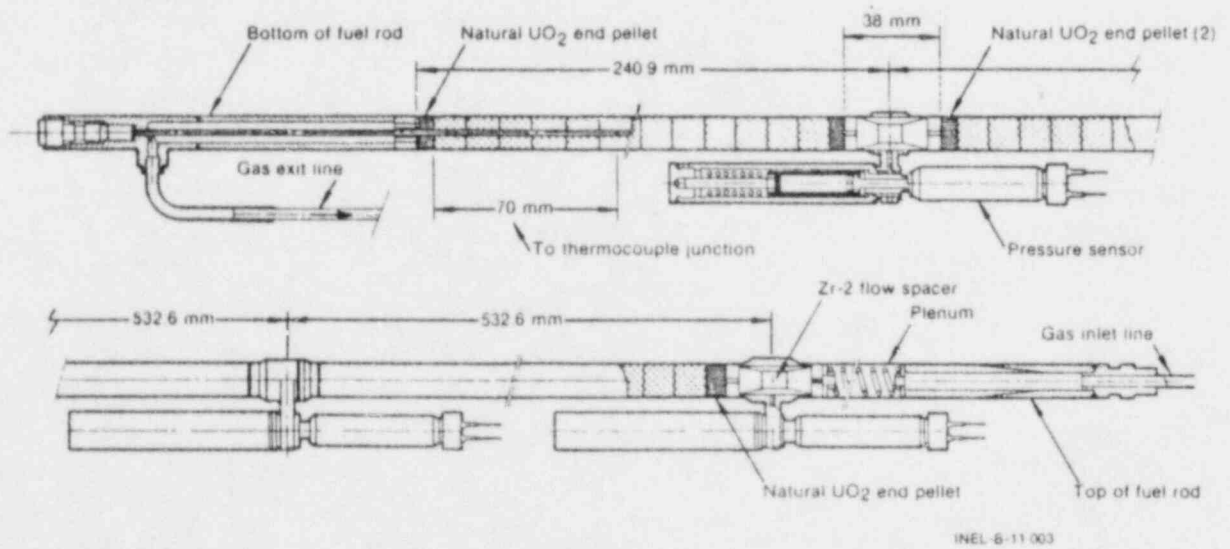


Fig. 3 Features of the two gas flow fuel rods, rods 2 and 4.

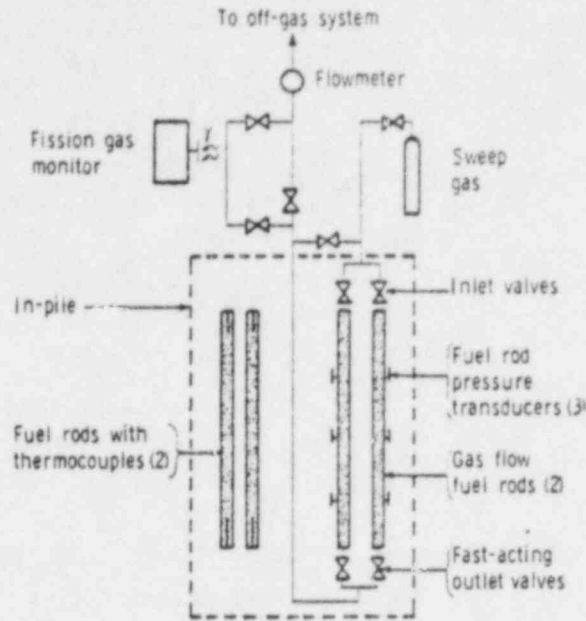


Fig. 4 Simplified schematic of in core fuel rod sweep gas system.

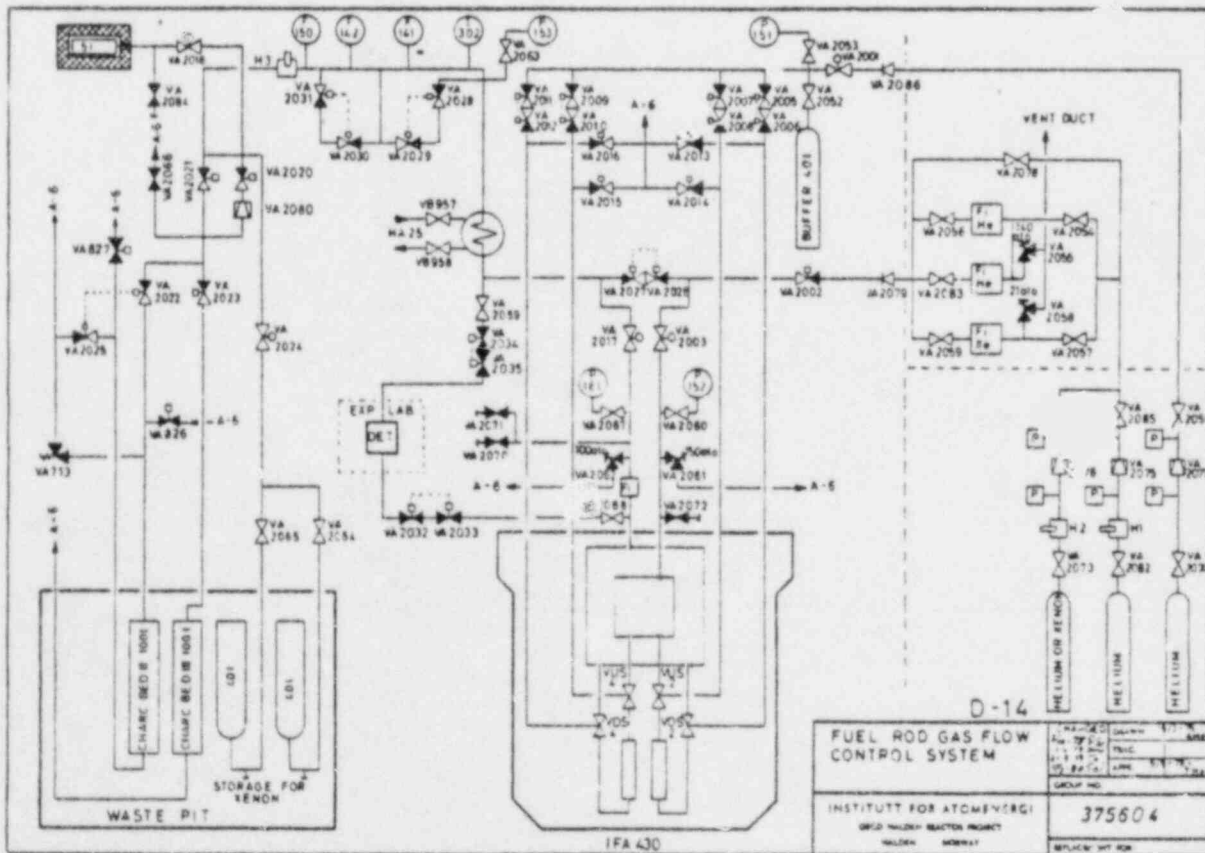


Fig. 5 IFA-430 gas supply system.

ramps to full power but these processes slowed or stopped during subsequent ramps so that at the time of the present tests, the fuel was quite stable.

3.3 Instruments

The principal objective of the tests reported here was to establish the temperature response of the fuel in each of the gas flow fuel rods as a function of fill gas pressure and xenon content. The fuel centerline temperatures were measured with a W3%Re thermocouple (TF-3) in the 0.23 mm gap rod (Rod 2) and by a W5%Re thermocouple (TF-6) in the 0.10 mm gap rod (Rod 4).

Power at each thermocouple position was measured indirectly using an array of nine self-powered neutron detectors which were calibrated calorimetrically.¹¹

Pressure of the gas was measured with pressure transducer P-152, shown in Figure 5, which is a Foxboro Bourdon tube type with a range from 0.1 to 15 MPa.

A discussion of error for each of the instruments and for the data system is contained in Appendix C.

3.4 Experimental Procedure

The tests were conducted as a series of staircase power changes with gas pressure being adjusted in a stepwise fashion through the complete 0.1 to 5.1 MPa range at each power level. At the completion of a power staircase, the fill gas was exchanged and another power staircase initiated. Figure 6 illustrates the complete sequence of test steps as conducted during the period 14-17 August, 1979. Additional data were taken in December 1979 at a higher power level to augment the 10% Xenon data base.

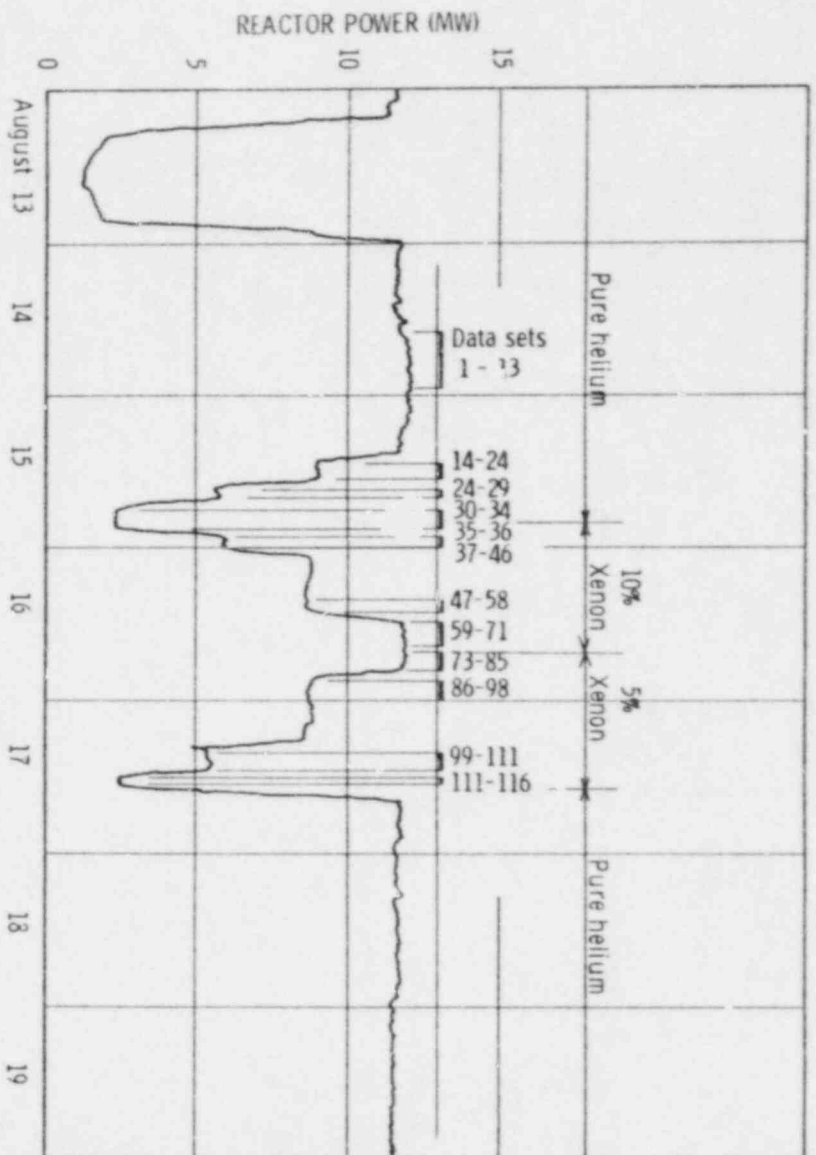


Fig. 6 Reactor power schedule during xenon and pressure tests on IFA 430, August '79

A data set of usually 10 or more temperatures with associated rod powers for each of the two rods was recorded over a period of about 10 minutes, for each pressure.

At each power level, reactor control was placed in servo-mode to hold power as constant as possible. After the gas pressures were established, the temperatures were allowed to fully stabilize (usually about 10 minutes) before the temperature data were recorded. The data system recorded all variables each 40 to 60 seconds. The data sets were averaged to remove noise arising from low-level randomness of reactor flux levels, and in this way were condensed to pairs of single temperatures and powers for each rod together with the standard deviation of each data set. In August, 1979, 116 sets of data were taken for each thermocouple followed in December by 13 more sets representing a total of approximately 2800 individual temperature-power pairs.

Pressure, as measured by the P-152 sensor, was recorded manually from a digital voltmeter at each pressure level and later converted to pressure (see Appendix C). All sequences of pressure data begin with the highest pressure (5.1 MPa) proceeding in a stepwise fashion down to atmospheric pressure (0.1 MPa). As each pressure level was reached, the vent valves (2020 and 2021 in Figure 5) were closed and the fuel rod and gas system were allowed to come to pressure equilibrium as evidenced by stability of pressure measured by P-152.

As shown in Figure 6, the first experiments were conducted with 100% helium fill gas in order to establish the control or reference data and to gain experience with the procedures before xenon gases were introduced. After accumulation of 34 data sets for each fuel rod from four pressure runs over four power levels, the gas was exchanged to 10% xenon - 90% helium and a similar series of tests performed. Finally, the 10% xenon gas

was removed and replaced with 5% xenon - 95% helium for the third power series. This involves sweeping ~ 20 L of exchange gas through each rod and pressurizing to ~ 5 MPa to ensure that the exchange gas penetrates the cracks in the fuel and is better than 99% of the desired concentration. Complete details of the gas exchange procedure are given in Appendix D.

4. RESULTS

As an overview of the results, temperature-power data sets acquired during the experiments are shown in Figures 7 and 8. The data points have been connected by faired curves; the mean power levels and standard deviations of the power are listed to the right of each curve. The effect of the addition of xenon to the fill gas is to cause higher fuel temperatures and is clearly apparent in both rods with the larger effect being in the wide-gap rod, as expected. The effect of increasing pressure is also apparent, causing a reduction of temperature as the pressure is increased from 0.1 to ~2.0 MPa and a slight rise in temperature as pressure increases from ~2.0 to 5.0 MPa, with the exception of the 0.23 mm gap rod with 10% Xe fill gas. Both the pressure and xenon effects are examined in greater detail in the following sections. A listing of all the data shown in Figures 7 and 8 is located in Appendix A.

4.1 Fuel Temperature as a Function of Power

Figures 9, 10 and 11, show the temperature-power relationship for each rod for 100% helium, 5% xenon and 10% xenon respectively, for the two extremes of pressure studied, viz., 0.1 and 5.1 MPa. The lines are linear regression straight line fits utilizing the zero power temperature of 508 K (moderator temperature at the time of these tests) as an additional data point. The data correlate to straight lines extremely well except for the December 1979 data which lie slightly above the line in some instances. The linearity of the temperature-power data allowed the data pairs to be interpolated to uniform power levels of 5, 10, 15, 20 and 25 kW/m for ease of presentation and analysis. Unavoidable variance of the reactor power (usually less than 1%) and slight differences in power from Rod 2 to Rod 4 were eliminated in this way. The interpolated data, together with the interpolation method, are presented in Appendix A.

4.2 The Influence of Pressure on Fuel Temperature

The effect of pressure on temperature can best be examined by measuring the temperature change (temperature decrement) from some

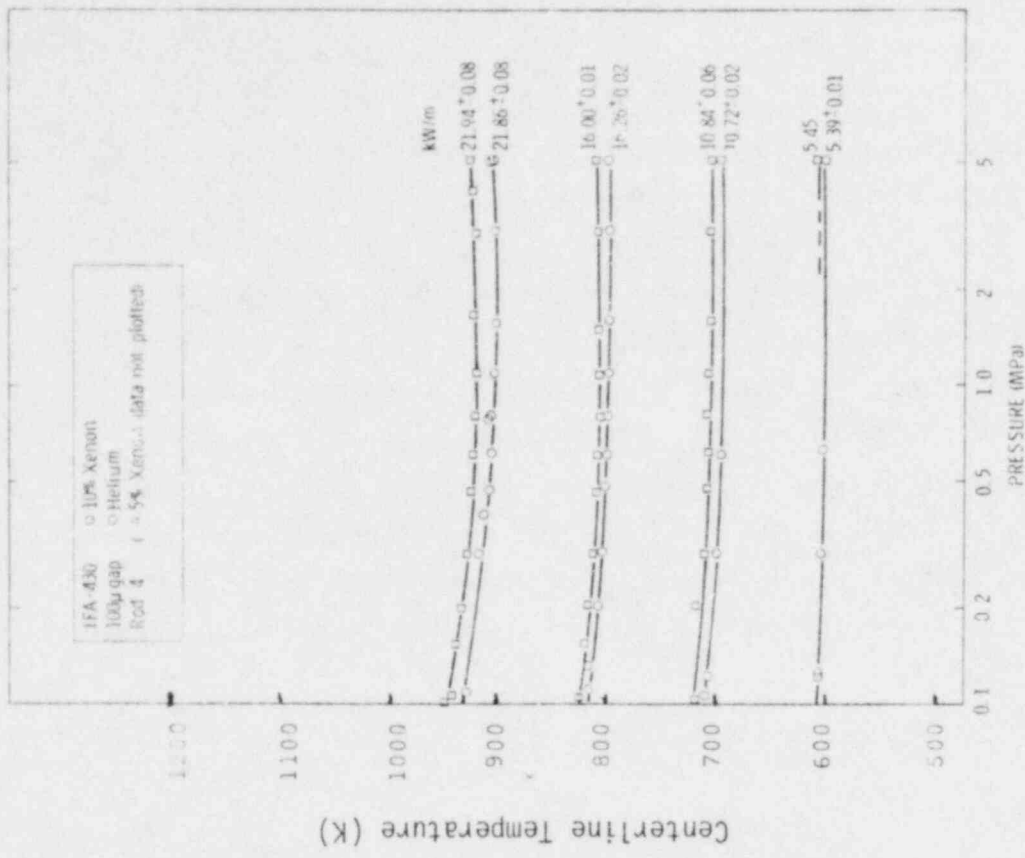


Fig. 8 Summary of rod 4 fuel centerline temperature data as a function of gas pressure. Linear power at the thermocouple position is listed for each data set.

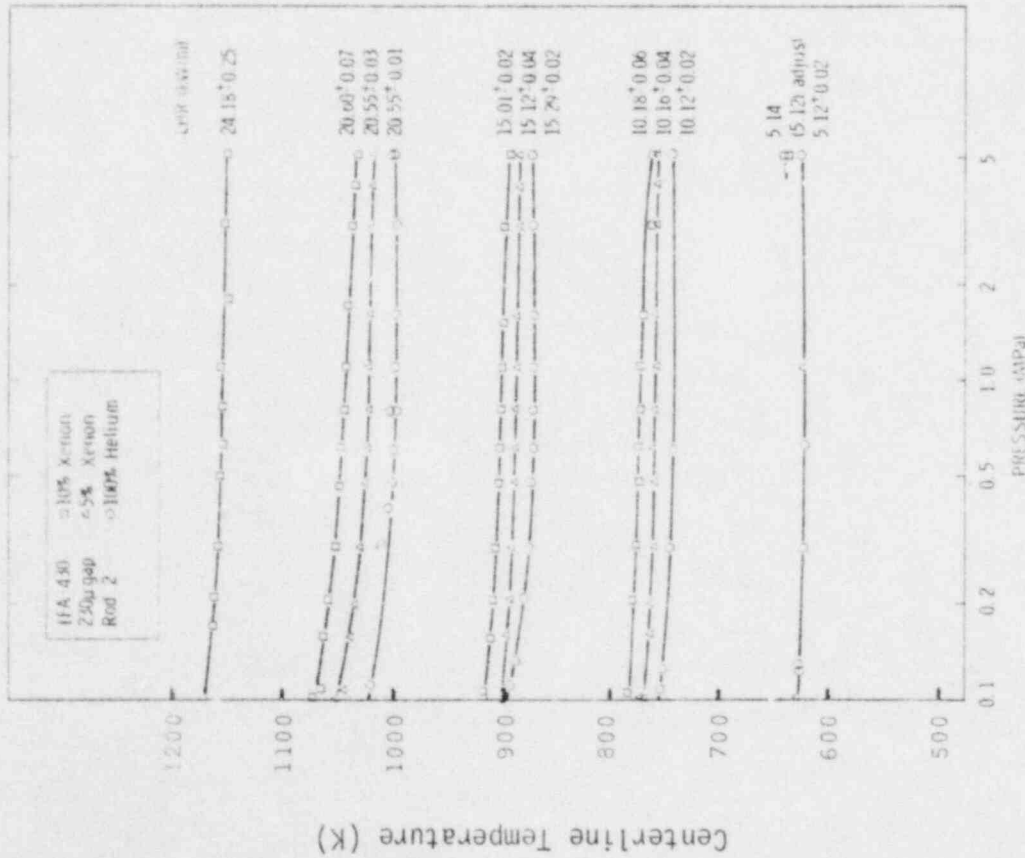


Fig. 7 Summary of rod 2 fuel centerline temperature data as a function of gas pressure. Linear power at the thermocouple position is listed for each data set.

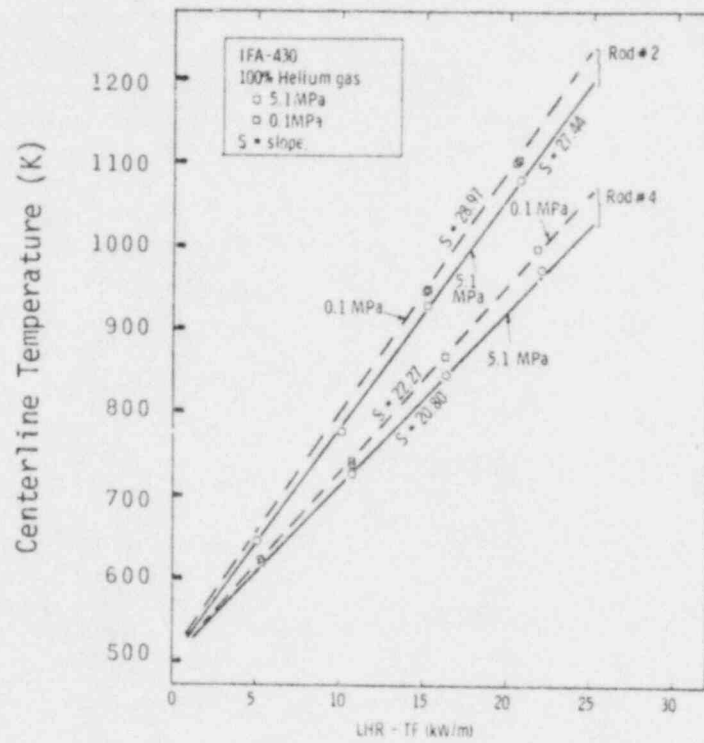


Fig. 9 Fuel centerline temperature as a function of linear power at the thermocouple position, rod 2 and rod 4, 0.1 and 5.1 MPa pressure, helium gas.

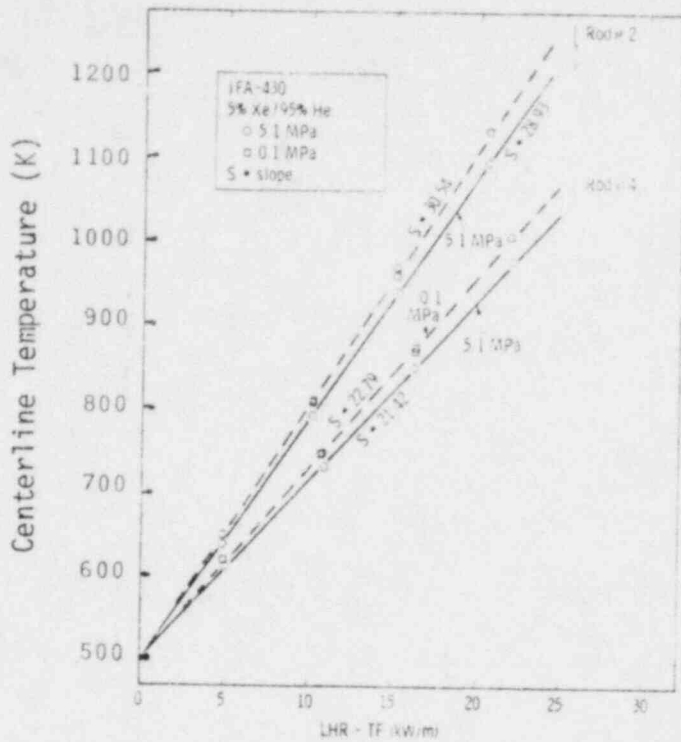


Fig. 10 Fuel centerline temperature as a function of linear power at the thermocouple position, rod 2 and rod 4, 0.1 and 5.1 MPa pressure, 5% xenon gas.

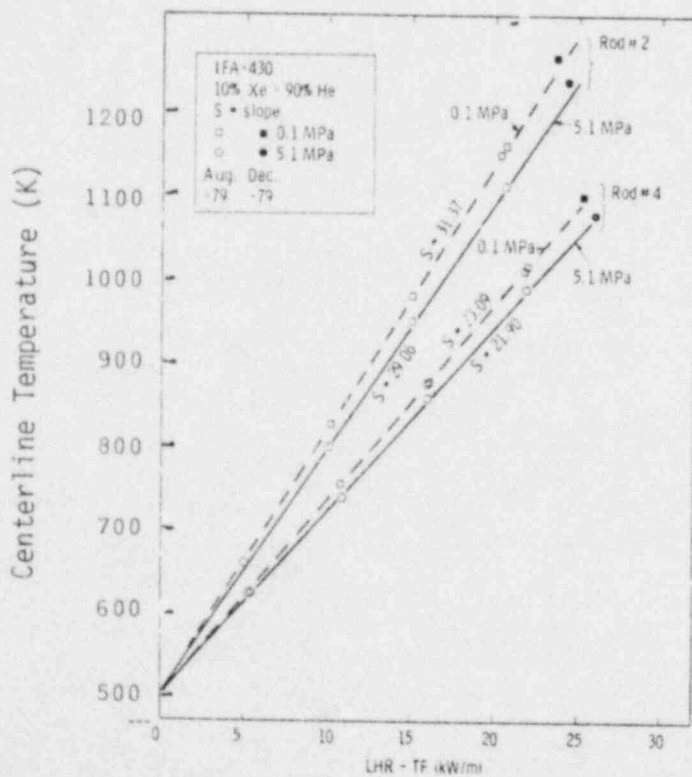


Fig. 11 Fuel centerline temperature as a function of linear power at the thermocouple position, rod 2 and rod 4, 0.1 and 5.1 MPa pressure, 10% xenon gas.

reference level as pressure is increased. In the present work, the temperature reference, T_{std} was determined for each combination of fuel rod, gas type and power level by extrapolation of the data to a standard gauge pressure level corresponding to 0.1 MPa. The T_{std} values for each pressure run are shown in Appendix B and the calculated temperature decrements are listed in Appendix A and plotted in Figures 12 through 17.

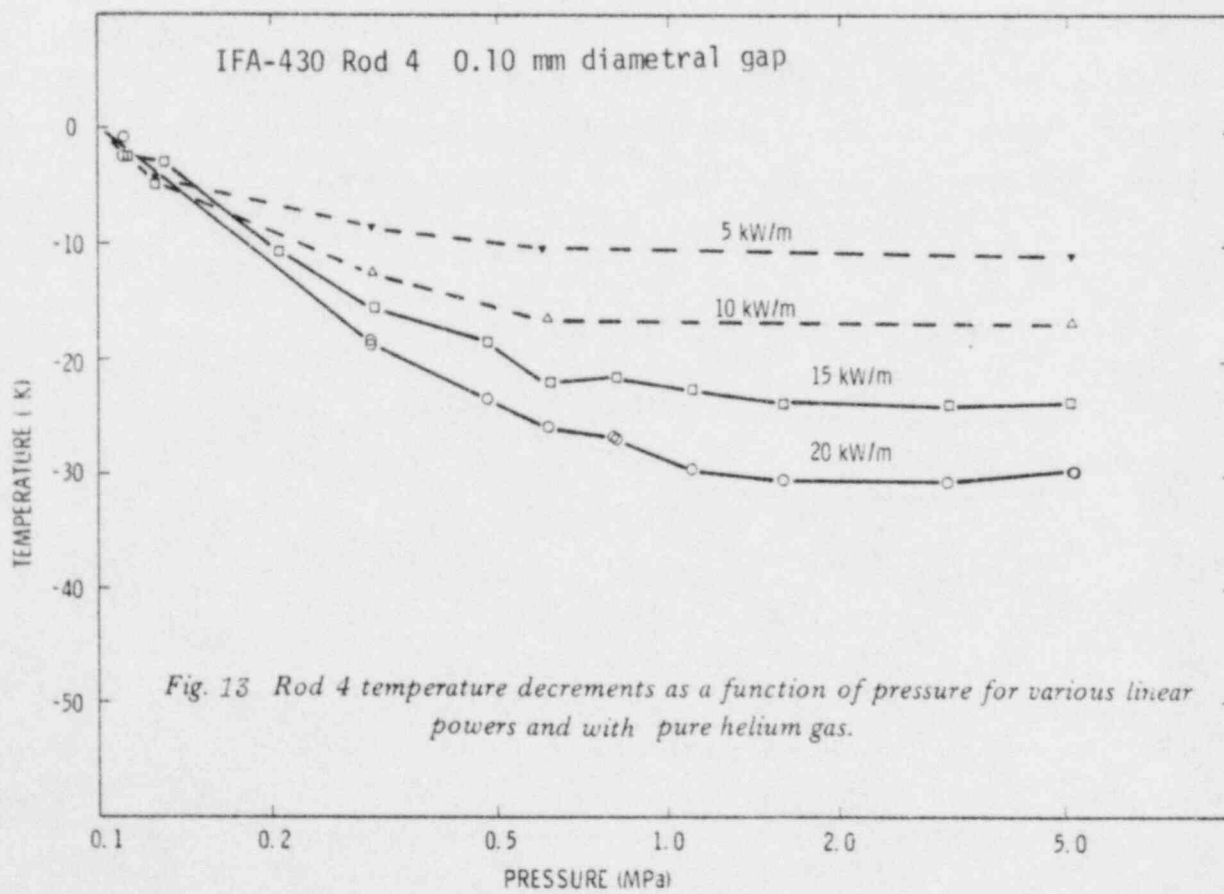
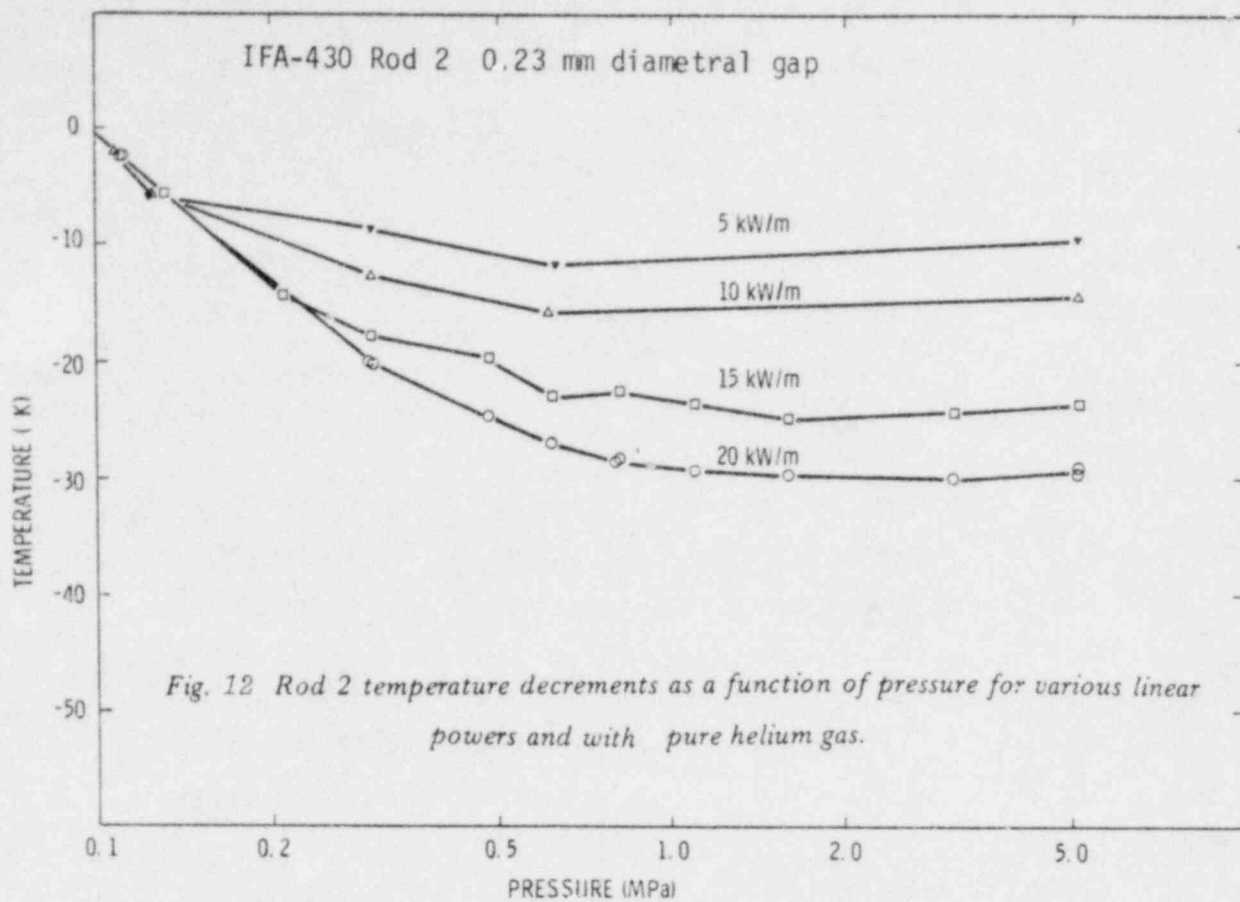
4.2.1 Form of Pressure Dependence

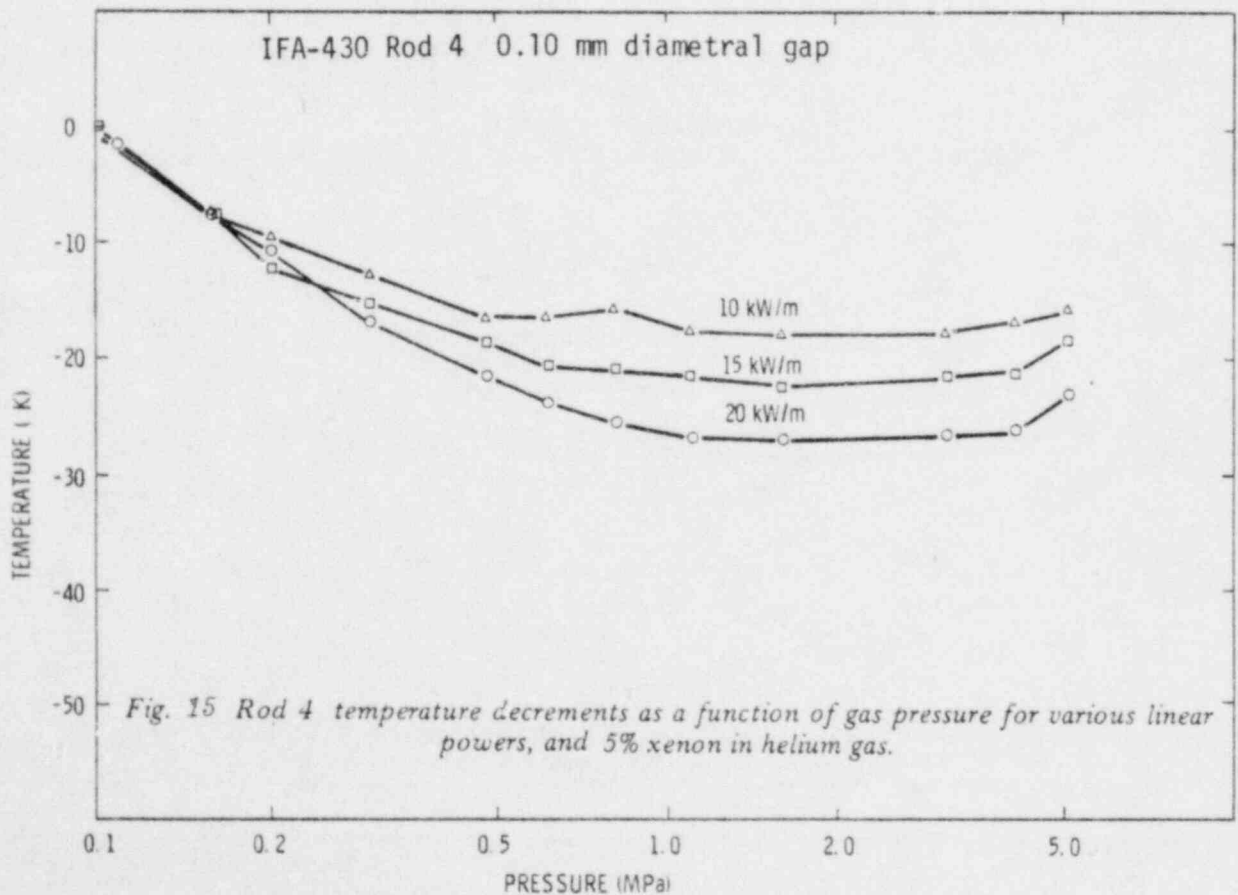
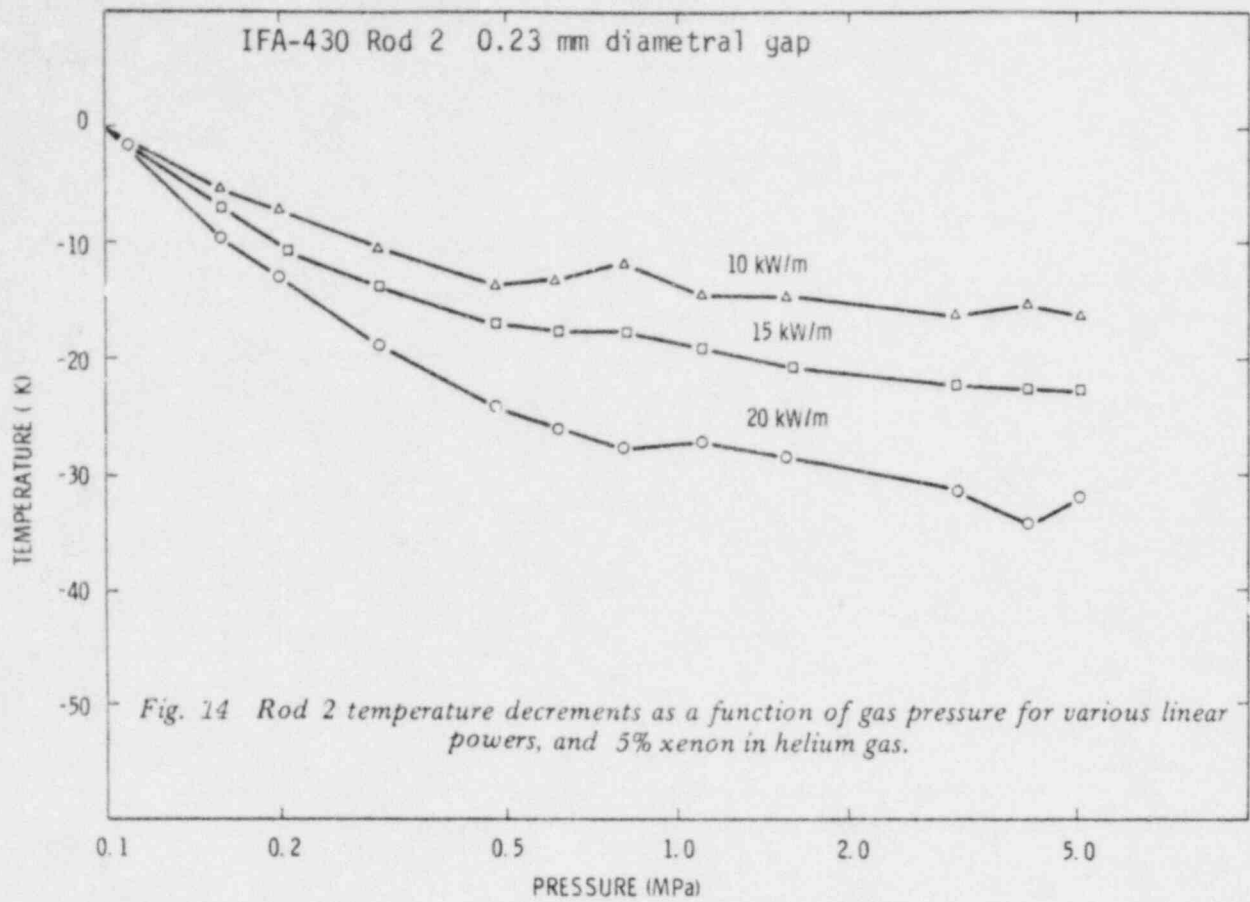
All of the pressure data support the general form of the temperature jump model which predicts that $\Delta TC \propto (1 - P_0/P)$. With pure helium, the data, Figures 12 and 13, show that temperature decrements decrease rapidly (the change becomes more negative) as the pressure is increased from 0.1 to 1.0 MPa, and above 1.0 MPa exhibit only a slight change. The slight upward curvature seen in the data in the 1.0 to 5.0 MPa range is a result of expansion of the cladding due to the increased pressure and subsequent increased gap width resulting in lower gap conductance. Figures 14 and 15 show the same fuel temperature versus rod internal pressure behavior with 5% xenon gas but with slight changes in fuel temperature at high pressures which are not predicted. Lower temperatures were measured in Rod 2 when the pressure was varied between 2 and 5 MPa whereas Rod 4 data show the opposite trend. When Rod 2 was filled with 10% xenon gas, unexpected changes in fuel temperatures at high pressure were again observed but with greater experimental significance, as shown in Figures 16 and 17.

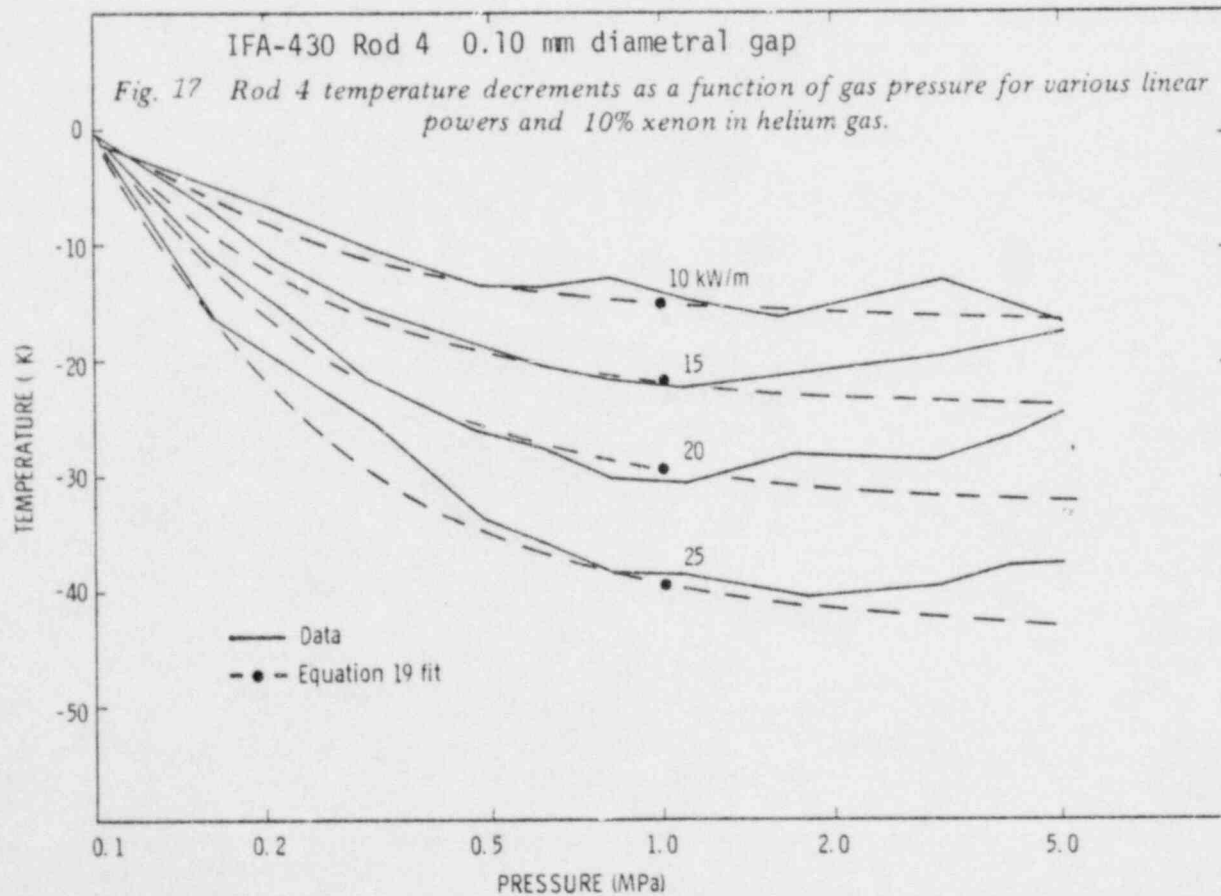
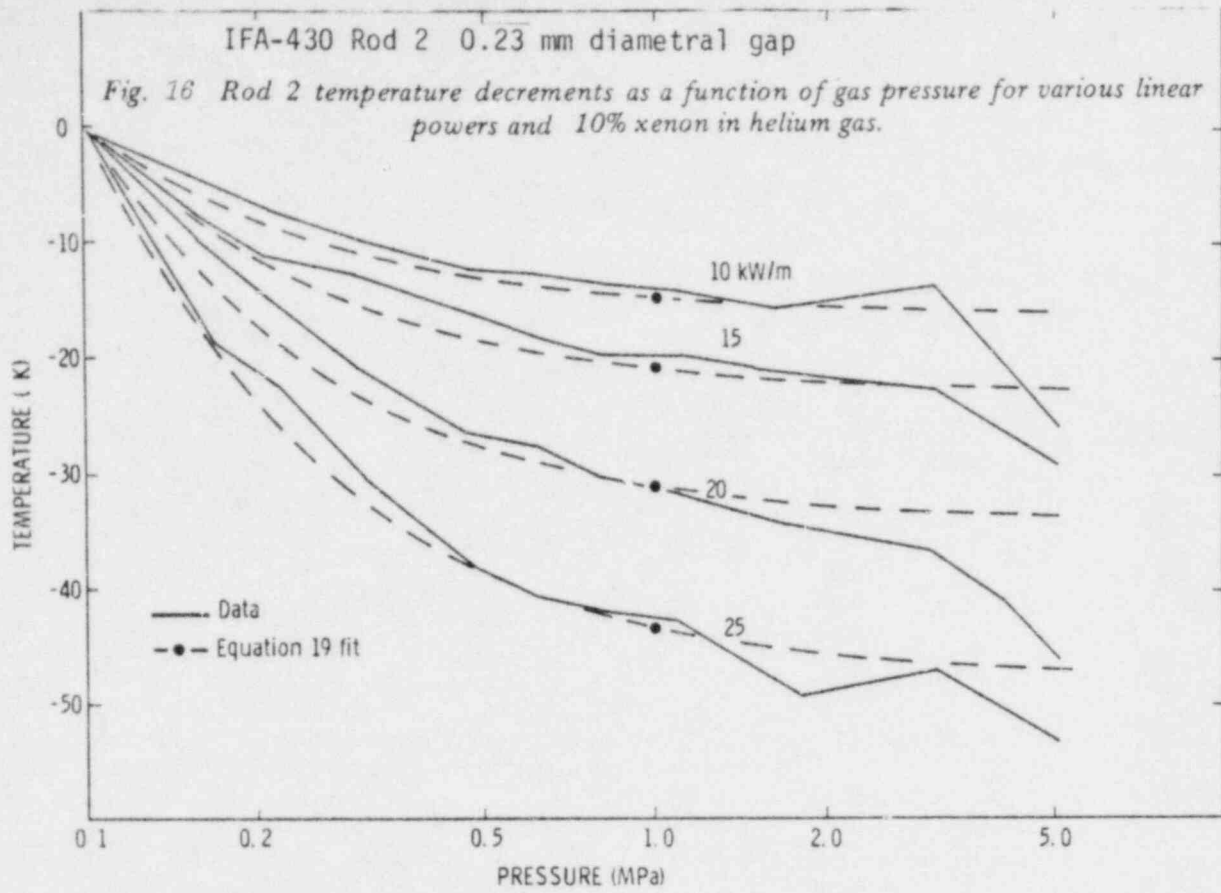
The calculated pressure response using Equation (19) normalized to a good fit with the data at ~ 1.0 MPa is shown in Figures 16 and 17. At pressures below about 2 MPa the data follow the calculated response within experimental error; at pressures above 2 MPa the data and calculated response differ significantly.

4.2.2 Dependence of Pressure Effects on Power

The temperature jump model predicts that for all combinations of gases, gap size and pressure, the gap temperature drop, $\Delta TG = \Delta TC/R$,







should be proportional to power. The temperature decrements at $P = 1.0$ MPa are tabulated in columns 2, 3 and 4 of Table 1 for each fuel rod. These data are averaged (column 5), divided by R (column 6), and the results plotted in Figure 18, where the expected proportionality between the gap temperature drop and power is shown.

4.2.3 Dependence of Pressure Affects on Gap Width

Equation (19) predicts that gap width should have only a very weak influence on mean gas temperature (appearing as $T^{1/2}$). To test this prediction, pressure decrement data for 0.10 mm and 0.23 mm gap rods are plotted together in Figure 19. Note that for helium the decrements for the two rods are very close. With 5% and 10% xenon, Figure 19 shows that from atmospheric pressure (0.1 MPa) up to about 2.0 MPa, data from both rods also lie together, within experimental error. However, at pressures above 2.0 MPa, the differing trends for lower temperatures in Rod 2 and higher temperatures in Rod 4 imply a possible gap dependence which is not understood.

4.2.4 Calculation of Temperature Jump Distance

Since the data support the temperature jump model, it appears that the data could be used to calculate absolute temperature jump distance. Equation (20) indicates that $2\bar{g}$ could be calculated if the center-to-surface temperature derivative, R , is known [Equation 17]. Estimates of R , described in Appendix F together with a discussion of error, are shown in Figure 20. Temperature decrements for pure helium experiments were taken from Figures 12 and 13 at the maximum pressure (~ 5.0 MPa). Helium data are used because they do not display the unpredicted trends at high pressures seen for both the 5% and 10% xenon data. Helium thermal conductivities were computed using the MATPRO¹² equation

$$k_{\text{He}} = (3.366 \times 10^{-3}) T^{0.668} \text{ W/mK}, \quad (26)$$

TABLE 1. TEMPERATURE DECREMENT DATA AT P = 1.0 MP^a

<u>Linear Power</u> <u>kW/m</u>	<u>Rod 2 Decrement, (K)</u>				<u>Average</u>	<u>Average/R</u>
	<u>Helium</u>	<u>5%Xe</u>	<u>10%Xe</u>			
5	6.5	-	-	6.5	6.1	
10	15.5	14.0	14.5	14.7	12.6	
15	23.5	19.0	20.0	20.8	16.6	
20	29.0	28.5	31	29.5	29.7	

	<u>Rod 4 Decrement, (K)</u>					
5	10.5	-	-	10.5	9.8	
10	16.5	17.5	15.0	16.3	14.1	
15	22.5	21.5	22.0	22.0	17.6	
20	28.5	26.5	30.0	28.3	20.8	
25	-	-	39.5	39.5	27.24	

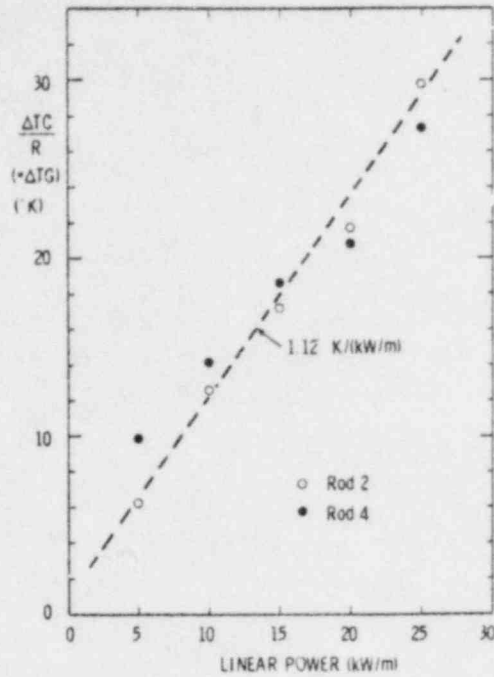


Fig. 18 Average temperature decrements (0.1 - 1.0 MPa) adjusted by R as a function of linear power. Data taken at 1.0 MPa. Linear regression fit.

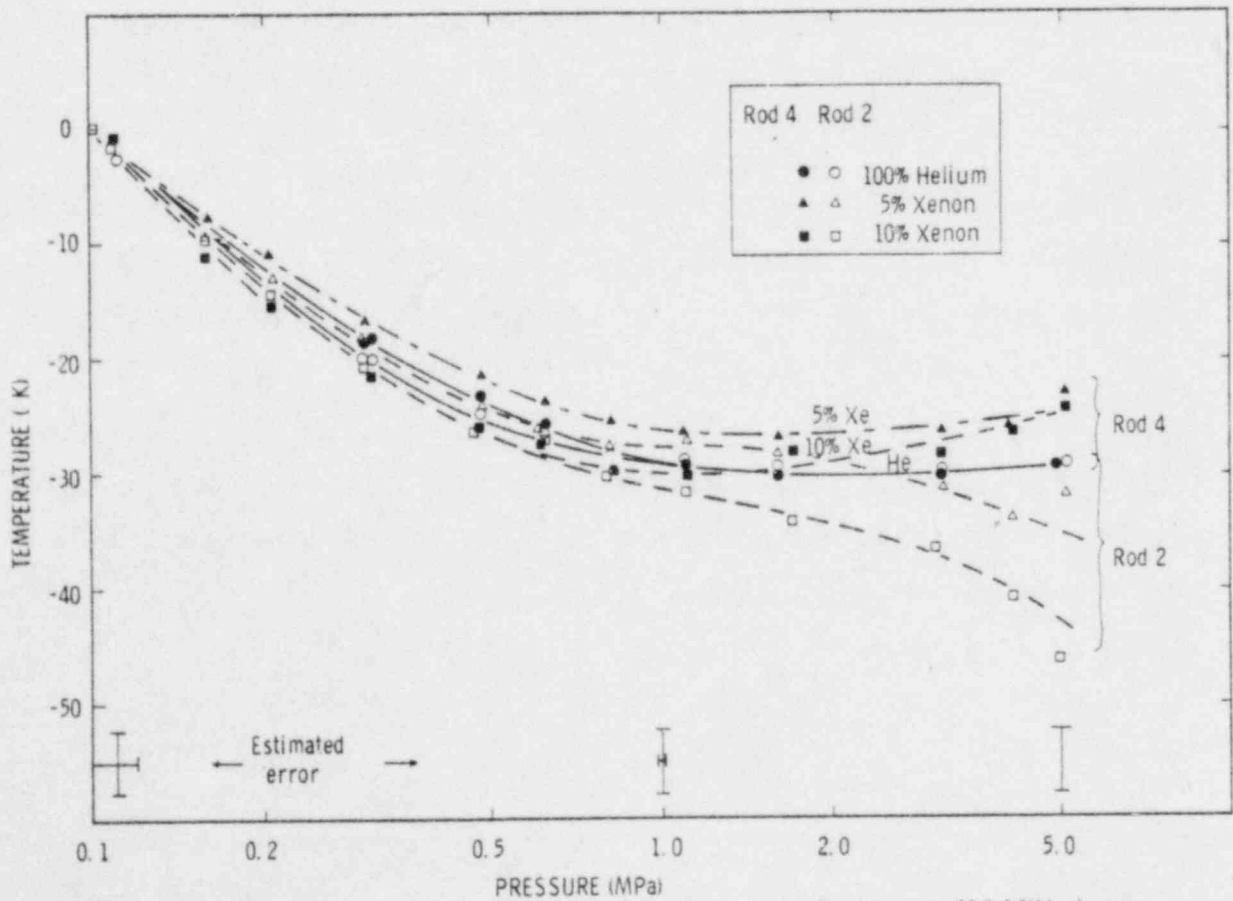


Fig. 19 Comparison of rod 2 and rod 4 temperature decrements (20 kW/m) for all three gas mixtures.

where T is the mean gap gas temperature (K). Although the mean gap gas temperature cannot be precisely known without detailed knowledge of the gap, gas conductivity is not strongly dependent upon the temperature. For the present purposes, gap gas temperatures were estimated with the Halden fuel code FTEMP2.¹³ The calculated gap gas temperatures are probably quite close to actual temperatures, but even if a very large error of, say, 50 K existed in these predictions, Equation (26) would yield a change in conductivity of only about 5%.

Table 2 contains the data together with results of the calculations for $2\bar{g}$ for both fuel rods at each of three power levels. The uncertainty is seen to diminish steadily with increased power so that the values for 20 kW/m power levels represent the best estimate of $2\bar{g}$.

Predictions of $2\bar{g}$ by the Lloyd model, under the same conditions as the 20 kW/m data, yield combined jump distances of $2\bar{g} = .006$ mm for Rod 2 and $2\bar{g} = 0.006$ mm for Rod 4, representing an average underprediction by the Lloyd model of 35%. Under-predictions of this magnitude may be the result of uncertainties in the accommodation coefficient of helium, Equation (6), since reported values⁷ of this quantity have ranged to a factor of 10 lower than those used in the Lloyd model.

Another explanation of the variance between experimental data and the Lloyd model might be found in the physical condition of the fuel pellets. As noted earlier, cylindrical cracks could multiply the number of gas-solid interfaces and produce higher values of $2\bar{g}$. Such cracks would not have to be strictly cylindrical, but in the limit, could be manifest as badly chipped or fragmented surfaces with the fragments locked in place by the cladding.

TABLE 2. CALCULATION OF $\bar{2}g$

$$\bar{2}g = \frac{(1.02) (\Delta TC) k_{\text{gas}}}{Rq}$$

LHR (kW/m)	q (kW/m ²)	ΔTC (K)	T' (K)	k Helium ^a (W/mK)	R	$\bar{2}g \times 10^3$ (mm)
<u>Rod 2, helium, 0.1 MPa:</u>						
10	294	14.5 + 2.8	588	0.2383	1.16 + 0.02	10.3 + 2.3
15	441	23.5 + 2.8	613	0.2450	1.25 + 0.03	10.6 + 1.8
20	589	29.5 + 2.8	634	0.2506	1.36 + 0.05	9.4 + 1.4
<u>Rod 4, helium, 0.1 MPa:</u>						
10	294	16.5 + 2.8	560	0.2306	1.16 + 0.02	11.3 + 2.3
15	441	23.5 + 2.8	576	0.2350	1.25 + 0.03	10.2 + 1.8
20	589	29.5 + 2.8	589	0.2385	1.36 + 0.05	9.0 + 1.4

a. From Equation (26).

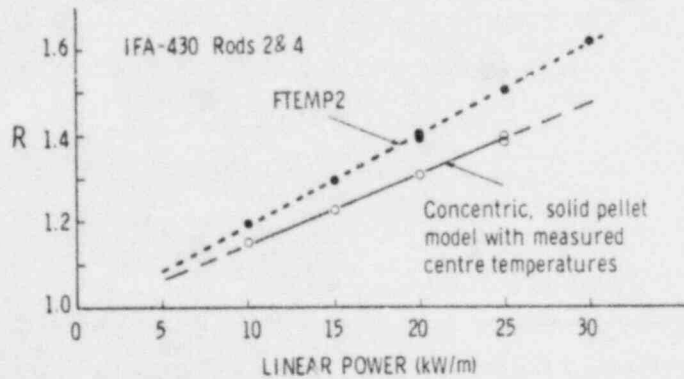


Fig. 20 $R = dTC/dTS$, based upon solid pellet model, MATPRO, UO_2 properties, and measured centre temperatures. Results of model with «eccentricity» modeled via a contact area function are also shown.

4.3 The Influence of Xenon on Fuel Temperature

Using pure helium experiments to establish reference temperatures, the temperature increments for 5% and 10% xenon gases are shown in Figures 21 through 24 for the power levels of 10, 15, 20 and 25^a kW/m. Focusing first on the data taken at 0.1 MPa, the experimental data strongly support a linear relationship between temperature and xenon fraction for both fuel rods and straight lines have been fitted to these data. At mid-pressures (~1.1 MPa) the data still support linear relationships but at the highest pressures (~5 MPa), previously noted diverging temperature trends complicate the interpretation. This divergence is most significant in Rod 2 with 10% xenon gas.

It was stated earlier that the model [Equation (29)] predicts a nearly linear relationship between temperature and xenon concentration. To illustrate this further, Equation (29) has been evaluated using the input data listed in Table 2 and plotted for the case of 20 kW/m power for various gap widths in Figure 25. It is clear that for the experimental data to confirm the predicted curvature more data of better accuracy is required.

Looking next at dependence upon power, it is noted that temperature increments in Equation (25) are proportional not only to power but also to gap width, d , which itself is dependent upon power due to thermal expansion. If we make the approximation that the gap closes linearly with power, that is

$$d = d_0 - \beta q \quad (27)$$

a. The singular data points for 25 kW/m do not correlate well with other data and are shown only for completeness. These experiments were conducted 4 months later and, since helium reference temperatures were not taken at that time, extrapolated reference temperatures are used.

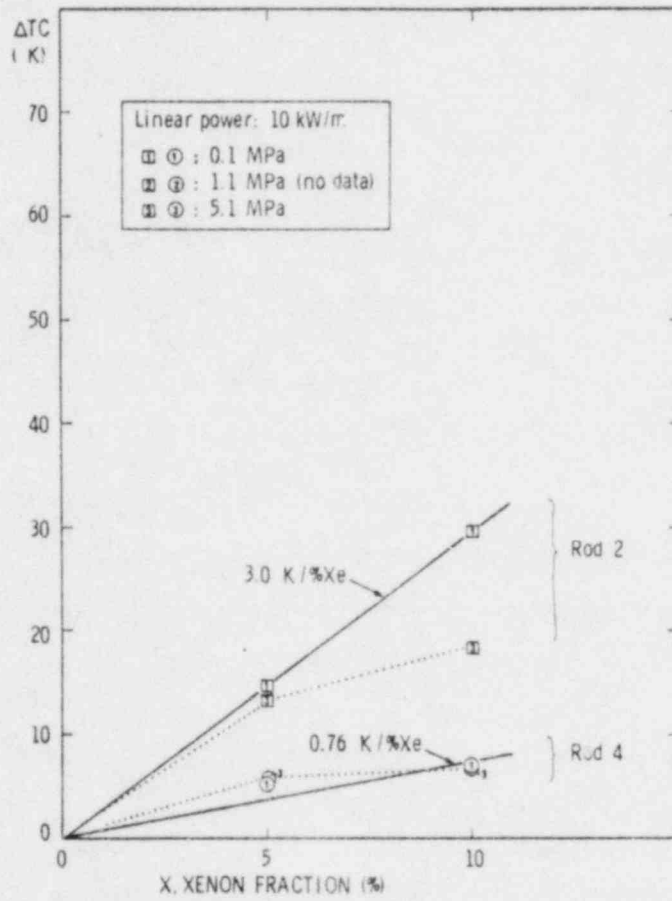


Fig. 21 Temperature rise due to xenon, IFA 430, rods 2 and 4 at 10 kW/m and pressures of 0.1, 1.0 and 5.1 MPa.

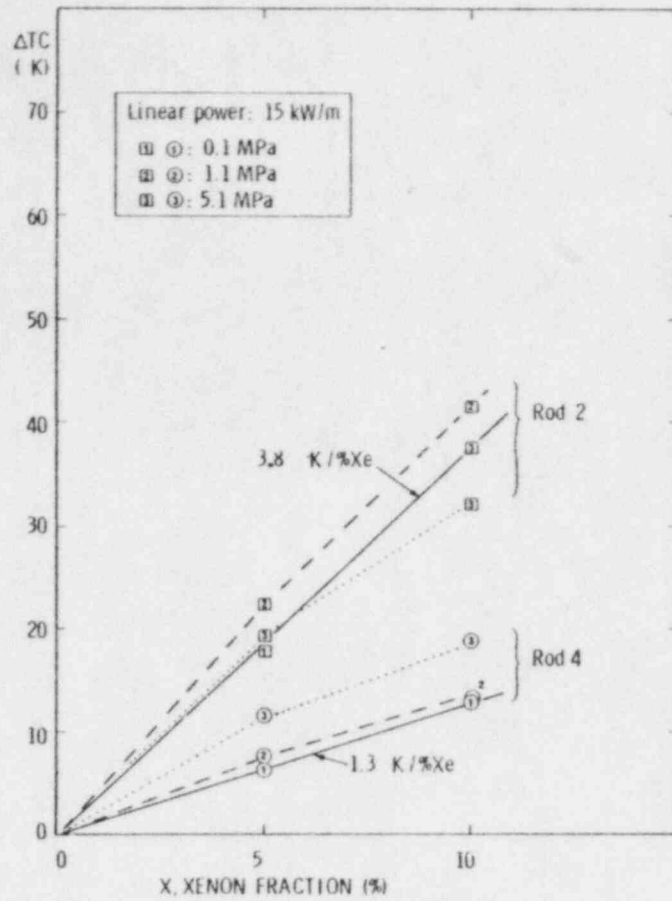


Fig. 22 Temperature rise due to xenon, IFA 430, rods 2 and 4 at linear power 15 kW/m and pressures of 0.1, 1.0 and 5.1 MPa.

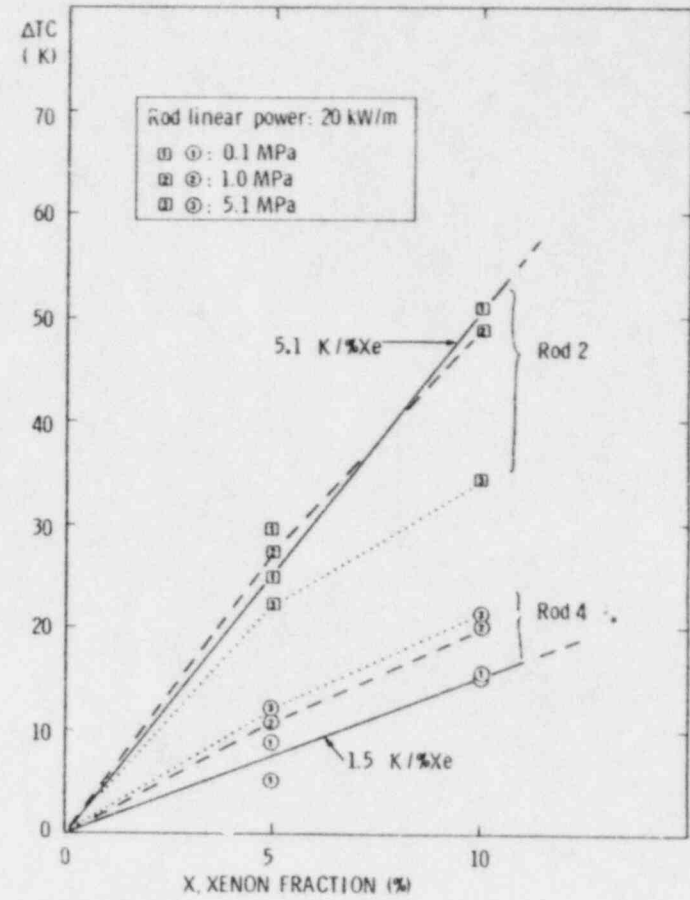


Fig. 23 Temperature rise due to xenon in IFA 430, rods 2 and 4. Pressures of 0.1, 1.0, and 5.1 MPa, linear power at 20 kW/m.

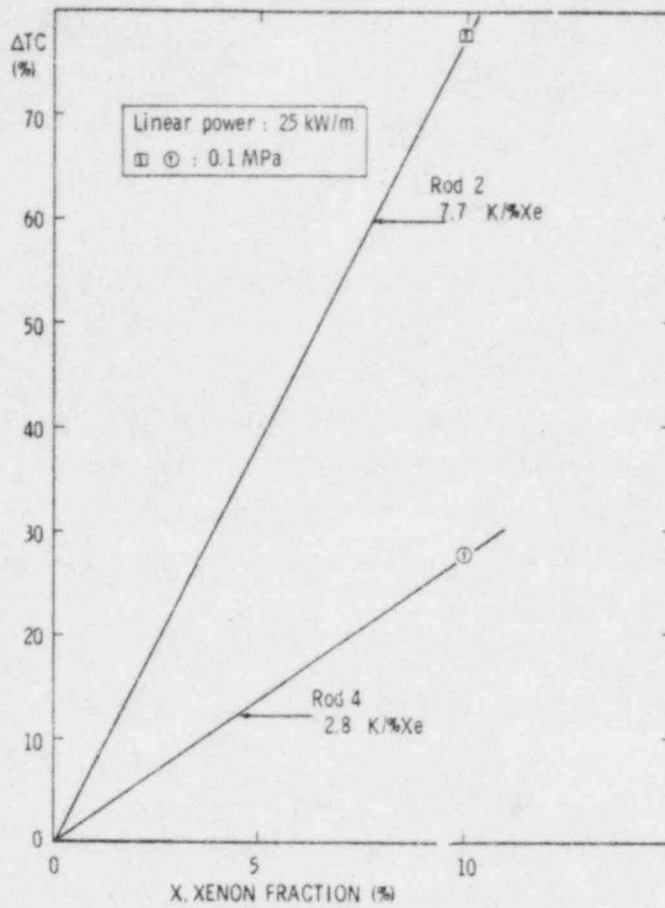


Fig. 24 Temperature rise due to xenon, IFA 430 rods 2 and 4, 0.1 MPa. (Since a pure helium reference was not taken at the time of these tests, this temperature increment is not considered to be as accurate as the lower power data.)

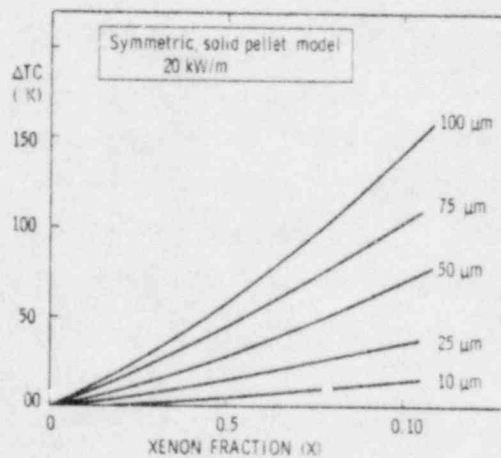


Fig. 25 Predicted xenon temperature increments for 20 kW/m power level, simple model, and various radial gap widths.

then

$$\Delta TC = Rq \left[\frac{3x}{1-3x} \frac{(d_o - \beta q)}{k_{He}} - \frac{2.25x}{P} \right] \quad (28)$$

Using calculated¹³ gap coefficients, β , Equation (28) has been evaluated for 10% xenon at 0.1 MPa for several initial gaps and is plotted in Figure 26. The temperature increment (ΔTC , figure 25) increases as the power increases, and, comparing the 0.48 mm gap curves of Figures 26 and 27, reaches a maximum at a power at which the gap has been reduced by about a factor of two; the temperature increment then decreases as the power is increased further. Data from the present experiment, are also shown in Figure 26 for comparison. Although the experiments did not reach sufficiently high power to define a peak in ΔTC for either rod, the available data seem to fit within the family of curves. In absolute terms the data lie close to the 0.025 mm and 0.05 mm curves (Figure 26). Rod 2 data fit well to an initial gap of about 0.055 mm, which is half of the 0.118 mm radial gap predicted by thermal expansion in the concentric pellet model. Similarly, Rod 4 data fit best to curves in the 0.025 mm to 0.030 mm range, whereas 0.048 mm is the predicted radial gap at zero power, and ~ 500 K.

4.4 Calculation of Gap Width

Equation (25) can be used with the measured temperature increment (ΔTC) data to estimate the gap width. Temperature increments measured in the 10% Xe fill gas experiments were used, along with estimates of R and g , as shown in Table 3, to calculate the radial gap widths using Equation (25). The estimated error of each term in Equation (25) (irrespective of the model itself) is also shown in Table 3; conventional error propagation was used to estimate the uncertainty in the gaps calculated with Equation (25). The Equation-(25)-calculated gaps are compared with the calculated gap using only thermal expansion

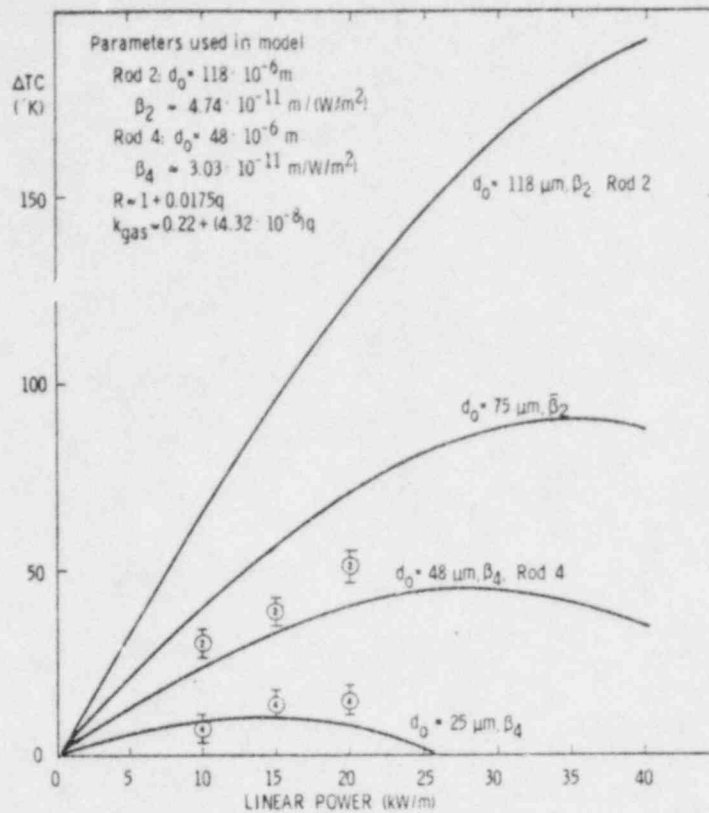


Fig. 26 Expected temperature increments for 10% xenon in the concentric solid pellet model expanding thermally (solid lines) for several initial radial gaps. Data from xenon experiments are also shown.

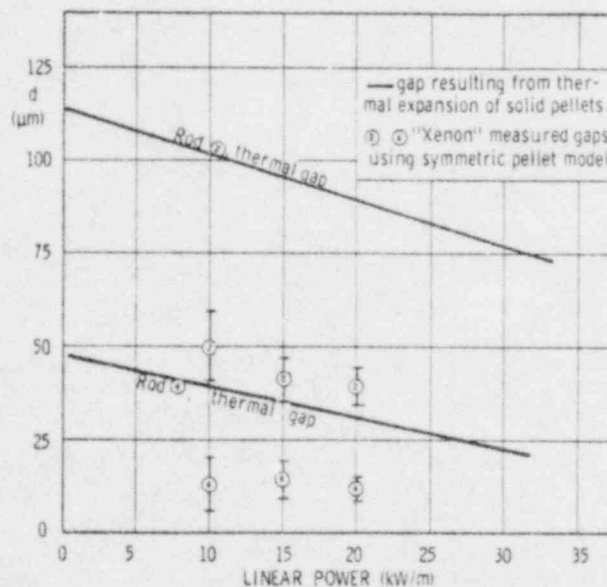


Fig. 27 «Effective» radial gap widths as measured by xenon exchange for IFA 430, rods 2 and 4, compared to the concentric gap widths predicted by differential thermal expansion alone.

TABLE 3. INPUT DATA, UNCERTAINTY AND CALCULATED RADIAL GAPS USING EQUATION 25, AND MEASURED ΔTC .

LHR (kW/m)	q (10^5 W/m ²)	R	Rod-2			Rod-4		
			k_{He} (W/m·K)	ΔTC (K)	gap (mm · x · 10 ³)	k_{He} (W/m·K)	ΔTC (K)	gap (mm · x · 10 ³)
10	2.94	1.16	0.2383	30	50 + 9	0.2306	7.6	13 + 7
15	4.41	1.25	0.2450	38	41 + 6	0.2350	13	14 + 5
20	5.89	1.36	0.2506	51	39 + 5	0.2385	15	12 + 3
Uncertainty	+ 5%	+ 2%	+ 10%	+ 4°K		+ 10%	+ 4°K	

[Equation (28)] in Figure 27 and, as suggested by Figure 26, the Equation-(25)-calculated gaps are about a factor of two less than the gap calculated using the concentric pellet model with thermal expansion.

4.5 Comparison with FRAP-T Calculations

This section provides a comparison of the measured data with the FRAP-T³ (Fuel Rod Analysis Program-Transient) calculated thermal response of the fuel. Two versions of the FRAP computer code were used to calculate the fuel response to changes in gap fill gas composition and pressure: (a) FRAP-T5^a, the most recently published version of the FRAP-T code and; (b) FRAP-T6^b an experimental version of the FRAP code, currently being developed by EG&G Idaho for the U.S. Nuclear Regulatory Commission.

The significant difference which is of interest to this analysis, between the FRAP-T5 and FRAP-T6 versions, is in the fuel-cladding gap conductance models.

The model for the gap conductance used in FRAP-T5 is basically a modification of the formulation due to Ross and Stoute¹⁴ which, for non-contact (fuel-cladding) conditions, assumes the gap between fuel and cladding is axisymmetric and that heat is transferred across the gap by conduction through the gas and by radiation. Thus, in FRAP-T5,

$$h_g = \frac{k_g}{t_g + (g_1 + g_2)} + h_r \quad (29)$$

where

h_g = gap conductance
 k_g = conductivity of gas in gas gap

-
- a. FRAP-T5 VERSION 7/26 Configuration Control Number H-000583B.
 - b. FRAP-T6 VERSION 67 Configuration Control Number H-002483B.

- t_g = gap thickness
- g_1 = temperature jump distance at cladding inside surface
- g_2 = temperature jump distance at fuel outside surface
- h_r = radiant heat transfer conductance.

The radiant heat transfer coefficient is computed using the following equation

$$h_r = \sigma F_e (T_f^2 + T_c^2) (T_f + T_c) \quad (30)$$

where

- h_r = radiant heat transfer
- σ = Stefan-Boltzmann constant
- F_e = emissivity factor
- T_f = temperature of outside surface of fuel
- T_c = temperature of inside surface of cladding.

The emissivity factor is computed by the equation

$$F_e = \left[\frac{1}{e_f} + \frac{r_f}{r_c} \left(\frac{1}{e_c} - 1 \right) \right]^{-1} \quad (31)$$

where

- F_e = emissivity factor
- e_f = emissivity of fuel surface
- e_c = emissivity of cladding inside surface
- r_f = outside radius of fuel
- r_c = inside radius of cladding.

The temperature jump distance term ($g_1 + g_2$) is computed by an empirically derived equation presented in the GAPCON-THERMAL-1¹⁵ code report. The equation is

$$g_1 + g_2 = 5.448 \frac{\mu}{P} \left(\frac{T}{M} \right)^{1/2} \quad (32)$$

where

$(g_1 + g_2)$	=	jump distance (cm)
μ	=	viscosity of gas (g/cm \cdot s)
P	=	pressure of gas (psi)
T	=	temperature of gas (K)
M	=	molecular weight of gas.

The gap conductance model used in FRAP-T6 is that from the GAPCON-THERMAL-2¹⁶ code. The gas conductance and temperature jump distance terms and the assumed pellet location within the cladding differs from that used in FRAP-T5. The gap conductance in FRAP-T6 is

$$h_g = \frac{k_g}{t_g + 1.8(g_1 + g_2)} + h_r \quad (33)$$

thus differing from the FRAP-T5 (Equation 29) model by the added 1.8 term on the temperature jump distance.

The temperature jump distance used in FRAP-T6 is from GAPCON-THERMAL-2¹⁶

$$g_i = \frac{Ck_g}{\sum_j \frac{a_j P_j}{M_j T_i}} \quad \begin{array}{l} i = 1,2 \\ j = 1, \dots, N \end{array} \quad (34)$$

where C is a constant dependent upon the units of k_g , P_j is the partial pressure of the j th gas, M_j is the molecular weight, a_j the accommodation coefficient (a function of temperature) and T_i the temperature at the gas-solid interface (before temperature jump). This model has been derived from the Lloyd equation, and is similar to the model used in Section 2, Equation (3). The accommodation coefficients are as given in Equations (6) and (7) for helium and xenon. For mixed gases the accommodation coefficient is given by

$$a_j = (a_{Xe} - a_{He}) \frac{M_j - 4}{128} + a_{He} \quad (35)$$

The gap conductance calculated with FRAP-T5 assumes the pellet is located axisymmetrically within the cladding. The FRAP-T6 model assumes the pellet is located one-half the fabricated gap size off-center within the cladding and calculates the average gap conductance for the non-uniform gap. The pellet and gap are divided into three pie shaped segments, the gap conductance is computed for each segment, based on the average gap size in each section, and the gap conductance of the three segments is averaged to give an average gap conductance which is used in the fuel temperature calculations.

In both the FRAP-T5 and -T6 models, the conductivity of a mixed gas is given by¹²

$$k_{mix} = \frac{\sum_{i=1}^n k_i}{1 + \sum_{\substack{j=1 \\ j \neq i}}^n \psi_{ij} \frac{x_j}{x_i}} \quad (36)$$

where

$$\psi_{ij} = \phi_{ij} \left[1 + 2.41 \frac{(M_i - M_j)(M_i - 0.142 M_j)}{(M_i + M_j)^2} \right] \quad (37)$$

and

$$\phi_{ij} = \frac{\left[1 + \left(\frac{k_i}{k_j} \right)^{1/2} \left(\frac{M_i}{M_j} \right)^{1/4} \right]^2}{2^{3/2} \left(1 + \frac{M_i}{M_j} \right)^{1/2}} \quad (38)$$

and

- n = number of components in mixture
- M_i = molecular weight of the chemical species i
- x_i = mole fraction of the chemical species i
- k_i = thermal conductivity of the chemical species i.

The thermal conductivity equations of the individual rare gases are based on the correlative work of Gandhi and Saxena.¹⁷ The resulting expressions are

$$k_{\text{helium}} = 3.366 \times 10^{-3} T^{0.668} \quad (39)$$

$$k_{\text{argon}} = 3.421 \times 10^{-4} T^{0.701} \quad (40)$$

$$k_{\text{xenon}} = 4.0288 \times 10^{-5} T^{0.872} \quad (41)$$

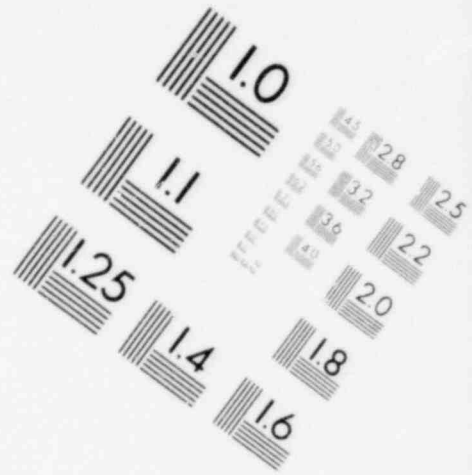
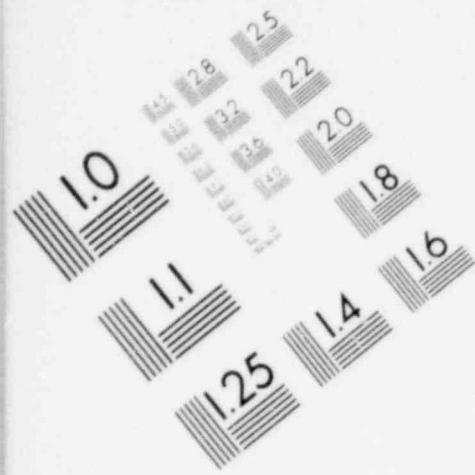
$$k_{\text{krypton}} = 4.726 \times 10^{-5} T^{0.923} \quad (42)$$

where

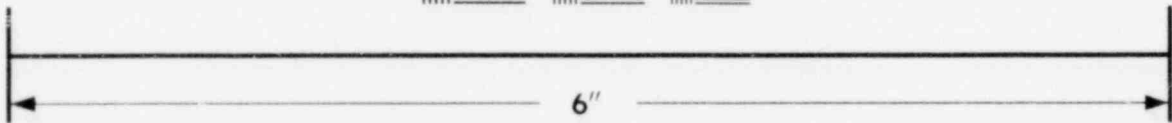
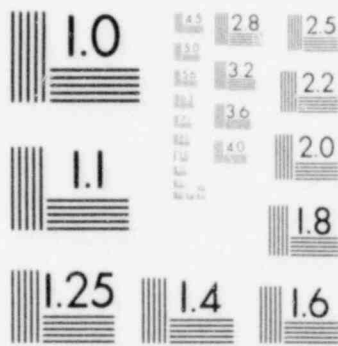
- k = thermal conductivity (W/m K)
- T = gas temperature (K).

4.5.1 Xenon Effects

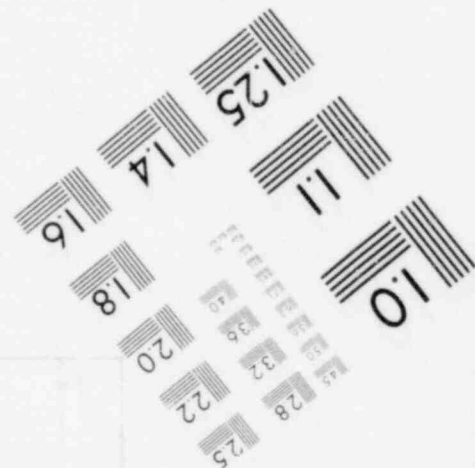
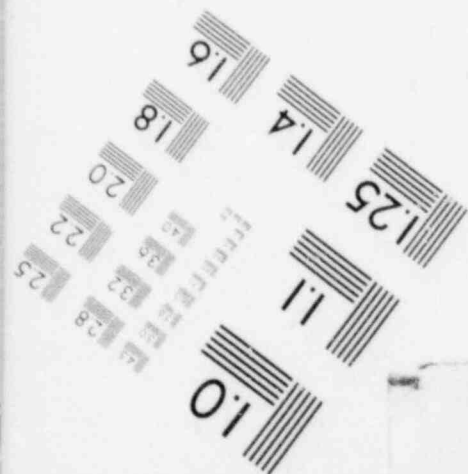
The effect of the addition of Xe to the He fill gas, as discussed in Section 4.3, is to reduce the gap conductance. Figure 28 shows the gap conductance as a function of gap size for 100% He and 90% He/10% Xe fill gas at 1.0 MPa, as computed with FRAP-T5 and -T6 for the 0.23 mm gap rod. Qualitatively, the gap conductance calculated by FRAP-T6 increases at a faster rate than that calculated by FRAP-T5 as the gap closes and quantitatively, is higher than that calculated by FRAP-T5 for radial gaps less than ~ 0.110 mm.

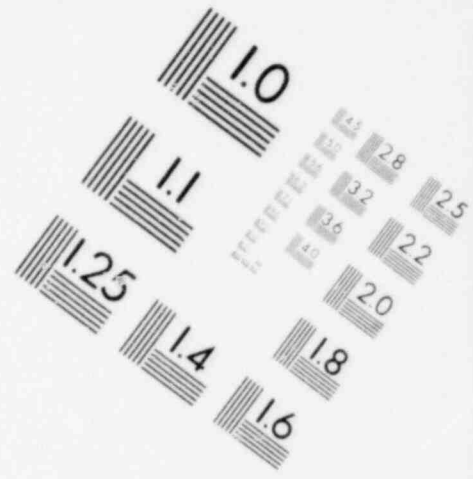
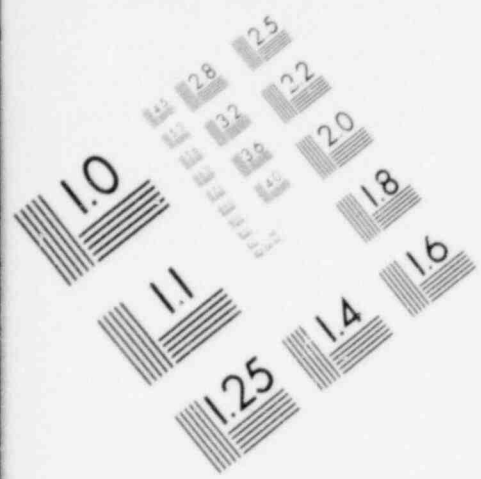


**IMAGE EVALUATION
TEST TARGET (MT-3)**

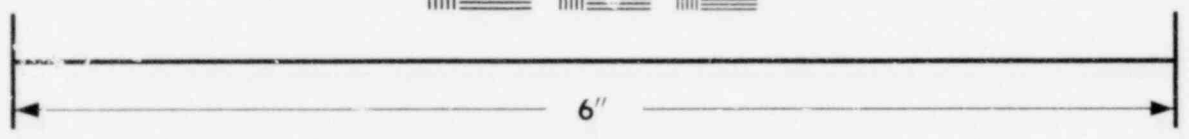
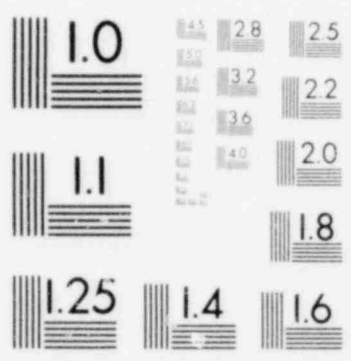


MICROCOPY RESOLUTION TEST CHART

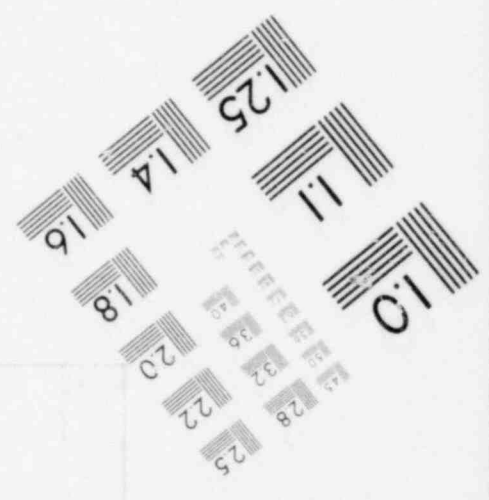
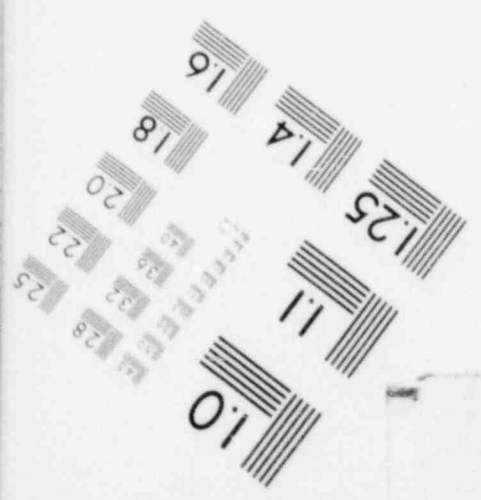




**IMAGE EVALUATION
TEST TARGET (MT-3)**



MICROCOPY RESOLUTION TEST CHART



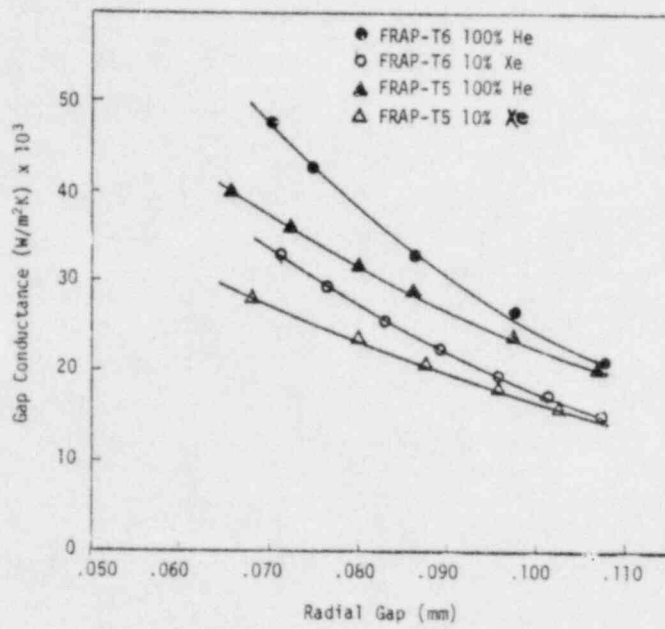


Fig. 28 FRAP-T5 and -T6 calculated gap conductance as a function of radial gap size for 1.0 MPa fill gas pressure and 0.115 mm fabricated radial gap width.

The 0.23 mm gap rod centerline temperatures calculated with FRAP-T5 and -T6 are compared with the measured centerline temperatures in Figures 29 and 30. In general the FRAP calculated temperatures are a few percent higher than the measured temperatures, and the FRAP-T6 experimental code calculations are slightly closer to the data than FRAP-T5. Figure 31 shows the measured and FRAP-T5 calculated fuel centerline temperatures for the 0.10 mm gap rod (FRAP-T6 calculated data were not available for this rod); the trends are the same as for the 0.23 mm gap rod. In Figures 32 and 33 the centerline temperature at 10 and 20 kW/m is plotted as a function of percent Xe in the fill gas. It appears that the FRAP calculations are diverging from the data. To look at this more closely the increase in centerline temperature from that measured with 100% He fill gas is plotted as a function of the percent Xe in the fill gas in Figure 34. The FRAP calculated temperatures are higher than the data, as shown earlier, and appear to be diverging from the measured data. The FRAP-T6 model does predict temperatures closer to the measured temperatures than FRAP-T5; however, the divergence between the measured and calculated temperatures indicate that the FRAP results should be used with caution at high Xe concentrations until further data (at higher Xe concentrations) are available.

4.5.2 Pressure Effects

The pressure influences the fuel centerline temperature through the temperature jump distance contribution to the fuel-cladding gap conductance, as shown in Equations (29), (32) and (34). The measured effect of fill gas pressure ranging from 0.1 to 5.0 MPa was shown in Figure 19 and discussed previously in Section 4.2. Figure 35 compares the measured centerline temperature change as a function of pressure with the FRAP-T5 calculated change for the 0.1 mm gap rod. The FRAP-T5 results generally agree with the data for both the 100% He and 10% Xe/90% He cases; however the calculated decrease in fuel centerline temperature with 100% He is slightly greater than the data. Figure 36 presents the FRAP-T5 calculated and measured temperature change data for the 0.23 mm gap rod at 20 kW/m with 100% He and 95% He/5% Xe fill gas; the FRAP-T5 calculations

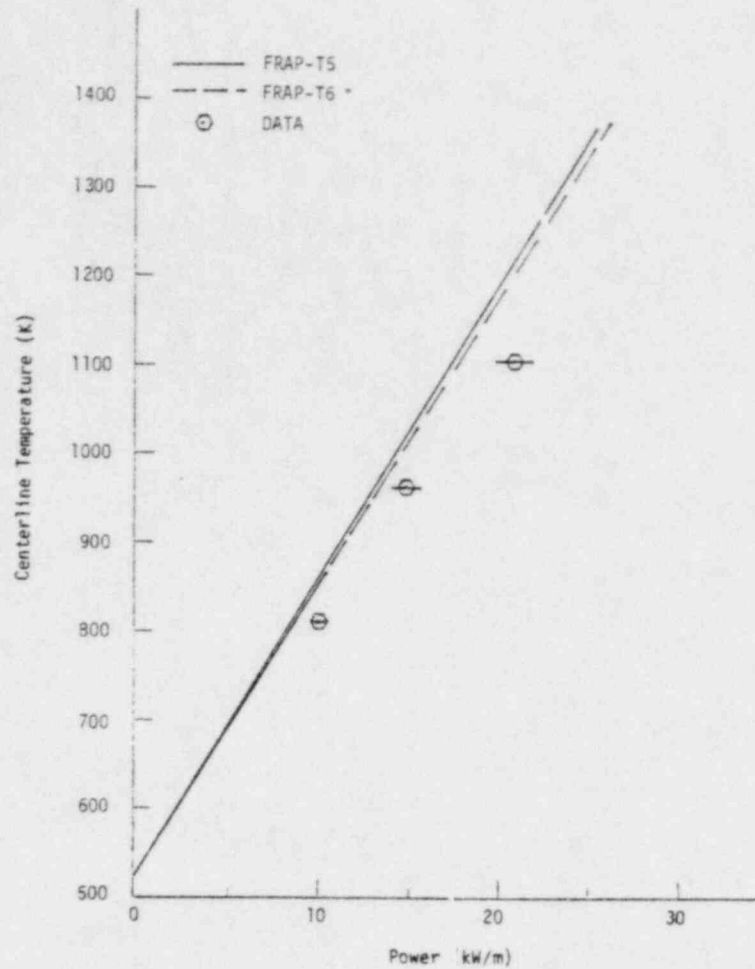


Fig. 29 FRAP-T5 and -T6 calculated fuel centerline temperatures compared with data for 10% Xe fill gas at 1.0 MPa in the 0.23 mm-diametral-gap rod.

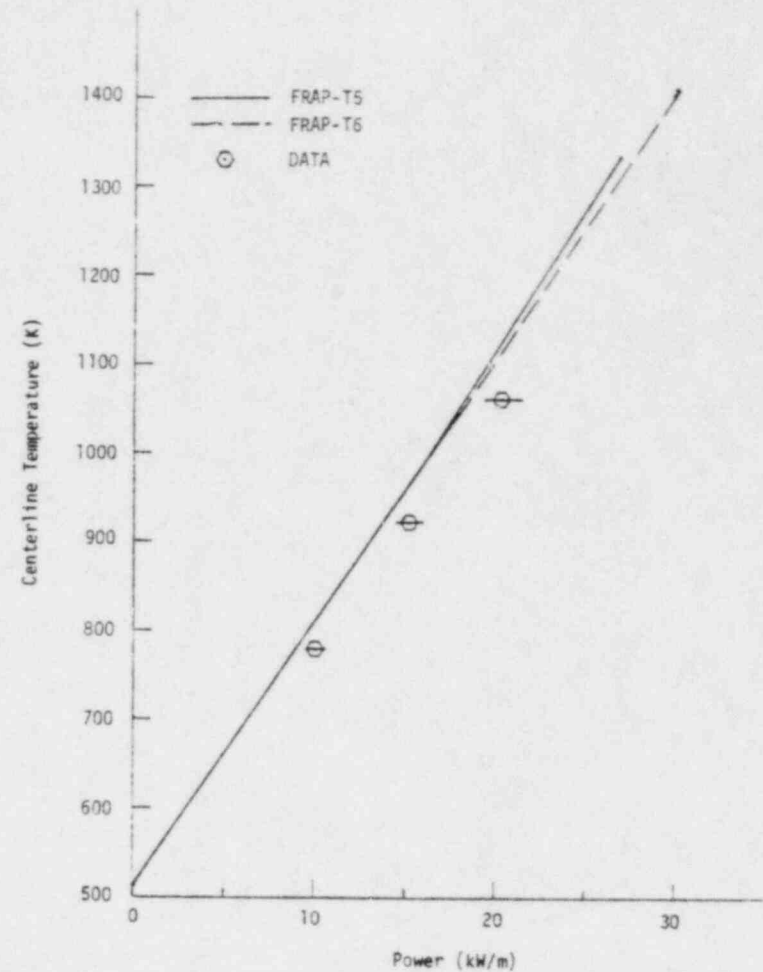


Fig. 30 FRAP-T5 and -T6 calculated fuel centerline temperatures compared with data for 100% He fill gas at 1.0 MPa in the 0.23 mm-diametral-gap rod.

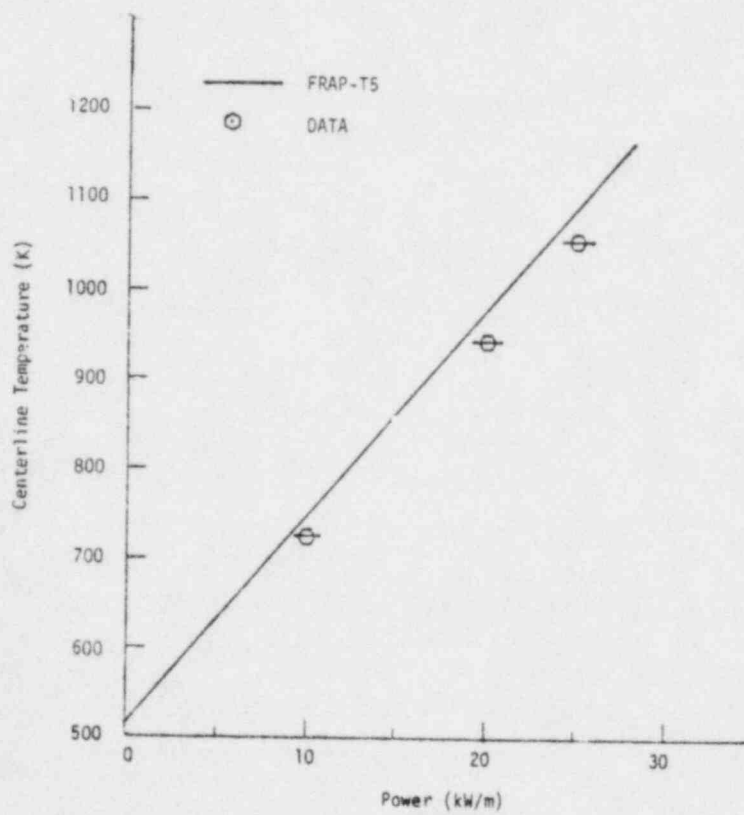


Fig. 31 FRAP-T5 calculated fuel centerline temperature and data for 10% Xe fill gas at 1.0 MPa in 0.10 mm-diametral-gap rod.

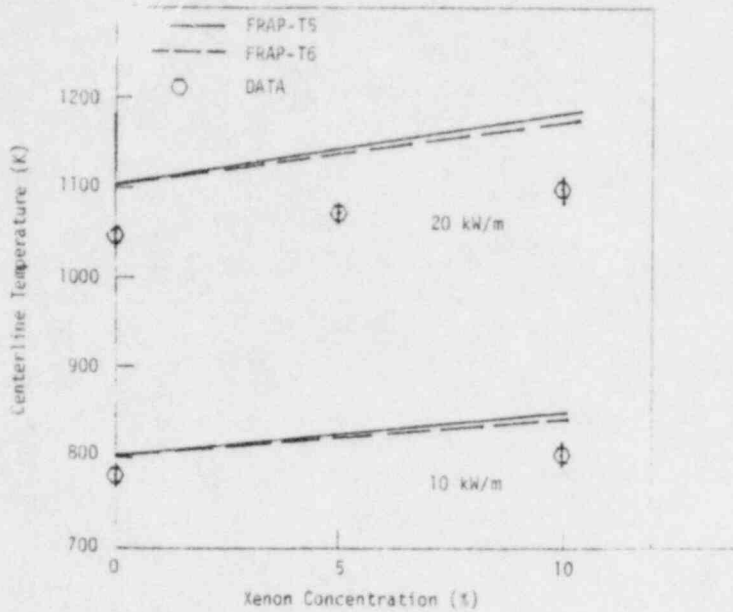


Fig. 32 Measured and FRAP calculated fuel centerline temperature as a function of Xe concentration in the fill gas for the 0.23 mm-diametral-gap rod at 1.0 MPa fill gas pressure.

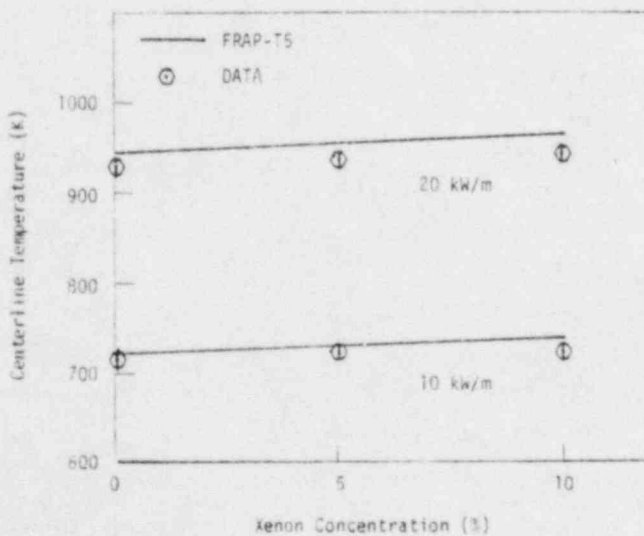


Fig. 33 Measured and FRAP calculated fuel centerline temperature as a function of Xe concentration in the fill gas at a pressure of 1.0 MPa in the 0.10 mm-diametral-gap rod.

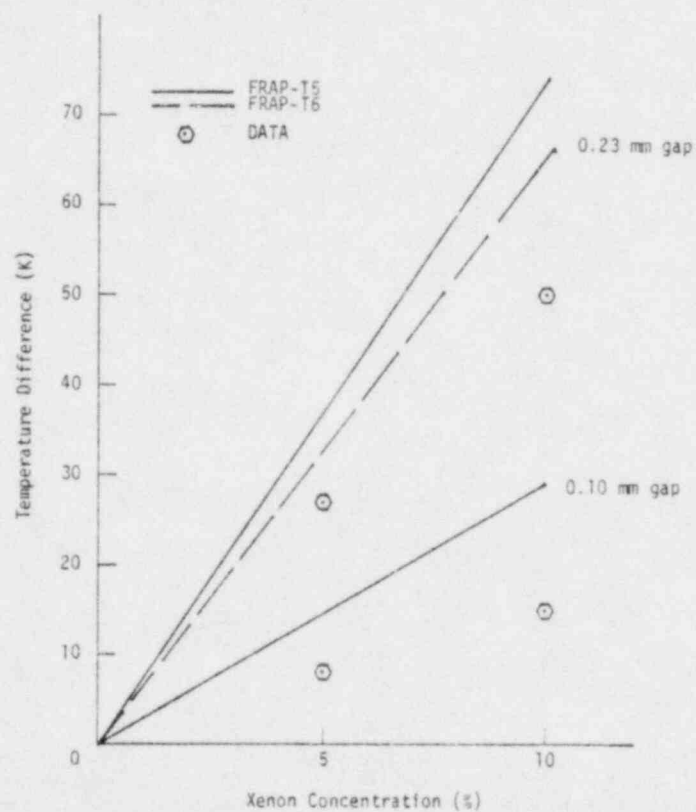


Fig. 34 Measured and FRAP calculated temperature change due to increasing xenon concentration for the 0.10 and 0.23 mm-diametral-gap rods, 20 kW/m.

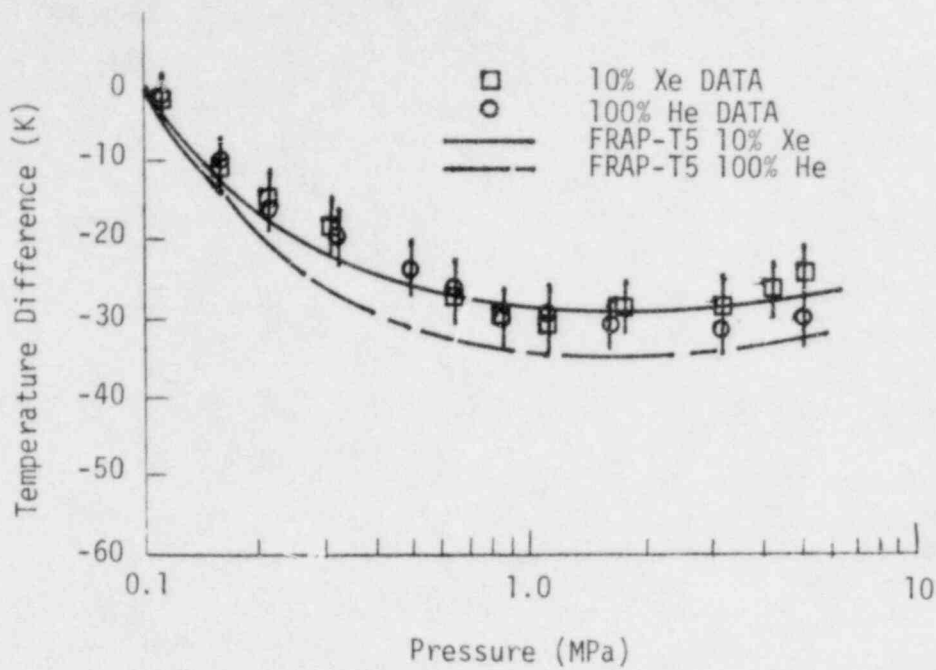


Fig. 35 Measured and FRAP calculated centerline temperature change as a function of fill gas pressure with 100% He and 10% Xe/90% He fill gas in the 0.1 mm-diametral-gap rod, 20 kW/m.

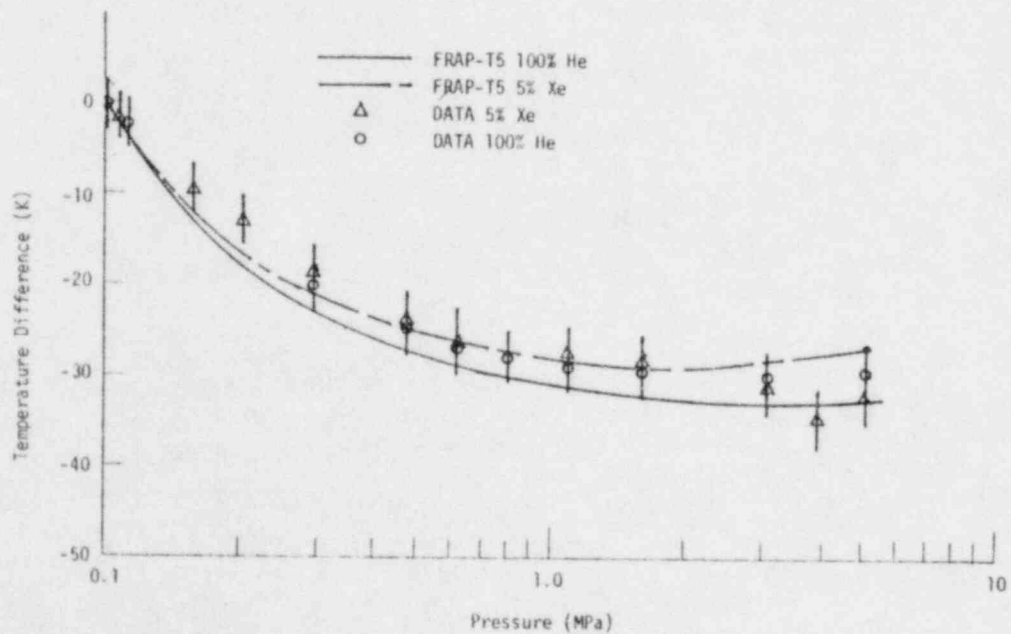


Fig. 36 Measured and FRAP calculated centerline temperature change due to increasing fill gas pressure for 0.23 mm-diametral-gap rod, 20 kW/m.

agree very well with the data. In the case of the 0.23 mm gap with 10% Xe fill gas, however, the FRAP-T5 and -T6 calculated temperature change does not follow the data trend at pressures above 2.0 MPa as shown in Figure 37.

Figure 38, which shows the measured temperature drop data at 10, 15, and 20 kW/m powers for the 0.23 mm gap rod with 10% Xe/90% He fill gas, further illustrates the unexpected decreases in temperatures at pressures above 2.0 MPa. As mentioned previously the downward trend in the data at pressures above 2.0 MPa is not presently understood. The FRAP code indicates that as the pressure increases from 2.0 to 5.0 MPa the gap increases, due to cladding expansion, which should lead to increasing centerline temperature and a smaller (absolute) temperature difference. The contribution of the Xe temperature jump distance is only 1-2% of the gap conductance and is not expected to be the cause of the discrepancy between the calculated and experimental results.

In summary the effects of increased fill gas pressure are: (1) to decrease fuel temperatures (enhance gap conductance) in the range 0.1 to 2.0 MPa (FRAP calculations agree very well); (2) insignificant in the range 2.0 to 5.0 MPa for the 0.10 mm gap rod at Xe concentrations less than 10% and for the 0.23 mm gap rod at Xe concentrations less than 5%, (FRAP calculations agree); and (3) to decrease fuel temperatures in the range 2.0 to 5.0 MPa in the 0.23 mm gap rod at a Xe concentration of 10 %, (a trend not predicted by the FRAP gap conductance models).

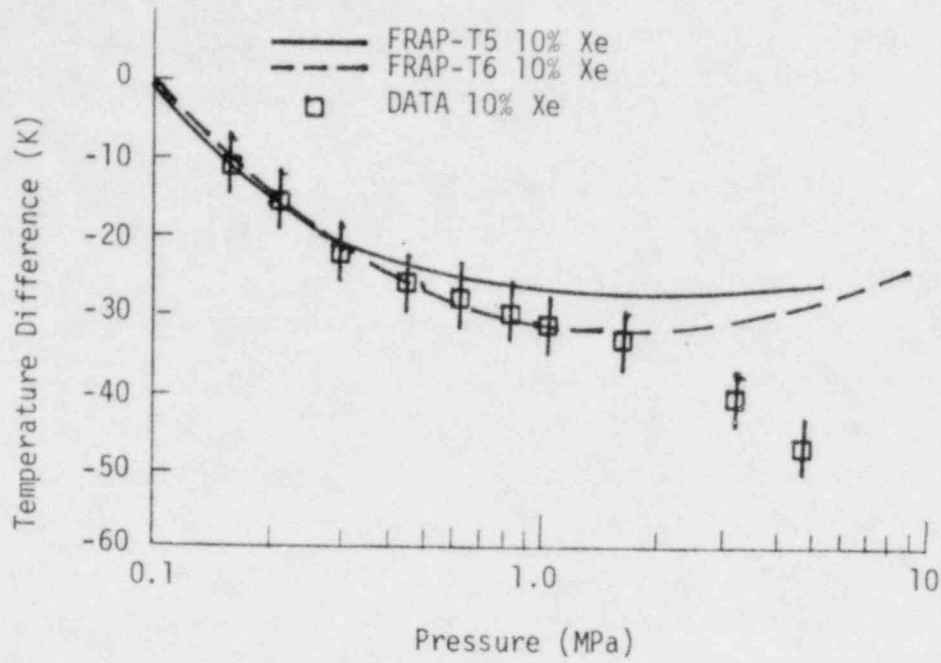


Fig. 37 Temperature difference data and FRAP-T5 and -T6 calculations for 20 kW/m power level, 10% Xe in the 0.23 mm-diametral-gap rod.

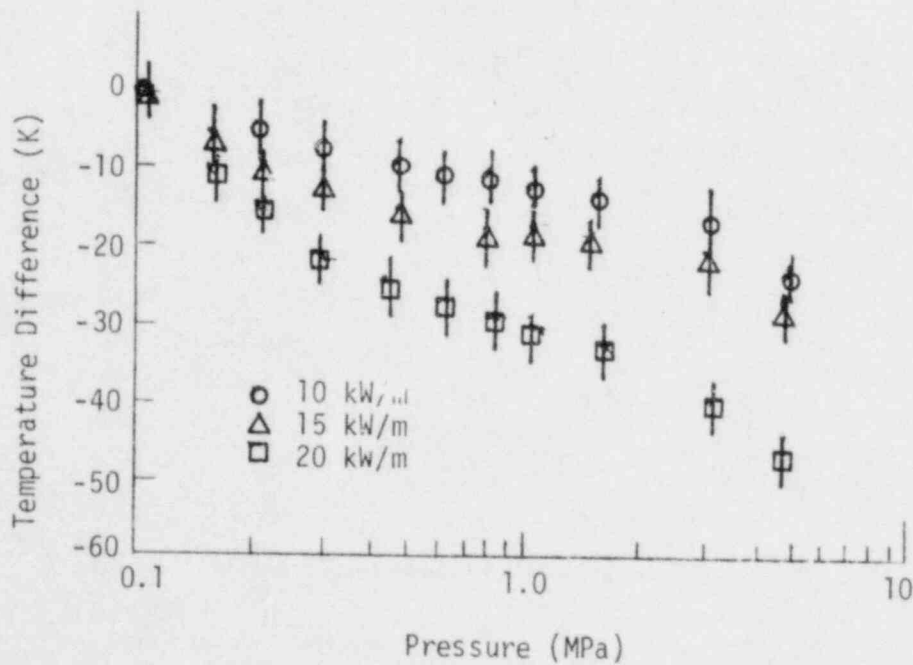


Fig. 38 Measured change in fuel centerline temperature as a function of fill gas pressure for 10% Xe in the 0.23 mm-diametral-gap rod.

5. CONCLUSIONS

The measured effects of fuel rod fill gas pressure and composition on fuel temperature has been analyzed and compared with a simple analytical model and with FRAP computer code calculations. The analysis and comparison has led to the following conclusions:

- (1) The results of the experiments support the use of on-line fuel rod fill gas control and fuel temperature measurement as a viable, in-pile, non-destructive technique for measuring fuel-cladding gap heat transfer characteristics. Temperature changes resulting from fill gas pressure and composition variance can be measured with sufficient precision to determine the temperature jump distance effect and measure small changes in fuel-cladding gap conductance.
- (2) The effect of fill gas pressure is predictable, both by the analytical model and the FRAP computer code with the exception of the data from the 0.23 mm gap rod with 5% or 10% Xe in the fill gas at pressures above ~ 2.0 MPa.
- (3) There is an apparent increase in gap conductance for the 0.23 mm gap rod with 10% Xe in the helium fill gas when the pressure is increased from 2.0 to 5.0 MPa. This behavior is not predicted by the simple analytical model or FRAP and is currently unexplained. The data show that the trend exists at all power levels (10 to 25 kW/m) and is consistently repeatable.
- (4) The qualitative effect of the concentration of xenon in the fill gas is predicted except for the case of the 0.23 mm gap rod with 10% xenon in the fill gas. Quantitatively, the simple model overpredicts temperature change due to Xe by about a factor of two, and the FRAP calculations are high by from 30 to 100% of the measured values. In absolute terms, the FRAP code calculated fuel centerline temperatures are only 2 to 7% higher than the measured temperatures.

- (5) The temperature jump distance term of the gap conductance, as determined from the experimental data, follows theory in that it is inversely proportional to pressure and independent of gap size and gas thermal conductivity. Although theory predicts a slight dependence on gas species no measurable change in the temperature jump distance was observed when pure helium was replaced by helium with 10% xenon fill gas. The temperature jump distances determined with the data are about 50% longer than predicted by the Lloyd model, indicating that (a) the accommodation coefficients used in the model may be too high or that (b) pellet surface chips and cracks may result in multiple gas-solid interfaces which are not taken into account in the model.
- (6) The effective gap size determined from the temperature increase due to xenon concentration in the fill gas data are smaller by a factor of about 2 than the gap predicted by simple thermal expansion of the fuel. This confirms the previous results¹¹ which indicated that the IFA-430 fuel had significantly cracked and relocated, resulting in a reduction of the effective gap size, and points out an area where further experimentation and model development are necessary.
- (7) Comparison of the experimental data with the FRAP-T5 and -T6 calculations show that:
- (a) FRAP adequately models the effect of fill gas pressure on fuel temperature in the range 0.1 to 5.0 MPa for fill gas compositions ranging from pure helium to helium with 10% xenon in fuel rods with 0.1 and 0.23 mm fuel-cladding gap sizes with one exception. For the combination of a 0.23 mm gap with >5% xenon in the fill gas, at pressures above 2.0 MPa the data indicate a continued increase in gap conductance while FRAP calculations predict an essentially constant gap conductance.

- (b) The FRAP calculated fuel centerline temperature is 3 to 7% higher than the measured temperature for a range of xenon concentrations of 0 to 10% (in helium) of the fill gas. However, the FRAP calculated centerline temperature as a function of xenon concentration in the fill gas diverges from the measured temperatures, indicating that the FRAP calculations must be used with caution at higher xenon concentrations.
- (c) The FRAP-T6 calculated fuel centerline temperatures are slightly closer to the measurements than the FRAP-T5 values.

6. REFERENCES

1. United States Nuclear Regulatory Commission, Division of Reactor Safety Research, Water Reactor Safety Research Program-A Description of Current and Planned Research, NUREG-0006, February 1979.
2. R. W. Miller, et al., "The Influence of Gas Pressure and Composition on Fuel Temperature Observed in the USNRC/Halden Assembly IFA-430," ANS Topical meeting on Thermal Reactor Safety, Knoxville; Tennessee, April 1980.
3. L. J. Siefken et al., FRAP-T5-A Computer Code for the Transient Analysis of Oxide Fuel Rods, NUREG/CR-0840, TREE 1281, June 1979.
4. E. H. Kennard: Kinetic Theory of Gases. 1st Ed., New York, McGraw Hill Book Co., 1938, pp 311-325.
5. W. R. Lloyd, D. P. Wilkins, P. R. Hill: "Heat Transfer in Multi-Component Monatomic Gases in the Low, Intermediate and High Pressure Regime," Nuclear Thermionics Conference, 1978.
6. S. K. Loyalka, "Temperature Jump in a Gas Mixture," Physics-Fluids-17, 897, 1974.
7. D. D. Lanning, C. R. Hann, Review of Methods Applicable to the Calculation of Gap Conductance in Zircaloy-Clad UO₂ Fuel Rods, BNWL-1894, UC-786, April 1975.
8. J. E. Gernier, S. Begej: Ex-Reactor Determination of Thermal Gap and Contact Conductance Between Uranium Dioxide-Zircaloy-4 Interfaces, NUREG/CR-0330, PNL-2696 R3, April 1979.
9. A. Ullman, et al., "Thermal Accommodation Coefficients of Inert Gases on Stainless Steel and UO₂," Journal of Nuclear Materials 51, 277, 1974.
10. L. S. Tong, J. Weisman: "Thermal Analysis of Pressurized Water Reactors," American Nuclear Society Monograph, 1970.
11. A. D. Appelhans, et al. Cracking and Relocation of UO₂ Fuel During Initial Nuclear Operation, NUREG/CR-1425, EGG 2032, May 1980.
12. MATPRO-Version 10, A Handbook of Material Properties for Use in the Analysis of Light Water Reactor Fuel Rod Behavior, TREE-NUREG-1180, U.S. National Technical Information Office, 1978.
13. T. J. Bjorlo, et al., FUEL-TEMP-; A Computer Programme for Analyzing the Steady State Thermal Behaviour of Oxide Fuel Rods HPR-211, Sanderstolen, 1977.

14. A. M. Ross and R. L. Stoute, Heat Transfer Coefficient Between UO₂ and Zircaloy-2, AECL-1552 June 1962.
15. C. R. Hann, C. E. Beyer, L. J. Parchen, GAPCON-THERMAL-1: A Computer Program for Calculating the Gap Conductance in Oxide Fuel Pins, BNWL-1778 September 1973.
16. C. E. Beger et al., GAPCON-THERMAL-2: A Computer Program for Calculating the Thermal Behavior on an Oxide Fuel Rod, BNWL-1898, November 1975.
17. J. M. Gandhi and S. C. Saxena, Correlated Thermal Conductivity Data of Rare Gases and Their Binary Mixtures at Ordinary Pressures, Journal of Chemical and Engineering Data, 13, 3, 1968.

APPENDIX A

COMPILATION OF TREATED RAW DATA

At each stabilized situation representing a specific power, gas and gas pressure, the CALIB^a data logging system collected usually 11 data sets (set = temperature and linear power at the thermocouple) each separated by 40 to 60 s. These "raw" data were subsequently averaged yielding the treated raw data listed in Table A-1 together with standard deviations. The table is organized in chronological order exactly as the data were taken. The table also shows corrections to the absolute temperature accounting for a small depression of moderator temperature in the early tests, and temperature decrements referenced from T_{std} at one atmosphere (0.1 MPa) for each pressure run.

a. CALIB is the acronym for the data logging system used for the IFA-430 experiments during the Xe/He gas pressure tests.

Table A-I. EXPLANATION

Data from IFA-430 Xenon, Pressure and Power Tests of 14th - 17th Aug., 1979 & 14th Dec., 1979

Column no.	EXPLANATION
1	Step Number. Each step represents a stable condition of power, pressure, and gas type, during which a set of usually 11 fuel centreline temperatures were accumulated by the "CALIB"* data system over about 10 minutes. These were later averaged in columns 6 & 8.
2	CALIB* record numbers, first and last, used for the data set.
3	Gas mixture.
4	Pressure transducer P-152 voltage output, read by DVM manually.
5	Pressure at P-152 calculated from (5) by equation: $MPa = (V - 0.957)(4.12) + (0.1)$.
6, 7	<p>TF-3 averaged temperatures and standard deviation, s followed by linear power, TF-3R, at the thermocouple as follows:</p> <div style="text-align: center;"> </div> <div style="display: flex; justify-content: space-between; margin-top: 10px;"> <div style="width: 45%;"> <p>(Temperature change from T_{std}. The temperature, T_{std}, at 0.100 MPa for any group of data sets with constant power and gas constituency is calculated by adjusting the nearest data points by approximate slopes of 22°C/ata for Rod no. 2 and 17°C/ata for Rod no. 4. Then $(\delta\delta-\delta) = T_{std} - TTT.T$.)</p> </div> <div style="width: 45%;"> <p>(The power to which the temperatures (xxx.xx) have been adjusted, always nearest multiple of 5 kW/m.)</p> <p>Adjusted Temperatures. The raw average, xxx.xx, is corrected for an abnormal coolant temperature (235°C versus 240°C) and adjusted to standard power levels (PP.P) by the equation $(TTT.T) = (xxx.xx - T_{mod})(PP.P/yy.y) + 240^\circ C$ $T_{mod} = 235^\circ C$ in data sets 1 through 116, August 1979. $= 240^\circ C$ in data sets 1 through 14, December 1979.</p> </div> </div>
8,9	TF-6 and TF6R data - same as TF3 above.

* "CALIB" is the name of the data logging system used at the reactor for the collection of these data.

Table A-I. IFA-430 Xenon Exchange Tests
 Aug. 14 - 17, 1979 ($T_{mod} = 235^{\circ}\text{C}$)

STEP No.	CALIB No. From/Through	GAS			ROD NO. 2				ROD NO. 4			
		Mixture	P-152, V (voltage)	MPa (absolute)	TF-3 (°C)		LHRTF3 (kW/m)		TF-6 (°C)		LHRTF5 (kW/m)	
					ΔTC	TF-3 _{adj.}	LHRTF3 _{adj.}	s	ΔTC	TF-6 _{adj.}	LHRTF5 _{adj.}	s
1	353/362	100% He	2.168	5.083	801.2	2.4	20.68	.01	693.3	1.8	22.01	.02
					- 29.1	787.6			- 29.6	650.5		
2	366/375	"	1.128	0.804	801.95	2.1	20.69	.02	696.5	1.7	22.02	.02
					- 28.6	788.0			- 26.8	659.2		
3	379/399	"	1.008	0.310	810.53	2.3	20.68	.04	705.7	1.9	22.01	.05
	399/410	"	unstable		- 20.1	796.6			- 18.3	667.7		
	411/425	"	exhausting									
	425/432	"	unstable									
4	433/442	"	0.960	0.112	825.3	1.8	20.54	.03	720.2	2.0	21.85	.02
					- 2.1	814.8			- 2.5	683.5		
5	444/453	"	2.183	5.145	796.1	1.2	20.51	.02	690.0	1.2	21.85	.02
					- 29.5	787.2			- 29.5	656.5		
6	457/466	"	1.693	3.129	795.72	1.9	20.51	.02	689.0	1.6	21.85	.02
					- 29.9	786.8			- 30.4	655.6		
7	470/480	"	1.326	1.618	796.2	2.0	20.52	.02	689.7	1.6	21.87	.03
					- 29.7	787.0			- 30.2	655.8		
8	485/495	"	1.199	1.096	795.6	1.8	20.48	.02	690.0	2.1	21.81	.07
					- 29.2	787.5			- 29.5	656.5		
9	998/508	"	1.129	0.808	797.3	1.6	20.51	.04	692.3		21.81	
					- 28.33	788.3			- 26.9	659.1		
10	512/522	"	1.083	0.618	797.68	2.1	20.47	.01	693.1	2.0	21.81	.03
					- 26.9	789.8			- 25.9	660.1		
11	526/535	"	1.049	0.479	799.8	1.9	20.46	.03	695.0	1.8	21.81	.02
					- 24.5	792.1			- 23.4	662.6		
12	539/548	"	1.005	0.298	804.3	1.9	20.46	.02	700.6	1.4	21.80	.02
					- 20.1	796.5			- 18.8	667.2		
13	555/565	"	0.960	0.112	822.5	1.9	20.45	.02	719.7	1.7	21.73	.02
					- 2.2	814.5			- 0.9	685.1		
14	596/606	"	0.965	0.133	670.6	1.2	15.32	.02	592.3		16.30	
					- 5.34	666.5		15.0	- 3.0	568.8		15.0
15	610/619	"	2.169	5.087	651.7	1.9	15.32	.02	570.2	1.9	16.30	.01
					- 23.8	648.0			- 23.4	548.5		
16	625/635	"	1.695	3.137	650.7	1.5	15.30		569.3	1.3	16.28	.02
					- 24.2	647.6			- 23.8	548.0		
17	632/640	"	1.326	1.618	650.4	1.6	15.30		569.2	1.6	16.26	.02
					- 24.8	647.0			- 23.5	548.3		
18	655/665	"	1.200	1.100	650.9	1.3	15.28		570.0	1.4	16.25	
					- 23.5	648.3			- 22.6	549.2		
19	671/679	"	1.129	0.808	651.9	1.5	15.28		571.3	1.3	16.26	
					- 22.5	649.5			- 21.6	550.2		
20	682/692	"	1.083	0.618	651.2	1.1	15.27		570.7	1.5	16.25	
					- 23.0	648.8			- 22.0	549.9		
21	696/706	"	1.050	0.483	654.6	1.2	15.27		574.5	1.4	16.25	
					- 19.6	652.2			- 18.5	553.4		
22	709/719	"	1.006	0.302	656.6	1.6	15.27		576.8	1.3	16.26	
					- 17.8	654.0			- 16.5	555.3		

Table A-I. IFA-430 Xenon Exchange Tests
 Aug. 14 - 17, 1979 ($T_{mod} = 235^{\circ}\text{C}$)

STEP No.	CALIB No. From/Through	GAS			ROD NO. 2				ROD NO. 4			
		Mixture	P-152, V (voltage)	MPa (absolute)	TF-3 (°C)		LHRTF3 (kW/m)		TF-6 (°C)		LHRTF6 (kW/m)	
					ΔTC	TF-3 _{adj.}	LHRTF3 _{adj.}	LHRTF3 _{adj.}	ΔTC	TF-6 _{adj.}	LHRTF6 _{adj.}	LHRTF6 _{adj.}
23	724/734	100% He	0.983	0.207	660.4	1.8	15.28		581.7	1.4	16.25	
					- 14.2	657.6			- 11.8	560.0		
24	740/750	"	0.960	0.112	675.7	1.0	15.29		592.1	1.1	16.24	
					- 2.6	669.2			- 2.4	569.8		
25	769/779	"	0.959	0.108	518.4		10.10		469.7		10.70	
					- 1.8	520.2			- 0.7	459.4		
26	786/796	"	2.186	5.157	505.6		10.12		453		10.72	
					- 14.6	507.4			- 16.6	443.4		
27	809/819	"	1.083	0.618	505.1		10.15		453		10.72	
					- 15.9	506.1			- 16.6	443.4		
28	828/838	"	1.007	0.298	508.0		10.13		458		10.74	
					- 12.5	509.5			- 12.4	447.6		
29	846/856	"	0.963	0.125	515.5		10.14		466		10.74	
					- 5.4	516.6			- 4.9	455.0		
30	877/887	"	0.964	0.129	374.1	1.1	5.15		351.2	0.8	5.41	
					- 6.04	375.1			- 4.7	347.4		
31	894/904	"	2.182	5.141	370.0	0.8	5.14		344.5	0.9	5.40	.01
					- 9.8	371.3			- 10.7	341.4		
32	914/925	"	1.087	0.635	367.4	0.8	5.12		345.0	0.7	5.40	
					- 11.84	369.3			- 10.2	341.9		
33	935/945	"	1.005	0.298	370.1	1.1	5.10		346.5	0.8	5.38	
					- 8.6	372.5			- 8.5	343.6		
34	958/968	"	0.963	0.125	373.3	0.8	5.11		350.8	0.9	5.38	.01
					- 5.8	375.3			- 4.5	347.6		
	971/1004	EXCHANGE TO 10% XENON										
35	1005/1015 1016/1031	10% Xe Reflux	-2.184	5.157	386.1	0.8	5.17		351.8	0.7	5.45	
						386.2				347.1		
36	1032/1037	"	2.184	5.157	387.8	0.8	5.11		352.6	0.7	5.45	
						389.5				347.9		
37	1057/1067	10% Xe	2.179	5.129	525.5	3.9	10.17	.06	562.5	2.8	10.82	.06
					- 25.9	525.7			- 16.7	450.3		
38	1071/1081	"	1.699	3.153	534.2	1.6	10.03	.06	463.4	2.1	10.67	.06
					- 13.3	538.3			- 12.9	454.1		
39	1088/1098	"	1.328	1.627	536.0	2.3	10.17		463.2	2.0	10.82	
					- 15.6	530.1			- 16.1	450.9		
40	1103/1113	"	1.200	1.100	538.3	1.3	10.19		465.0	1.1	10.84	
					- 14.0	537.6			- 14.8	452.2		
41	1116/1126	"	1.131	0.816	539.3	1.7	10.20		467.5	1.8	10.85	
					- 13.3	538.3			- 12.7	454.3		
42	1128/1138	"	1.084	0.623	540.7	1.1	10.23		467.3	0.9	10.88	
					- 12.7	538.9			- 13.5	453.5		
43	1141/1151	"	1.050	0.483	541.3	1.5	10.23		467.3	0.8	10.88	
					- 12.2	539.4			- 13.5	453.5		
44	1155/1165	"	1.007	0.306	543.6	2.0	10.23		470.4	1.4	10.87	
					- 9.9	541.7			- 10.4	456.6		

(AD) : A-1. IFA-430 Xenon Exchange Tests
 Aug. 14 - 17, 1979 ($T_{mod} = 235^{\circ}C$)

STEP No.	CALIB No. From/Through	GAS			ROD NO. 2			ROD NO. 4		
		Mixture	P-152, V (voltage)	MPa (absolute)	TF-3 ($^{\circ}C$)		LHRTF3 (kW/m)	TF-6 ($^{\circ}C$)		LHRTF6 (kW/m)
					ΔTC	TF-3 _{adj.}	LHRTF3 _{adj.}	ΔTC	TF-6 _{adj.}	LHRTF6 _{adj.}
45	1168/1178	10% Xe	0.983	0.207	546.4	1.5	10.23	473.2	1.1	10.87
46	1182/1192	"	0.958	0.104	- 7.2	544.4	10.21	- 7.9	459.1	10.86
					- 0.9	550.76		- 1.5	466.5	
47	1238/1248	"	0.958	0.104	703.5	1.9	15.00	601.0	1.2	15.96
48	1279/1284	"	2.183	5.145	- 0.9	708.5	15.01	- 0.7	584.0	15.99
49	1293/1301	"	1.693	3.129	675		15.01	584		16.00
50	1314/1320	"	1.306	1.536	- 29.3	680.1	15.00	- 17.3	567.4	16.00
51	1328/1335	"	1.199	1.096	682.0		15.00	561.8		16.00
52	1345/1349	"	1.129	0.808	- 22.7	686.7	15.00	- 19.6	565.1	16.00
53	1356/1362	"	1.083	0.618	683.7		15.00	580		16.00
54	1367/1375	"	1.049	0.479	- 20.7	688.7	15.00	- 21.3	563.4	16.00
55	1379/1388	"	1.199	1.096	684.9		15.00	579		16.00
56	1393/1401	"	1.129	0.808	- 19.5	689.9	14.99	- 22.2	562.5	15.98
57	1407/1415	"	1.083	0.618	684.9		15.01	579		16.00
58	1420/1428	"	1.049	0.479	- 19.5	689.9	15.01	- 21.8	562.9	16.00
59	1449/1459	"	1.005	0.298	686.8		15.01	581		16.00
60	1501/1511	"	1.005	0.298	- 18.0	691.5	15.01	- 20.3	564.3	16.00
61	1525/1535	"	1.049	0.479	683.6		15.01	552.7		16.00
62	1552/1558	"	1.005	0.298	- 16.1	693.3	15.02	- 18.7	566.0	16.00
63	1578/1588	"	0.983	0.207	692.2		15.02	586.5		16.00
64	1607/1617	"	0.983	0.207	- 12.8	696.6	15.03	- 15.2	569.5	16.00
65	1633/1643	"	0.971	0.158	694.2		15.03	590.7		16.00
66	1658/1668	"	0.971	0.158	- 11.1	698.3	15.02	- 11.2	573.5	16.00
					697.1		15.02	595.3		16.00
					- 7.9	701.5		- 6.9	577.8	
					705.1		15.05	602.3		16.01
					- 0.9	708.5		- 0.6	584.1	
59	1449/1459	"	0.959	0.108	873.6	1.7	20.39 .03	735.0	1.6	21.70 .03
60	1501/1511	"	2.179	5.129	- 1.4	866.4	20.63	- 1.0	700.8	21.96
61	1525/1535	"	1.939	4.141	- 46.1	821.6	20.59	- 24.2	677.6	21.92
62	1552/1558	"	(1.670)	(3.034)	838.8	2.0	20.61	712.2	1.8	21.94
63	1578/1588	"	(1.351)	(1.721)	- 41.2	826.5	20.61	- 26.4	675.4	21.94
64	1607/1617	"	1.939	4.141	844.2		20.61	710.4	1.3	21.94
65	1633/1643	"	1.939	4.141	- 36.6	831.1	20.60	- 28.4	673.4	21.94
66	1658/1668	"	1.939	4.141	846.4	1.2	20.60	710.8	0.8	21.94
					- 34.1	833.6		- 28.1	673.7	
					849.3	2.2	20.61	708.2	1.8	21.95
					- 31.6	836.1		- 30.6	671.2	
					851.4	2.4	20.62	709.4	3.6	21.97
					- 29.9	837.8		- 29.9	671.9	
					853.8	2.1	20.61	711.9	2.1	21.97
					- 27.3	840.5		- 27.7	674.1	

Table A-I. IFA-430 Xenon Exchange Tests
 Aug. 14 - 17, 1979 ($T_{mod} = 235^{\circ}\text{C}$)

STEP No.	CALIB No. From/Through	GAS			ROD NO. 2				ROD NO. 4			
		Mixture	P-152, V (voltage)	MPa (absolute)	TF-3 ($^{\circ}\text{C}$)		LHRTF3 (kW/m)		TF-6 ($^{\circ}\text{C}$)		LHRTF6 (kW/m)	
					ΔTC	TF-3 _{adj.}	LHRTF3 _{adj.}	ΔTC	TF-6 _{adj.}	LHRTF6 _{adj.}		
67	1693/1703	10% Xe	1.047	0.470	856.0	2.2	20.65	714.4	1.9	22.00		
					- 26.2	841.5		- 26.0	678.3			
68	1720/1730	"	1.005	0.298	860.2	1.6	20.60	718.1	1.8	21.95		
					- 20.7	847.0		- 21.6	680.2			
69	1740/1750	"	0.983	0.207	867.3	1.9	20.62	725.2	1.0	21.95		
					- 14.5	853.7		- 15.2	686.7			
70	1755/1765	"	0.971	0.158	872.3	2.8	20.63	730.4	1.9	21.97		
					- 9.8	857.9		- 10.8	691.0			
71	1770/1780	"	0.957	0.100	883.1	1.6	20.65	742.5	1.2	21.98		
					(-0)	867.7		(-0)	701.8			
Change gas from 10% Xe to pure helium, and then to 5% Xe.												
72	1809/1819	Gas purity not assured - Reject this step		(0.1)	848.1		20.64	735.5		21.97		
					- 7.6	834.1						
73	1860/1870	5% Xe	2.184	5.149	821.2	4.9	20.58	705.1	2.1	21.94		
					- 32.1	809.7		- 23.0	668.5			
74	1884/1894	"	1.937	4.133	819.9		20.61	702		21.96		
					- 34.2	807.6		- 26.2	665.3			
75	1895/1915	"	1.694	3.132	821.8	1.6	20.57	701		21.93		
					- 31.2	810.5		- 26.5	665.0			
76	1926/1936	"	1.326	1.618	824.5	1.4	20.56	700.5		21.93		
					- 25.3	813.5		- 27.0	664.5			
77	1947/1957	"	1.199	1.096	825.2	2.2	20.54	700.5		21.92		
					- 27.1	814.7		- 26.8	664.7			
78	1970/1980	"	1.129	0.608	824.5	2.3	20.54	701.7		21.91		
					- 27.7	814.0		- 25.5	666.0			
79	1992/2002	"	1.083	0.618	826.6	2.6	20.55	703.2		21.90		
					- 26.0	815.7		- 23.9	667.6			
80	2014/2024	"	1.049	0.479	828.6	1.8	20.55	705.6	1.4	21.89		
					- 24.0	817.7		- 21.5	670.0			
81	2036/2046	"	1.005	0.298	833.1	2.0	20.52	710.0	1.7	21.86		
					- 18.8	822.9		- 16.9	674.6			
82	2056/2066	"	0.982	0.203	839.0	1.7	20.52	716.4	1.6	21.85		
					- 13.0	828.7		- 10.9	680.6			
83	2074/2084	"	0.971	0.158	842.7	1.9	20.53	720.0	1.5	21.86		
					- 9.7	832.1		- 7.8	683.7			
84	2090/2100	"	0.959	0.108	850.9	0.9	20.53	727		21.86		
					- 1.8	840.0		- 1.4	690.1			
85	2112/2122	"	0.955	0.092	859.1	5.1	20.51	733.0	1.2	21.85		
					+ 6.8	848.6		696.66				
86	2146/2156	"	0.955	0.092	696.5	1.6	15.19	602.3	1.3	16.20		
					+ 6.0	695.7		580.1				
87	2176/2187	"	2.187	5.161	667.2	2.2	15.18	579.4	1.6	16.15		
					- 22.6	667.1		- 18.3	559.9			

Table A-1. IFA-430 Xenon Exchange Tests
 Aug. 14 - 17, 1979 ($T_{mod} = 235^{\circ}\text{C}$)

STEP No.	CALIB No. From/Through	GAS			ROD NO. 2			ROD NO. 4		
		Mixture	P-152, V (voltaga)	MPa (absolute)	TF-3 $^{\circ}\text{C}$		LHRTF3 $\frac{\text{s}}{(\text{kW/m})}$	TF-6 $^{\circ}\text{C}$		LHRTF6 $\frac{\text{s}}{(\text{kW/m})}$
					ΔTC	TF-3 _{adj.}	LHRTF3 _{adj.}	ΔTC	TF-6 _{adj.}	LHRTF6 _{adj.}
88	2194/2204	5% Xe	1.940	4.145	666.5	1.7	15.15	576.3	1.4	16.14
					- 22.5	667.2		- 21.0	557.2	
89	2215/2225	"	1.695	3.137	666.3	1.7	15.13	575.5	1.2	16.13
					- 22.1	667.6		- 21.6	550.7	
90	2239/2249	"	1.328	1.627	668.4	1.5	15.15	575.0	1.1	16.14
					- 20.6	669.1		- 22.2	556.0	
91	2258/2268	"	1.201	1.104	669.4	1.6	15.13	575.3	1.2	16.12
					- 19.0	670.7		- 21.5	556.7	
92	2279/2289	"	1.131	0.816	670.2	1.7	15.11	576.5	1.7	16.15
					- 17.7	672.0		- 21.0	557.2	
93	2301/2311	"	1.084	0.623	669.4	1.4	15.08	576.0	1.5	16.09
					- 17.6	672.1		- 20.5	557.7	
94	2318/2328	"	1.050	0.483	671.2	0.9	15.12	578.1	0.5	16.11
					- 16.9	672.8		- 18.7	550.5	
95	2339/2349	"	1.006	0.302	673.8	1.6	15.10	581.3	1.3	16.08
					- 13.8	675.9		- 15.2	563.0	
96	2357/2367	"	0.983	0.207	677.4	1.1	15.11	585.0	1.2	16.10
					- 10.6	679.2		- 12.1	566.1	
97	2375/2385	"	0.972	0.162	679.8	1.4	15.07	588.8	1.7	16.06
					- 7.0	682.7		- 7.8	570.5	
98	2392/2402	"	0.957	0.100	687.4	1.1	15.09	597.1	1.3	16.06
					(-0-)	689.7		(-0-)	578.2	
99	2433/2443	"	0.957	0.100	535.2	1.0	10.11	476.8	0.5	10.74
					(-0-)	536.9		(-0-)	405.1	
100	2467/2477	"	2.183	5.145	520.8	1.4	10.18	461.1	1.0	10.80
					- 16.2	520.7		- 15.8	449.4	
101	2487/2497	"	1.928	4.137	521.5	0.8	10.17	460.0	0.7	10.80
					- 15.2	521.7		- 16.8	448.3	
102	2507/2517	"	1.694	3.133	521.6	0.9	10.21	459.5	1.3	10.83
					- 16.2	520.7		- 17.8	447.3	
103	2528/2538	"	1.327	1.623	522.7	1.4	10.19	459.4	1.6	10.83
					- 14.6	522.3	0.0	- 17.9	447.2	
104	2545/2555	"	1.199	1.096	522.3	0.9	10.17	459.4	1.1	10.81
					- 14.4	522.5		- 17.5	447.6	
105	2559/2569	"	1.129	0.808	525.2	1.0	10.18	461.5	0.7	10.82
					- 11.8	525.1		- 15.8	449.3	
106	2577/2587	"	1.083	0.618	525.6	1.1	10.24	462.0	0.8	10.88
					- 13.1	523.8		- 16.5	448.6	
107	2593/2603	"	1.049	0.479	523.9	1.5	10.19	461.2	1.7	10.84
					- 13.4	523.5		- 16.4	448.7	
108	2606/2616	"	1.005	0.298	524.9	1.1	10.12	463.5	1.3	10.76
					- 10.4	526.5		- 12.7	452.4	
109	2621/2631	"	0.982	0.203	527.8	1.1	10.11	466.3		10.74
					- 7.2	529.7		- 9.7	455.0	
110	2636/2646	"	0.971	0.158	529.0	0.9	10.09	468.5	0.8	10.73
					- 5.5	531.4		- 7.3	457.8	

Table A-I. IFA-430 Xenon Exchange Tests
 Aug. 14 - 17, 1979 ($T_{mod} = 235^{\circ}\text{C}$)

STEP No.	CALIB No. From/Through	GAS			ROD NO. 2				ROD NO. 4			
		Mixture	P-152, V (voltage)	MPa (absolute)	TF-3 (°C)		LHRTF3 (kW/m)		TF-6 (°C)		LHRTF6 (kW/m)	
					ΔTC	TF-3 _{adj.}	LHRTF3 _{adj.}	LHRTF3 _{adj.}	ΔTC	TF-6 _{adj.}	LHRTF6 _{adj.}	LHRTF6 _{adj.}
111	2652/2662	5% Xe	0.955	0.092	535.1 + 0.3	1.3 537.2	10.10		475.6 - 0.9	1.7 464.2	10.73	
112	2680/2690	"	0.955	0.092	374.9	0.5 384.5	4.84		348.7	1.0 351.7	5.09	
113	2701/2711	"	2.182	5.141	369.0		4.81		342.0		5.05	
114	2725/2735	"	1.200	1.100	368.0		4.82		440.0		5.07	
115	2744/2754	"	1.006	0.302	370.5		4.84		442.1		5.08	
116	2764/2774	"	0.954	0.088	376.2	0.7 385.5	4.85		343.0		5.10	
The following tests were conducted on Dec. 14, 1979, with $T_{mod} = 240^{\circ}\text{C}$:												
1	2618/2628	10% Xe 90% He	2.175	5.12	966.7 - 53.1	3.5 986.7	24.33	.02	808.4 - 37.3	2.3 786.1	26.02	.04
2	2632/2643	"	1.912	4.05	980.7 - 38.3	2.8 1001.5	24.30		808.1 - 37.4	2.2 786.0	26.01	
Reject the step for unstable temperature												
3	2666/2676	90% He	1.683	3.1	976.1 - 46.2	2.8 993.6	24.42		808.5 - 39.7	1.5 783.7	26.14	
4	2677/2687	"	1.683	3.1	975.5 - 47.8	2.8 992.0	24.45		809.1 - 39.5	1.7 783.9	26.16	
5	2704/2714	"	1.368	1.8	972.4 - 49.1	3.2 990.7	24.39		806.9 - 40.2		26.09	
6	2724/2734	"	1.200	1.1	977.9 - 42.3	2.9 997.6	24.35		807.5 - 38.4	1.7 785.0	26.03	
7	2743/2753	"	1.131	0.82	976.5 - 41.8		24.29		806.4 - 38.2	2.2 785.2	25.97	
8	2771/2781	"	1.085	0.63	976.7 - 40.3	3.1 999.5	24.25		807.4 - 35.9	1.7 787.5	25.91	
9	2792/2802	"	1.051	0.49	978.1 - 38.2	4.3 1001.6	24.23	.06	809.2 - 33.8	3.3 789.6	25.89	
10	2814/2824	"	1.007	0.31	979.8 - 30.2	3.7 1009.6	24.03		812.2 - 25.1	1.7 798.4	25.62	.02
11	2831/2841	"	0.985	0.22	984.6 - 22.5	2.7 1017.3	23.95	.04	817.1 - 20.3	2.5 803.1	25.62	
12	2842/2852	"	0.973	0.17	984.95 - 18.9	2.6 1020.9	23.85		818.7 - 16.3	2.1 807.1	25.51	
13	2880/2890	"	0.956	0.10	996.9 (-0-)	2.2 1039.8	23.66	.05	830.6 (-0-)	1.8 823.4	25.31	.05

APPENDIX B

CALCULATION AND TABLE OF T_{std}

Each set of pressure measurements from about 5 MPa down to atmospheric pressure (~ 0.1 MPa) usually culminated with a pressure just slightly above true atmospheric pressure. Although the difference was always less than the uncertainty of the absolute measurement, corrections to a standard one atmosphere pressure were made to eliminate any bias between separate sets of pressure measurements. The correction, or extrapolation, of the fuel centerline temperature (T_{std}) to a pressure of one atmosphere (0.1013 MPa) was made by performing a least-square fit of the data for each set of pressure measurements and then using the fitted line to calculate the temperature at one atmosphere (0.1013 MPa). Typically, slopes of the temperature versus pressure functions were in the range of 15-20 K/kPa at pressures near atmospheric (~ 0.1 MPa) and so the corrections to a standard atmosphere (0.1013 MPa) were usually less than 2 K.

Table B-1 lists the reference temperatures (T_{std}) for each set of pressure measurements.

TABLE B-1. T_{std}

Fill Gas	Linear Power (kW/m)	T_{std} (K)	
		Rod 2	Rod 4
100% Helium	5	654.1	625.1
	10	795.0	733.0
	15	944.8	844.8
	20	1089.7	959.0
5% Xe/95% He	10	809.9	738.1
	15	962.7	851.2
	20	1114.8	964.5
10% Xe/90% He	10	824.6	740.0
	15	982.4	857.7
	20	1140.7	975.0
	25 ^a	1312.8 ^a	1096.4 ^a

a. Data from December 14, 1979.

APPENDIX C

DISCUSSION OF MEASUREMENT ERRORS

An outstanding feature of the "raw" data as shown in Figures C-1 and C-2 is its smoothness and regularity. This freedom from randomness exhibits itself even in the much expanded graphs of ΔT in Figures C-3 and C-4. The level of error in measurements will be reviewed by discussing random errors and systematic errors separately.

TEMPERATURE

All of the fuel temperature data in the report were obtained from W3%/W25% Re (Rod 2) and W5%Re/W26%Re (Rod 4) fuel centerline thermocouples with chromel-alumel extension cables referenced to a controlled temperature junction box as shown in Figure C-5.

Systematic Error

Principal sources of systematic error in the temperature measurement system include:

- Calibration error of the fuel thermocouple materials (manufacturer specifications place this error to within 1% of ISA tables up to 2000°C),
- Calibration error of the Chromel-Alumel extension cable,
- Temperature of the thermoelement extension cable junction,
- Temperature induced decalibration,
- Transmutation induced decalibration,

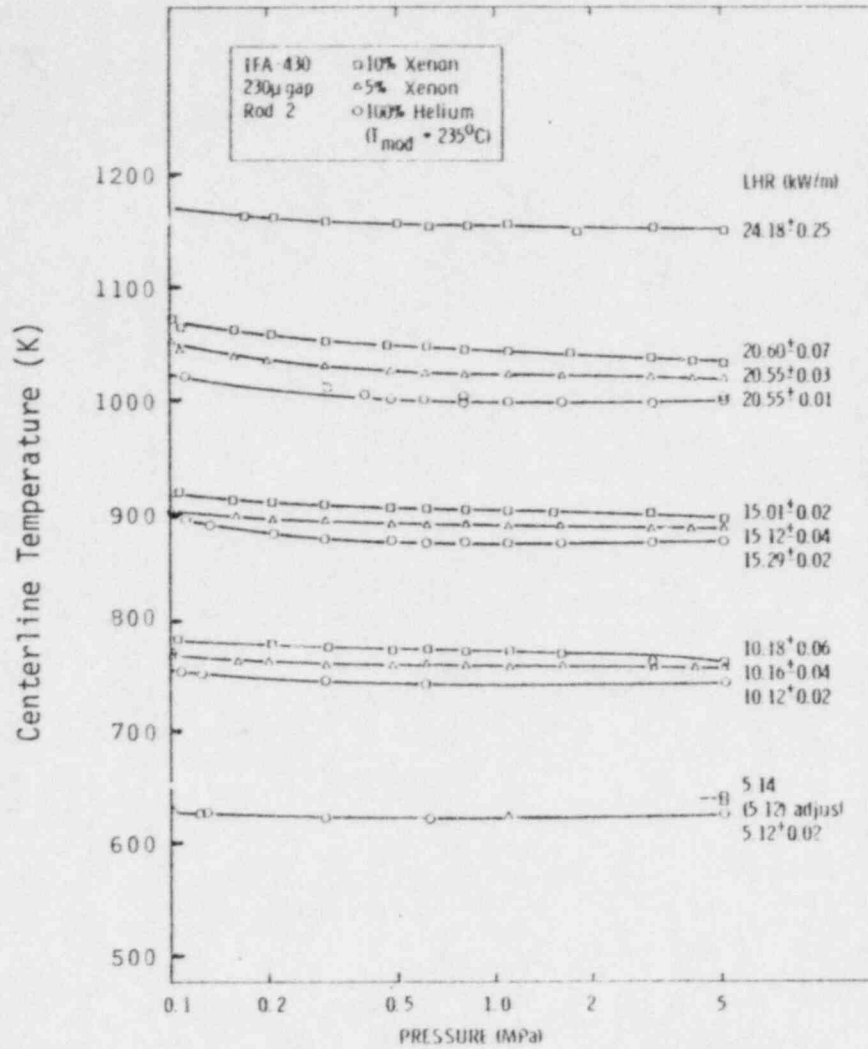


Fig. C-1 Summary of rod 2 fuel centerline temperature data as a function of gas pressure. Linear power at the thermocouple position is listed for each data set.

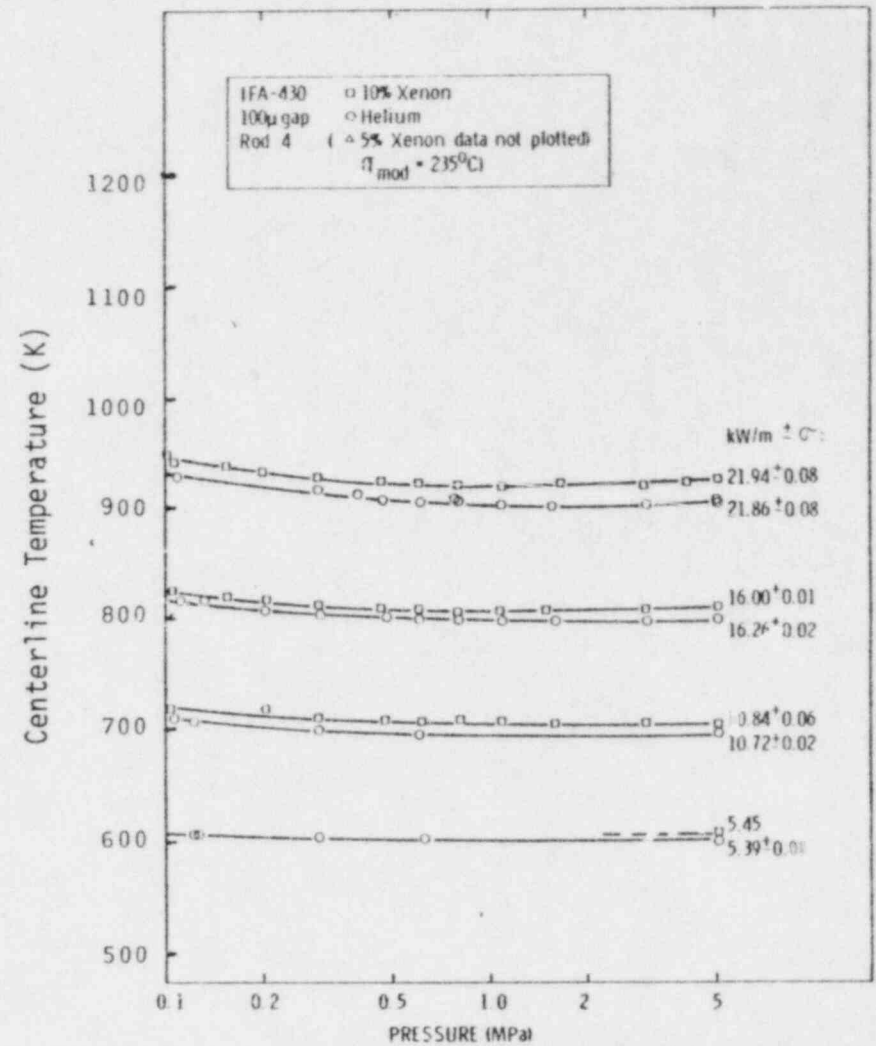
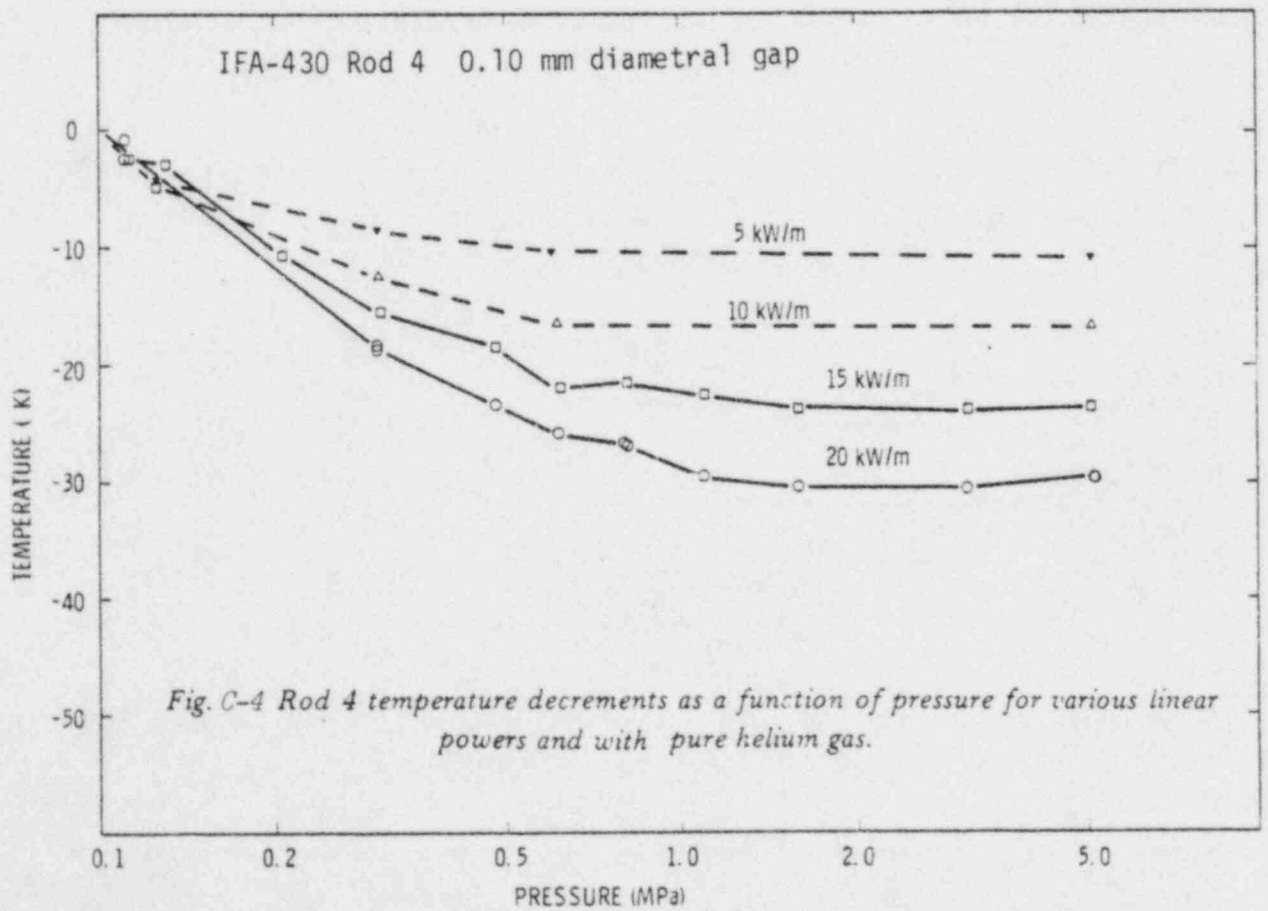
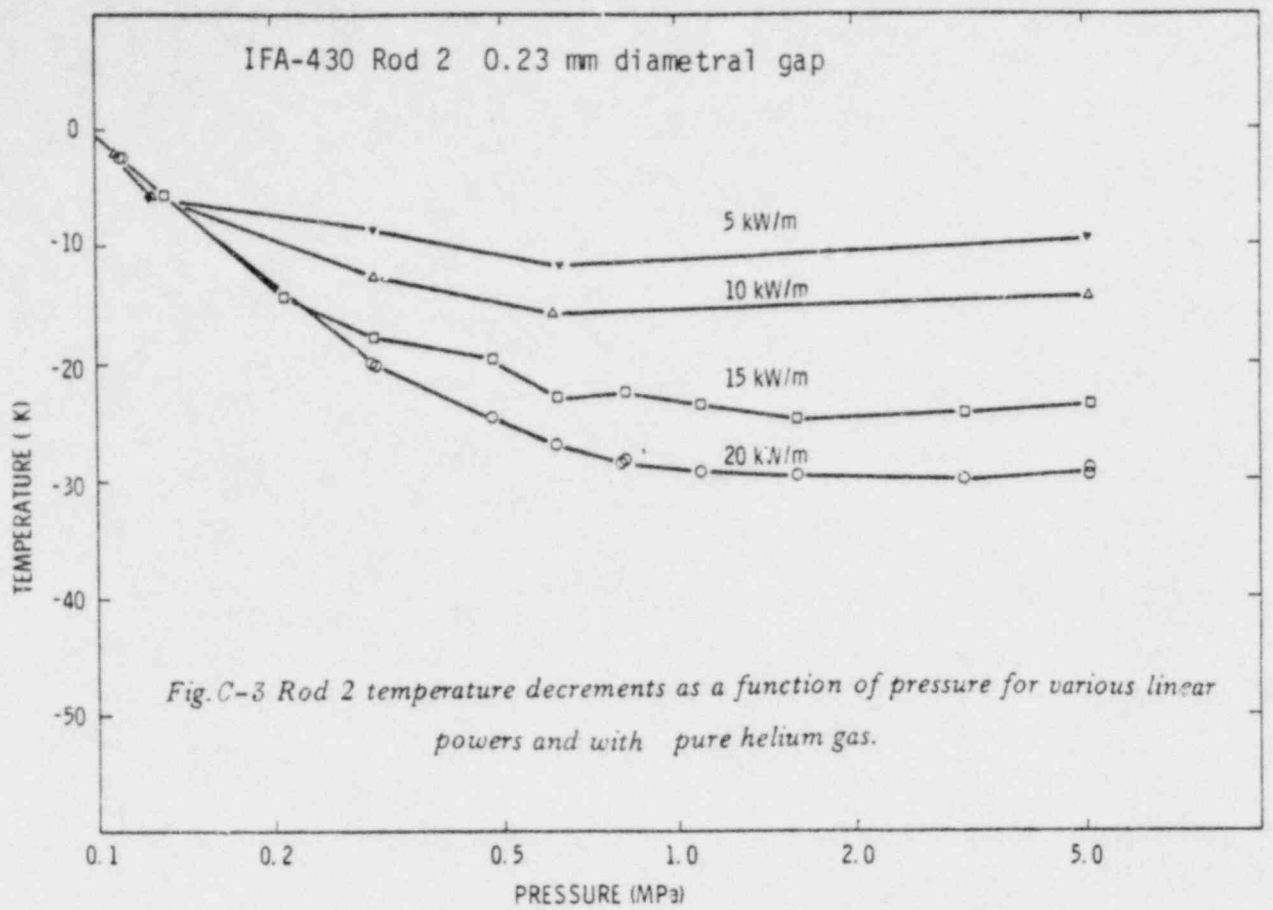


Fig. C-2 Summary of rod 4 fuel centerline temperature data as a function of gas pressure. Linear power at the thermocouple position is listed for each data set.



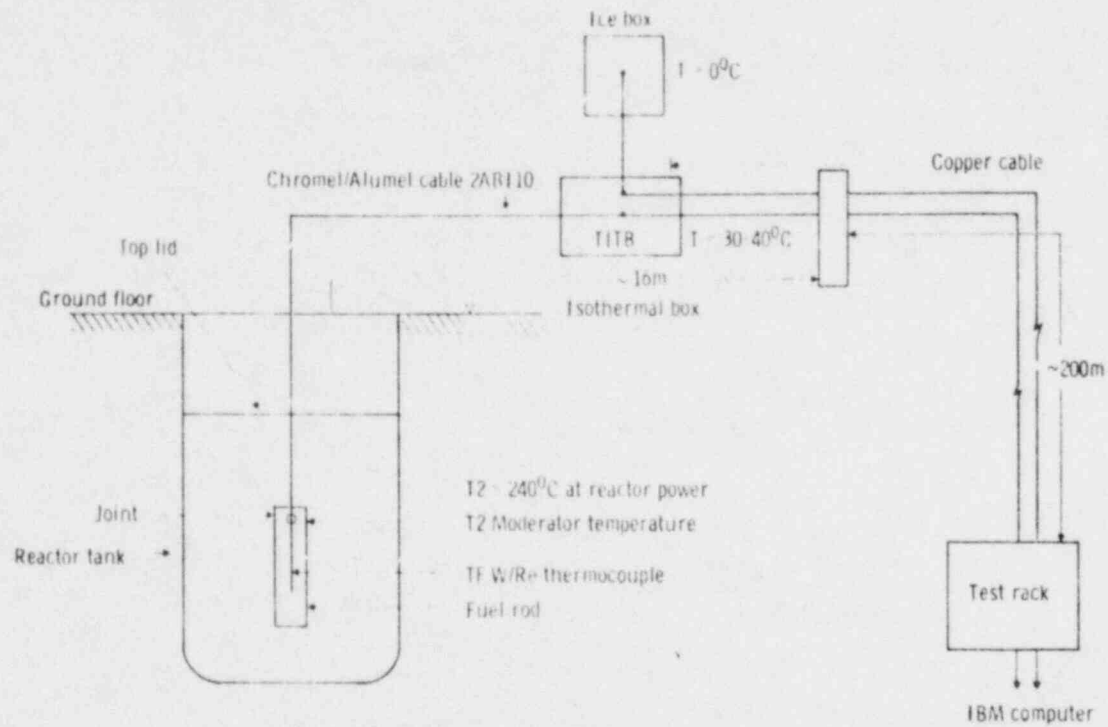


Fig. C-5. Circuitry for high temperature fuel thermocouples in the HBWR.

- Reference temperature error, and
- Signal conditioning and voltage conversion error.

Errors such as voltage drop due to wetted cables and shorting of thermoelements were not observed during these tests. Brakas et al.,^{C-1} in a review of the above systematic errors, concludes that the combined uncertainties of the measurement and conversion technique result in an uncertainty of ± 6 K for normal, undegraded circuits; this does not include calibration errors. For the temperatures in this study, which ranged up to a maximum of about 1200 K, calibration errors may be as large as ± 9 K and measurement errors ± 6 K. Fordestrommen^{C-2} concluded that transmutation in the HBWR of W5Re thermocouples could result in an error of -1.0 to -3.0% per 10^{20} n/cm² fluence after the first 3×10^{20} n/cm² exposure.

At 2,500 kWd/kg UO₂ average burnup, IFA-430 thermocouples would have accumulated only about 7×10^{19} n/cm² and therefore no significant decalibration is expected.

In the calculation of differential temperature it is reasonable to expect most of the systematic errors to diminish in importance or even to disappear. The major sources of systematic error for differential temperature are examined below.

1. Calibration errors. If one can assume that the slope of voltage output relative to real temperature, viz $[dV/dT]_T$, for the manufacturers product thermocouples is a monotonic function closely following the standard ISA tables, then the guaranteed $\pm 1\%$ absolute deviation from ISA tables cancels completely in the calculation of temperature differences and this error source may be essentially dismissed. Similar error at the chromel-alumel junction would also cancel. On the other hand, if

thermocouple output can meander between the $\pm 1\%$ limits, the error in temperature differences is significantly higher. While this behavior, which would still meet manufacturers' specifications, seems unlikely, the authors have no information to deny its existence.

2. Decalibration. Decalibrations due either to transmutation or thermal and chemical changes are expected to be monotonic, long-term effects which would not change thermocouple output significantly during the course of these experiments. Thus, they cancel in the differencing process, and are estimated to be less than 1% in the absolute measurement.
3. Reference Temperature error. Reference temperature error can also be dismissed. Thermocouple extension cables terminate in an insulated junction box whose temperature is in turn measured by chromel-alumel thermocouples referenced to an ice bath. Absolute error of the junction box temperature is listed by Brakes^{C-1} as 1.8 K which reflects about 3.6 K error into the fuel temperatures because of the use of chromel-alumel lead cables. Chromel-alumel has a temperature coefficient double that of the Tungsten-Rhenium types; nevertheless, variance of the reference box temperature during the experiments is expected to be insignificant and this error is likewise eliminated in the temperature difference calculation.
4. Measuring and conversion errors. Fuel centerline thermocouple outputs are processed through analog-to-digital converters (ADC) and thence to an IBM-1800 computer where conversion to degrees Celsius is performed using a polynomial fit to the standard ISA tables. In this process, a least-significant-bit error of $\pm 1.28 \text{ K}^{\text{C-3}}$ is introduced. Brakes^{C-1} estimates a $\pm 4 \text{ K}$ error possible in the polynomial fit, and a combined signal conditioning error of $\pm 6 \text{ K}$. In all of the measuring-converting process, it appears that accumulated errors are constant and systematic with the exception of

least-significant-bit and drift of the AEC electronics, which is so low ($\pm 0.6\%$ full scale over 6 months)^{C-3} it can be ignored. Thus, that measuring and conversion errors do not add significant error to temperature differences.

Least-significant-bit errors are random and appear in the measured random error which is discussed next.

Random Error

Each of the 258 temperature-power data sets listed in Appendix A, Table A-1 is the average usually of 11 or more individual measurements. For each data set the standard deviation of the individual measurements has been computed and, except for a very few cases, the random standard deviations are less than ± 2 K. Thus, the effective standard deviation(s) for temperature differences is given by,

$$s \leq \sqrt{2^2 + 2^2} = 2.8 \text{ K} \quad (\text{C-1})$$

Temperature Error Summary

Absolute measurements

Random error: $s = \pm 2 \text{ K}$

Systematic error:

1. Calibration $\pm 1\%$
2. Decalibration $< - 1\%$
3. Reference Temperature $\pm 4 \text{ K}$

- | | | |
|----|-------------------------------|---------------------|
| 4. | Extension cable | $\pm 4 \text{ K}$ |
| 5. | Measurement and
Conversion | $\pm 6.0 \text{ K}$ |

Temperature Differences

Random error: $s = \pm 2.8 \text{ K}$

Systematic error: probably much less than random.

POWER

The importance of power measurements in the present study derives mainly from the need to normalize all temperature measurements to standard power levels. Thus, precision and randomness play an important role, whereas absolute power measurement is less important. The rod powers were measured with a precision of a few tenths-percent. Randomness in the power measurement was usually 0.1% and occasionally as high as 0.6%. Absolute accuracy is more uncertain; the power calibration for IFA-430 showed a randomness of about $\pm 2\%$ and a total error of probably 4-5%, the uncertainty in the power at the thermocouple (LHRTF) is estimated to be $\sim 10\%$.

PRESSURE

The measurement of pressure is one in which improvement could be beneficial. The pressure transducer used for the study (P-152, Figure C-5) is a Bourdon tube type with a range of 0-16 MPa. Accuracy is specified at 0.5% of full scale (0.08 MPa), an amount which does not significantly influence most of the measurements. Fuel centerline temperatures, however, are strongly influenced by pressure in the region of 0.1 to 0.2 MPa and instrument error based simply on the 0.5% of full scale specification would result in an uncertainty of 40 to 80% of the measured pressure in this region. However, at one atmosphere (0.1 MPa absolute) the instrument (P-152) received repeated

calibration, so the 0.5% error is not strictly applicable. A review of data taken when the system had sufficient time to thoroughly equilibrate to atmospheric pressure shows that absolute error in the 0.1 to 0.2 MPa pressure range is in fact much better; repeatability near one atmosphere appears to be about 0.01 MPa and is therefore estimated to be the absolute error in 0.1 to 0.2 MPa range.

REFERENCES

- C-1 M. J. Brakas et al.: "HBWR Signal Inaccuracies," Enlarged HPG Meeting, Sanderstolen 1976.
- C-2 N. T. Fordestrommen: Analysis of the Present HBWR Data Base on W/Re Thermocouple Decalibration, IDG-Note 2632, October 1979.
- C-3 Sather: Specifications for Electronics Used for In-Core Signals, IDG-Note 2435, February 1978.

APPENDIX D

GAS EXCHANGE PROCEDURE

The two gas flow fuel rods in IFA-430 are connected via short lines and remotely operated valves to a high pressure tank, located within the assembly with a volume of three liters (L). The tank in turn is connected to the external gas flow circuit and gas supply tanks via long lines, several valves and filters. To exchange gas in the fuel rods requires first that the supply lines and the high pressure tank be flushed and filled with the exchange gas.

The supply line consists of about 18 m of 2-mm-ID line plus about 200 m of 6-mm-ID line containing a total volume of six L or less. With the introduction of 6L of exchange gas, the supply line is assumed to be flushed so that undiluted exchange gas is beginning to purge the high pressure tank. If perfect mixing is assumed in the tank, the average isobaric exchange gas concentration in the tank, C_T , is related to the flow rate, f , by the relation

$$\dot{C}_T = (C_{in} - C_T) f/3 \quad (D-1)$$

where C_{in} is the exchange gas concentration. Assuming the original gas to be pure helium, the concentration of exchange gas as a function of time, t , is

$$C_T = C_{in} [1 - \exp(-ft/3)] \quad (D-2)$$

Choosing arbitrarily that flushing should continue until $C_T = 0.99C_{in}$, that is, 99% pure exchange gas, then

$$\frac{C_T}{C_{in}} = 0.99 = 1 - \exp(-ft/3) \quad (D-3)$$

and $ft = 14 \text{ L}$.

Thus, after about 14 L of exchange gas has purged the tank, the tank concentration should be within 1% of the exchange gas concentration. Combining this with the approximate 6 L volume of the supply line results in a total gas purge volume of about 20 L necessary to purge the gas flow supply line and high pressure tank. After the tank has been purged, only a small flow through each fuel rod is required to purge the rod plenum and the open flow paths around the fuel.

Exchange of gases which reside in deep cracks in the fuel is more difficult, however, since many of these pockets of gas are expected to lie stagnant during the purging process. The method adopted here to exchange these gases was to follow the initial purge (which takes place at low pressure) with pressurization to 5 MPa. Accessible gas pockets should, in this way, be mixed on a 50-to-one basis with the new exchange gas, achieving a concentration within a few percent of the exchange gas concentration.

In practice, since there are currently no flow integrating circuits for IFA-430 and since the flow rates rapidly change as inlet and exhaust circuits are operated (making them difficult to read) conservative estimates of total flow were made during the actual exchange to assure adequate replacement of gas. In the exchange from 90% He/10% Xe fill gas to 95% He/5% Xe fill gas, helium was first flushed through the system so that both exchanges to xenon mixtures proceeded from the same initial condition.

APPENDIX E

DESIGN CHARACTERISTICS OF IFA-430

A detailed description of IFA-430 is contained in Reference E-1. The following table provides a brief summary of the design characteristics.

TABLE E-1. IFA-430 DESIGN CHARACTERISTICS

FUEL ROD POSITION	1	2	3	4
ROD DESIGNATION	Rod-1	Rod-2	Rod-3	Rod-4
FUEL				
Chemical Constituents	UO ₂	- ^a	-	-
Enrichment (%)	10.05	-	-	-
Form	Pellet	-	-	-
- Dishing	None	-	-	-
- Chamfer	0.12 mm x 45°	-	-	-
- Density	10.367	10.367	10.381	10.381
Fuel OD (mm)	10.68	10.68	10.81	10.81
Thermocouple hole	c	d	c	d
Active Length (mm)	1283	1183	1283	1183
Total Enriched weight (kg)	1.177	1.096	1.205	1.123
Pellet Length (mm)	12.7	-	-	-
				} = 4932 mm } = 4.601 kg
INSULATORS				
Chemical Constituents	Nat. UO ₂	-	-	-
Form	Pellet	-	-	-
Length each (mm)	6.0	-	-	-
Number in rod	2	6	2	6
GAS, FILLER				
Chemical Constituents	Helium	Ar/He/Xe Variable	Helium	Ar/He/Xe Variable
Pressure (MPa absolute)	0.48	variable	0.48	variable
Volume (cc)	19.0	N.A.	16.4	N.A.
CLADDING				
Alloy	Zr-II	-	-	-
Treatment	SR Annealed	-	-	-
Outside Dia. (mm)	12.787	-	-	-
Thickness (mm)	1.939	-	-	-
Welding	End plugs - EB, Seal Weld - TIG	-	-	-
Gap (diametral, mm)	0.23	0.23	0.10	0.10
INSTRUMENTS, Rod				
Centerline Temperature(TF)	TF-1,-2, (b,t) ^e	TF-3	TF-4,-5(b,t)	TF-6
Off-Center Temperature(TP)	Tp-1,-2,-3	none	Tp-4,-5,-6	none
Gas Pressure (PF)		PF-1,-2,-3(b,m,t) ^f		
PF-4,-5,-6(b,m,t)				
SHROUD: Material Zr-II;		Dia. Inside: 71.0 mm;		Thickness 1.0 mm

a. Dash indicates same specification as Rod 1.
 b. Gas Flow rods have two interruptions in the fuel stack each of 50 mm to accommodate flow bodies and insulator pellets, see Reference E-1.
 c. Centerline and off-center thermocouples-see Reference E-1.
 d. Centerline thermocouple hole, 1.9 mm diameter, extending 70 mm up from the bottom of the fuel stack.
 e. b = bottom, t = top of rod.
 f. b = bottom, m = middle, t = top of rod.

REFERENCES

- E-1 Appelhans et al., Cracking and Relocation of UO₂ Fuel During Initial Nuclear Operation, NUREG/LR-1425, EGG-2032, May 1980.

APPENDIX F

CALCULATION OF $R = \frac{d TC}{d TS}$

The axisymmetric, solid-pellet model^{F-1} for heat flux

$$qf = \frac{2\pi}{r_0} \int_{TS}^{TC} k dT$$

together with k and $\int k dT$ equations published in MATPRO^{F-2} are used to estimate the constant power derivative

$$R \equiv \left. \frac{d TC}{d TS} \right|_{q=\text{constant}} \approx \frac{k_{TS}}{k_{TC}},$$

where q = heat flux W/m^2

f = 0.90, flux depression factor with centerhole

r_0 = 0.54 cm, original radius of pellet

TC = measured fuel centerline temperature, and

TS = (calculated) pellet surface temperature.

K = UO_2 conductivity (W.mK)

Input data and results for the two IFA-430 fuel rods are listed in Table F-1.

Discussion of Error

An expected error of ± 10 K in the centerline temperature measurements is found to yield no significant change in R and an assumed large error in f of ± 0.05 produces only a 2% change in R. Although MATPRO shows about $\pm 10\%$ standard deviation on k, it is reasonable that similar fractional errors will exist at each temperature extreme, TS and TC, so that this source of error is largely reduced when the conductivities are ratioed. Probably the largest source of error in R comes from the assumption of an axisymmetric, solid-pellet model. Cylindrical cracks in the fuel will lower surface temperatures, as will eccentricity of the fuel pellets within the cladding. The Halden code FTEMP2^{F-3}, which models eccentricity by an empirical contact area function, was used to test the dependence of R on pellet eccentricity. Applying the recommended contact area function of E = 0.8, and code calculated temperatures, R takes on the values shown in the last column of Table F1. It appears prudent to use R-values between the two sets of calculations and assume an uncertainty band large enough to cover all calculations, thus the uncertainty in R = $\pm 0.16(R-1)$.

TABLE F-1. ESTIMATES OF R

Power kW/m	q kW/m ²	TC K	TS K	k _{TC} W/cmK	k _{TS} W/cmK	R (f=0.9)	R (FTEMP2)
Rod 2 with Helium at 0.1 MPa.							
10	294	795	668	0.0413	0.0473	1.145	1.185
15	442	945	732	0.0360	0.0441	1.225	1.287
20	589	1090	781	0.0321	0.0419	1.306	1.394
25	736	1313	876	0.0277	0.0382	1.378	1.505
Rod 4 with Helium at 0.1 MPa							
10	294	733	613	0.0440	0.0505	1.147	1.186
15	442	845	650	0.0393	0.0483	1.229	1.288
20	589	959	680	0.0356	0.0466	1.312	1.400
25	736	1096	720	0.0320	0.0446	1.397	1.517

REFERENCES

- F-1. L. S. Tong and J. Weisman: "Thermal Analysis of Pressurized Water Reactors." American Nuclear Society Monograph, 1970.
- F-2. MATPRO-Version 10, A Handbook of Material Properties for Use in the Analysis of Light Water Reactor Fuel Rod Behavior, TREE-NUREG-1180, U.S. National Technical Information Office, 1978.
- F-3. T. J. Bjorlo et al., FUEL-TEMP-2, A Computer Programme for Analyzing the Steady State Thermal Behavior of Oxide Fuel Rods, HPR-211, Sanderstolen, 1977.